AQUEOUS SOLUTION PROPERTIES OF POLY(*N*-ISOPROPYLACRYLAMIDE)

TOMOAKI KAWAGUCHI

2009

Contents

1 Introduction

1.1 Background

Acquiring a deeper understanding of phase behavior of polymer solutions is an interesting and important subject in thermodynamics of polymer solutions, and therefore considerable efforts[1–3] have been continuously devoted to the subject since Flory[4] and Huggins[5] broke ground for it. Even in these days, the phase behavior of polymer solutions is usually interpreted in the framework of the Flory–Huggins (FH) theory, in which the so-called FH entropy term is combined with an enthalpy term including the thermodynamic interaction coefficient χ. For binary solutions of non-polar polymers in non-polar solvents, which commonly exhibit upper-critical-solution-temperature (UCST) miscibility behavior in an ordinary temperature range, the FH theory with $\chi \propto T^{-1}$ may qualitatively explain experimental results. As for binary solutions of polar polymers in polar solvents, on the other hand, they show a variety of phase diagrams, *e.g.*, lower-critical-solution-temperature (LCST), hour-glass shaped, and closed-loop ones, other than the UCST one, since χ is not simply proportional to T^{-1} in such solutions because of interactions between permanent electric dipole moments of solute polymers and solvent molecules. In particular, the dipolar interactions are very strong in aqueous polymer solutions, in which χ may be appreciably varied by breakdown of the so-called hydrogen bond as the solution temperature is raised, and a special interest therefore has centered on aqueous solutions. For instance, phase behavior of aqueous polyoxyethylene (POE) solutions has been almost completely investigated both experimentally[6–8] and theoretically.[9] The aqueous POE solution could be a model system for a comprehensive study of aqueous polymer solutions, if it were easy to carry out a variety of experimental measurements other than the turbidity near room temperature.

Among aqueous polymer solutions studied so far, those of poly(*N*-isopropylacrylamide) (PNIPA) are considered to be suitable for a variety of experimental measurements near their phase-separation temperatures, since they show LCST miscibility behavior near the human body temperature.[10] Besides such experimental convenience, PNIPA itself is an attractive polymer because of its potential applications to drug-delivery devices and intelligent materials.[11,12] Not a few studies have therefore been made of phase behavior

of its aqueous solutions both experimentally[13–21] and theoretically,[22] in which the cloud-point curve in the solution is always considered to be the binodal as in the cases of other polymer-solvent systems.[1–3] The cloud point in aqueous PNIPA solutions has been shown to have some salient and unusual features: it is rather insensitive to the concentration of the solutions,[13–21] and at a given concentration it decreases with decreasing the molecular weight of PNIPA.[17,18] Unfortunately, however, the literature data[13–21] for the cloud point is rather scattered and the difference between literatures beyond experimental error. It is therefore necessary to find the source of the difference and to inquire the reasons of such characteristic features. It is the purpose of this thesis.

Recently, Ray *et al.*[23] pointed out that the cloud point in an aqueous PNIPA solution appreciably depends on the stereochemical composition of the sample used. In addition, it seems to be sensitive to hydrophobic and electrostatic interactions between the end groups of the samples used. All the PNIPA samples used in the literatures[13–21] were synthesized by radical polymerization under different polymerization conditions from each other. The fraction f_r of racemo diads, specifying the stereochemical composition, of the samples so synthesized are considered to be almost independent of the solvent condition and the initiator used for the polymerization, so that the difference in the cloud point between the literature data may not be caused by the difference in f_r. The end groups of the samples synthesized by the use of different initiators are different from each other. The difference in the cloud point, however, exists not only between the samples having the different end groups but also between those having the same end group. Under these circumstances, the cause of the difference in the cloud point between the literature data is not clear.

The experimental procedures to determine the cloud point, such as the rate of increase in temperature and/or the manner of adopting a temperature as the cloud point, are somewhat different between the investigators,[13–21] so that the above-mentioned difference in the cloud point between the literature data is possible to be apparent and is not yet conclusive. It is therefore desirable to compare experimental data for the cloud point in aqueous PNIPA solutions determined following the same procedure in the same laboratory. In this study, we synthesize the PNIPA samples by radical polymerization in methanol, *tert*-butanol, benzene, and 1,4-dioxane by the use of azobis(isobutyronitrile) as an initiator, and then determine their cloud points in aqueous solutions, in order to examine whether or not the difference in the cloud point between the samples synthesized in different solvents really exists beyond experimental error.

If there is surely a difference in the cloud point between the samples so prepared, we have to go in search of its sources other than the above-mentioned differences in f_r and experimental procedure. Recent report by Gao and Frisken[24,25] tells us that PNIPA samples synthesized by radical polymerization in some conditions have random-branched

structure, suggesting that PNIPA samples synthesized by radical polymerization in general have branched structure and the number of branch points in the sample, depends on solvents used for polymerization. Since the number of the branch points does not seems so large that it can be detected by spectroscopic techniques, it is necessary for confirmation of the branched structure to examine dilute solution properties, *e.g.*, the mean-square radius of gyration $\langle S^2 \rangle$, second virial coefficient A_2, translational diffusion coefficient D, and intrinsic viscosity $[\eta]$ determined from static and dynamic scattering (LS) and viscosity measurements.

Further if the PNIPA samples synthesized by radical polymerization surely have the branched structure, it is desirable for us to prepare well-characterized *linear* PNIPA samples and to examine the cloud point of their aqueous solutions. Preparation of the linear PNIPA samples, for example, by living anionic polymerization requires some comments. It is known that living anionic polymerization of *N*-isopropylacrylamide (NIPA) is unfeasible because of acidity of its amide proton.[26,27] Recently, it has been shown that linear PNIPA may be synthesized by living anionic polymerization of protected NIPA whose amide proton is masked with a group properly chosen,[26–29] and that the living anionic polymerization of NIPA monomers masked with a methoxymethyl group by the use of diphenylmethylpotassium as an initiator,[27–29] leads to linear samples which have the same value of f_{r} as that of the samples synthesized by the radical polymerization.

1.2 Outline

The plan of this thesis is as follows.

In Chapter 2, the cloud point was determined for aqueous solutions of four kinds of poly(*N*-isopropylacrylamide) (PNIPA) samples synthesized by radical polymerization in methanol, *tert*-butanol, benzene, and 1,4-dioxane by the use of azobis(isobutyronitrile) (AIBN) as an initiator, in the range of the weight fraction w of the sample from 0.5 to 10%. It has then been found that the cloud points so determined for the samples synthesized in benzene and 1,4-dioxane are definitely lower than those for the samples synthesized in methanol and *tert*-butanol, although all the samples have almost the same stereochemical composition and the same end group. The observed deviation may be regarded as arising from the difference in the primary structure between the samples.

In Chapter 3, the mean-square radius of gyration $\langle S^2 \rangle$, second virial coefficient A_2, and intrinsic viscosity $[\eta]$ were determined in methanol at 25.0 °C for two kinds of PNIPA synthesized by radical polymerization in *tert*-butanol and benzene by the use of AIBN as an initiator. In all cases of the three quantities, it is found that the value is smaller for the PNIPA synthesized in benzene than for that synthesized in *tert*-butanol and the

difference between the two kinds of PNIPA increases with increasing the weight-average molecular weight M_w. The average chain dimension of the former PNIPA should then be smaller than that of the latter. Since the two kinds of PNIPA were shown to have the same stereochemical composition (and also the same chain end group), the difference in the average chain dimension may be regarded as arising from the difference in the primary structure, *i.e.*, the number of branch points. Considering the fact that the average dimension of a given polymer chain in general decreases with increasing the number of branch points, it may be concluded that the number is larger in the former PNIPA than in the latter. The behavior of the interpenetration function Ψ and the Flory–Fox factor Φ as functions of M_w is also examined, confirming the conclusion.

In Chapter 4, A_2 and $[\eta]$ were determined in methanol at 25.0 °C for PNIPA samples synthesized by living anionic polymerization in the range of M_w from 4.91×10^3 to 7.23×10^4, which are called L samples, and also for those by radical polymerization in *tert*-butanol and benzene by the use of AIBN as an initiator in the range of M_w from 1.23×10^4 to 7.83×10^4, which are called T and B samples, respectively. It is found for both A_2 and $[\eta]$ that their values for the three kinds of samples agree well with each other in the range of $M_w \lesssim 3 \times 10^4$ but deviate from each other as M_w is increased from 3×10^4, the value for the L sample being the largest and that for the B sample the smallest. The result is consistent with the fact that the average chain dimension is the largest for the L sample having no branch point and the smallest for the B sample having the largest number of branch points. From a simultaneous analysis of A_2 and $[\eta]$ for the L samples on the basis of the Kratky–Porod wormlike chain with excluded volume, the stiffness parameter λ^{-1} is estimated to be 18 Å, which is almost the same as those determined for typical flexible polymers. For the L samples, the cloud point was also determined in their aqueous solutions in the range of w of PNIPA from *ca.* 0.5 to *ca.* 10%. It is found that the cloud point in the range of $w \gtrsim 2\%$ decreases from *ca.* 32 °C to *ca.* 18 °C as M_w is decreased from 7.23×10^4 to 5.47×10^3. Such behavior may be regarded as arising from effects of hydrophobic chain end groups of the L samples.

In Chapter 5, transmittance of light passing through aqueous solutions of the L sample with $M_w = 7.23 \times 10^4$ was measured under a series of changes in temperature. It is then found that the transmittance is held at a constant value between 0 and 100% even at a temperature slightly higher than the cloud point, indicating that the macroscopic phase separation does not take place at the cloud point in the aqueous PNIPA solutions and therefore the cloud-point curve dose not correspond to the binodal. Static and dynamic light scattering measurements were also carried out for aqueous solutions of the L sample and the T sample with $M_w = 7.19 \times 10^4$ at temperatures considerably lower than the cloud point, the latter sample being considered to have random-branched structure. It

was found that both the PNIPA samples in aqueous solution form aggregates even at such temperatures, the number, size, and density profile of the aggregates depending on the kind of end group and also on the primary structure.

References

1. P. J. Flory, "Principles of Polymer Chemistry," Cornell Univ. Press, Ithaca, N.Y., 1953.
2. M. Kurata, "Thermodynamics of Polymer Solutions," Harwood Academic Publishers, Chur, 1982.
3. R. Koningsveld, W. H. Stockmayer, and E. Nies, "Polymer Phase Diagrams," Oxford University Press, New York, 2001.
4. P. J. Flory, *J. Chem. Phys.*, **10**, 51 (1942).
5. M. L. Huggins, *J. Phys. Chem.*, **46**, 151 (1942); *Ann. N. Y. Acad. Sci.*, **41**, 1 (1942); *J. Am. Chem. Soc.*, **64**, 1712 (1942).
6. H. L. Cox and L. H. Cretcher, *J. Am. Chem. Soc.*, **48**, 451 (1926).
7. G. N. Malcolm and J. S. Rowlinson, *Trans. Faraday Soc.*, **53**, 921 (1957).
8. S. Saeki, N. Kuwahara, M. Nakata, and M. Kaneko, *Polymer*, **17**, 685 (1976).
9. A. Matsuyama and F. Tanaka, *Phys. Rev. Lett.*, **65**, 341 (1990).
10. H. G. Schild, *Prog. Polym. Sci.*, **17**, 163 (1992).
11. A. Kikuchi and T. Okano, *Adv. Drug Deliv. Rev.*, **54**, 53 (2002).
12. E. S. Gil and S. M. Hudson, *Prog. Polym. Sci.*, **29**, 1173 (2004).
13. M. Heskins and J. E. Guillet, *J. Macromol. Sci. Chem.*, **A2**, 1441 (1968).
14. S. Fujishige, K. Kubota, and I. Ando, *J. Phys. Chem.*, **93**, 3311 (1989).
15. H. G. Schild and D. A. Tirrell, *J. Phys. Chem.*, **94**, 4352 (1990).
16. C. Boutris, E. G. Chatzi, and C. Kiparissides, *Polymer*, **38**, 2567 (1997).
17. Z. Tong, F. Zeng, X. Zheng, and T. Sato, *Macromolecules*, **32**, 4488 (1999).
18. F. Zeng, Ph. D. Thesis, South China University of Technology, 1997.
19. F. Afroze, E. Nies, and H. Berghmans, *J. Mol. Struct.*, **554**, 55 (2000).
20. R. G. de Azevedo, L. P. N. Rebelo, A. M. Ramos, J. Szydlowski, H. C. de Sousa, and J. Klein, *Fluid Phase Equilibria*, **185**, 189 (2001).
21. S. Furyk, Y. Zhang, D. Ortiz-Acosta, P. S. Cremer, and D. E. Bergbreiter, *J. Polym. Sci., Polym. Chem. Ed.*, **44**, 1492 (2006).
22. Y. Okada and F. Tanaka, *Macromolecules*, **38**, 4465 (2005).
23. B. Ray, Y. Okamoto, M. Kamigaito, M. Sawamoto, K. Seno, S. Kanaoka, and S.Aoshima, *Polym. J.*, **37**, 234 (2005).
24. J. Gao and B. J. Frisken, *Langmuir*, **19**, 5212 (2003).

25. J. Gao and B. J. Frisken, *Langmuir*, **19**, 5217 (2003).
26. T. Kitayama, W. Shibuya, and K. Katsukawa, *Polym. J.*, **34**, 405 (2002).
27. T. Ishizone and M. Ito, *J. Polym. Sci., Polym. Chem. Ed.*, **40**, 4328 (2002).
28. M. Ito and T. Ishizone, *Designed Monomers and Polymers*, **7**, 11 (2004).
29. M. Ito and T. Ishizone, *J. Polym. Sci., Polym. Chem. Ed.*, **44**, 4832 (2006).

2 Cloud Points in Aqueous Poly(*N*-isopropylacrylamide) Solutions

2.1 Introduction

As mentioned in Chapter 1, aqueous solutions of Poly(*N*-isopropylacrylamide) (PNIPA) have then been shown to have some salient and unusual features: the cloud point is rather insensitive to its concentration,[1–9] and at constant concentration it decreases with decreasing the molecular weight.[5,6] Unfortunately, however, the literature data[1–9] for the cloud point are rather dispersed and differ from each other, the difference being beyond experimental error. It is therefore necessary to ascertain the cause of the dispersion of the data prior to inquiring the reasons of such characteristic features.

Recently, Ray *et al.*[10] pointed out that the cloud point for the aqueous PNIPA solution appreciably depends on the stereochemical composition of the sample used. In addition, it seems to be sensitive to the hydrophobic and also electrostatic interactions between the end groups of the sample used, especially in aqueous solutions. All the PNIPA samples used in the previous studies[1–9] of the cloud point had been synthesized by aqueous redox polymerization by the use of a redox catalyst consisting of ammonium persulfate as an oxidative part and of sodium bisulfite,[1] tetramethylethylenediamine,[3] or sodium metabisulfite[8] as a reductive part, or by conventional radical polymerization in a mixture of benzene and acetone,[2] in benzene,[3,4] in *tert*-butanol,[5,6] in tetrahydrofuran,[7] or in methanol,[9] by the use of azobis(isobutyronitrile) (AIBN) as an initiator. The fraction f_r of racemo diads, specifying the stereochemical composition, of the samples so synthesized are considered to be almost independent of the solvent condition and the initiator used for the polymerization, so that the difference in the literature data for the cloud point may not be caused by the difference in f_r. The end groups of the samples synthesized by the use of the redox catalyst and that of AIBN are different from each other, the former end group being ionic. The difference in the cloud point, however, exists not only between the samples having the different end groups but also between those having the same end group. Under these circumstances, the cause of the difference in the cloud point between the literature data is not clear.

The experimental procedures to determine the cloud point, such as the rate of increase in temperature and/or the manner of adopting a temperature as the cloud point, are somewhat different between the investigators,[1–9] so that the above-mentioned difference in the cloud point between the literature data is not yet conclusive. It is therefore desirable to compare experimental data for the cloud point in aqueous PNIPA solutions determined following the same procedure in the same laboratory.

In this chapter, we synthesize the PNIPA samples by radical polymerization in methanol, *tert*-butanol, benzene, and 1,4-dioxane by the use of AIBN as an initiator, and then determine their cloud points in aqueous solutions, in order to examine whether or not the difference in the cloud point between the samples synthesized in different solvents really exists beyond experimental error.

2.2 Experimental

2.2.1 Materials

Four kinds of (original) PNIPA samples were synthesized by radical polymerization in methanol, *tert*-butanol, benzene, and 1,4-dioxane by the use of AIBN as an initiator. In each case, *N*-isopropylacrylamide (ca. 20 g), which had been recrystallized three times from a 8/2 mixture of *n*-hexane and benzene and then dried in a vacuum for 12 h, were polymerized in the solvent (ca. 150 mL) with AIBN (ca. 1 mol%) under dry nitrogen at 60 °C for 30 h, the conversion being almost 100%. The original samples so synthesized were purified by reprecipitation from acetone solutions into *n*-hexane and then separated into fractions of narrow molecular weight distribution by fractional precipitation using acetone as a solvent and *n*-hexane as a precipitant, or by a column elution method with a mixture 6/4 of *n*-hexane and acetone as an eluent. The test samples so prepared were dissolved in 1,4-dioxane, then filtered through a Teflon membrane of pore size 1.0 μm, and finally freeze-dried from their 1,4-dioxane solutions. They were dried in a vacuum at ca. 80 °C for ca. 12 h just prior to use.

The solvent methanol used for light scattering (LS) measurements was purified by distillation after refluxing over calcium hydride for ca. 6 h. The solvent tetrahydrofuran used for analytical gel permeation chromatography (GPC) was of reagent grade with no stabilizer. The solvent deuterated dimethyl sulfoxide used for ^{1}H NMR spectroscopy was of reagent grade. The solvent water used for the determinations of the cloud point was highly purified through a Milli-Q Labo water purification system of Millipore Co., its resistivity being 18.2 MΩ·cm.

2.2.2 Light Scattering

LS measurements were carried out to determine the weight-average molecular weight M_w for all the samples, in methanol at 25.0 °C. A Fica 50 light-scattering photometer was used with vertically polarized incident light of wavelength $\lambda_0 = 436$ nm. For a calibration of the apparatus, the intensity of light scattered from pure benzene was measured at 25.0 °C at a scattering angle of 90°, where the Rayleigh ratio $R_{Uu}(90°)$ of pure benzene was taken as 46.5×10^{-6} cm^{-1}.[11] The depolarization ratio ρ_u of pure benzene at 25.0 °C was determined to be 0.41±0.01. Scattered intensities were measured at seven or eight different concentrations and at scattering angles θ ranging from 30.0 to 142.5°, and then converted to the excess unpolarized (Uv) components ΔR_{Uv} of the reduced scattered intensities by the use of the scattered intensities from the solvent methanol. The data obtained were treated by using the Berry square-root plot.[12] For all the samples, corrections for the optical anisotropy were unnecessary since the degree of depolarization was negligibly small.

The most concentrated solution of each sample was prepared gravimetrically and made homogeneous by continuous stirring at room temperature for 1 day. It was optically purified by filtration through a Teflon membrane of pore size 0.10 μm. The solutions of lower concentrations were obtained by successive dilution. The weight fractions of the test solutions were converted to the polymer mass concentrations c by the use of the densities of the respective solutions calculated with the partial specific volumes v_2 of the samples and with the density ρ_0 of the solvent methanol. The values of v_2 in methanol at 25.0 °C were determined to be 0.903 cm^3/g irrespective of the kind of test sample, by the use of a pycnometer of the Lipkin–Davison type having the volume 10 cm^3. For the value of ρ_0 of methanol at 25.0 °C, we used the literature value 0.7866 g/cm^3.[13]

The refractive index increment $\partial n/\partial c$ was measured at wavelength 436 nm by the use of a Shimadzu differential refractometer DR-1. For the refractive index of methanol at 25.0 °C at wavelength of 436 nm, we used the literature value 1.3337.[13]

2.2.3 Analytical Gel Permeation Chromatography

The ratio of M_w to the number-average molecular weight M_n for all the PNIPA samples were evaluated by analytical GPC with five serially connected columns (Tosoh GMH_{xl} + $G5000H_{xl}$ + $G5000H_{xl}$ + $G4000H_{xl}$ + $G4000H_{xl}$) connected to a HPLC pump (Jasco PU-980) and a UV detector (Tosoh UV-8000) using tetrahydrofuran as an eluent and 12 standard polystyrene (PS) samples (Tosoh, $M_w = 2.8 \times 10^3 - 8.4 \times 10^6$, $M_w/M_n = 1.02 - 1.17$) as reference standards.

2.2.4 ^{1}H NMR

^{1}H NMR spectra for all the PNIPA samples in deuterated dimethyl sulfoxide at 170 °C were recorded on a JEOL JNM-A500 spectrometer at 500.2 MHz by the use of an rf pulse angle of 45° with a pulse repetition time of 8 s, where tetramethylsilane was added to each test solution as an internal standard.

2.2.5 Transmittance of Light

The intensity of light passing through the aqueous solution of each PNIPA sample at a given weight fraction w of the sample was monitored in order to determine its cloud point. All the measurements were carried out by the use of a self-made apparatus with incident light of wavelength 650 nm from a laser diode module, as described below. A cylindrical cell of outer diameter 10 mm containing a given test solution was immersed in a water bath, the test solution in the cell being stirred continuously. The temperature of the water bath was controlled to increase at the rate of ca. 1.5 °C/h. During continuous increase in temperature from 28 to 34 °C, the intensity of light passing through the cell was monitored by a photodiode. The output of the photodiode along with the solution temperature measured simultaneously by the use of a platinum resistance thermometer combined with a programmable digital multimeter (Yokokawa 7555) was recorded on a personal computer at intervals of 10 s.

The measurements were carried out at 8 different concentrations in the range of $0.5 \lesssim w \lesssim 10\%$ for each sample. The most concentrated solution of each sample was prepared gravimetrically and made homogeneous by continuous stirring for 1 day at ca. 20 °C. The solutions of lower concentrations were obtained by successive dilution.

2.3 Results and Discussion

2.3.1 Characterization

The values of M_w determined by LS measurements in methanol at 25.0 °C and M_w/M_n by analytical GPC using the standard PS samples as reference standards for all the PNIPA samples used in this work are given in the second and third columns of Table 2.1, respectively, the first letters M, T, B, and D in the sample codes in the first column indicating the solvents used for radical polymerization, *i.e.*, methanol, *tert*-butanol, benzene, and 1,4-dioxane, respectively. We note that the values of $\partial n/\partial c$ in methanol at 25.0 °C, which are necessary for the evaluation of M_w from the LS data, were determined to be 0.184_9, 0.185_7, 0.184_4, 0.183_7, 0.182_2, 0.185_7, 0.184_5, and 0.185_6 cm^3/g for the samples M6, M9, T5, T13, B5, B14, D5, and D13, respectively.

Table 2.1. Values of M_w, M_w/M_n, and f_r for Poly(*N*-isopropylacrylamide)

sample	M_w	M_w/M_n [a]	f_r
	synthesized in methanol		
M6	6.45×10^4	1.19	0.51
M9	9.44×10^4	1.17	0.52
	synthesized in *tert*-butanol		
T5	5.17×10^4	1.14	0.52
T13	1.31×10^5	1.23	0.52
	synthesized in benzene		
B5	4.65×10^4	1.17	0.52
B14	1.44×10^5	1.14	0.51
	synthesized in 1,4-dioxane		
D5	5.18×10^4	1.28	0.52
D13	1.27×10^5	1.18	0.52

[a]The values of M_w/M_n were determined by analytical GPC using standard PS samples as reference standards.

Figure 2.1 shows the ^{1}H NMR spectra for all the 8 samples in the range of the chemical shift δ from 0.7 to 2.4 ppm, where the signals from the methylene (a) and methine (b) protons in the main chain and the methyl protons (c) in the side group are included. According to Isobe et al.,[14] the signals in the ranges of $1.0 \lesssim \delta \lesssim 1.2$, $1.2 \lesssim \delta \lesssim 1.8$, and $1.9 \lesssim \delta \lesssim 2.2$ (in units of ppm) may be assigned to the c, a, and b protons, respectively. The three signals from the a protons in the range of $1.2 \lesssim \delta \lesssim 1.8$ may be further assigned to those in the meso (m), racemo (r), and m diads, respectively, from the right to the left, as explicitly shown in the spectra for the samples M6 and M9. In the last column of Table 2.1 are given the values of f_{r} determined from the intensities of those three signals from the a protons. All the PNIPA samples have almost the same value (0.51—0.52) of f_{r}, as has been expected.

2.3.2 Cloud Point

The (relative) transmittance of light through the aqueous solutions of the PNIPA samples M6, M9, T5, T13, B5, B14, D5, and D13, at the weight fraction w = 5.04, 4.93, 5.04, 5.07, 4.96, 5.09, 4.94, and 5.02%, respectively, in heating process are plotted against temperature in Figure 2.2. Here, the (relative) transmittance is defined as the ratio of the intensity of light passing through a test solution at a temperature to that at a lower temperature at which the test solution may be regarded as transparent. The light curves represent the values of M6, T5, B5, and D5 and the heavy ones represent those of M9, T13, B14, and D13, as indicated.

The transmittance as a function of temperature is expected to decrease steeply with increasing temperature at a threshold temperature, *i.e.*, the cloud point where the macroscopic phase separation takes place if the solution under consideration really shows the LCST miscibility behavior. From Figure 2.2, however, it is seen that the shape of the transmittance curve depends on the kind of sample and also on M_{w} and its decrease is rather gentle except for the samples M9 and T13. Such results arouse us some doubt if the decrease in the transmittance really corresponds to the macroscopic phase separation in all cases. We note that the shape of transmittance curve is independent of the rate of increase in temperature if it is slower than 1.5 °C/h.

The cloud point is experimentally determined to be the temperature at which a given test solution just begins to be turbid, *i.e.*, its transmittance just starts to decrease from 100%, in the heating process. Because of the situation mentioned above, it is difficult to determine such a temperature unambiguously, so that we adopt the temperature at which the transmittance becomes 90% as the cloud point, for convenience. The symbols ○, ◔, ▽, △, ▣, ◫, ◇, and ◈ in Figure 2.2 represent the cloud points so determined for the samples M6, M9, T5, T13, B5, B14, D5, and D13, respectively.

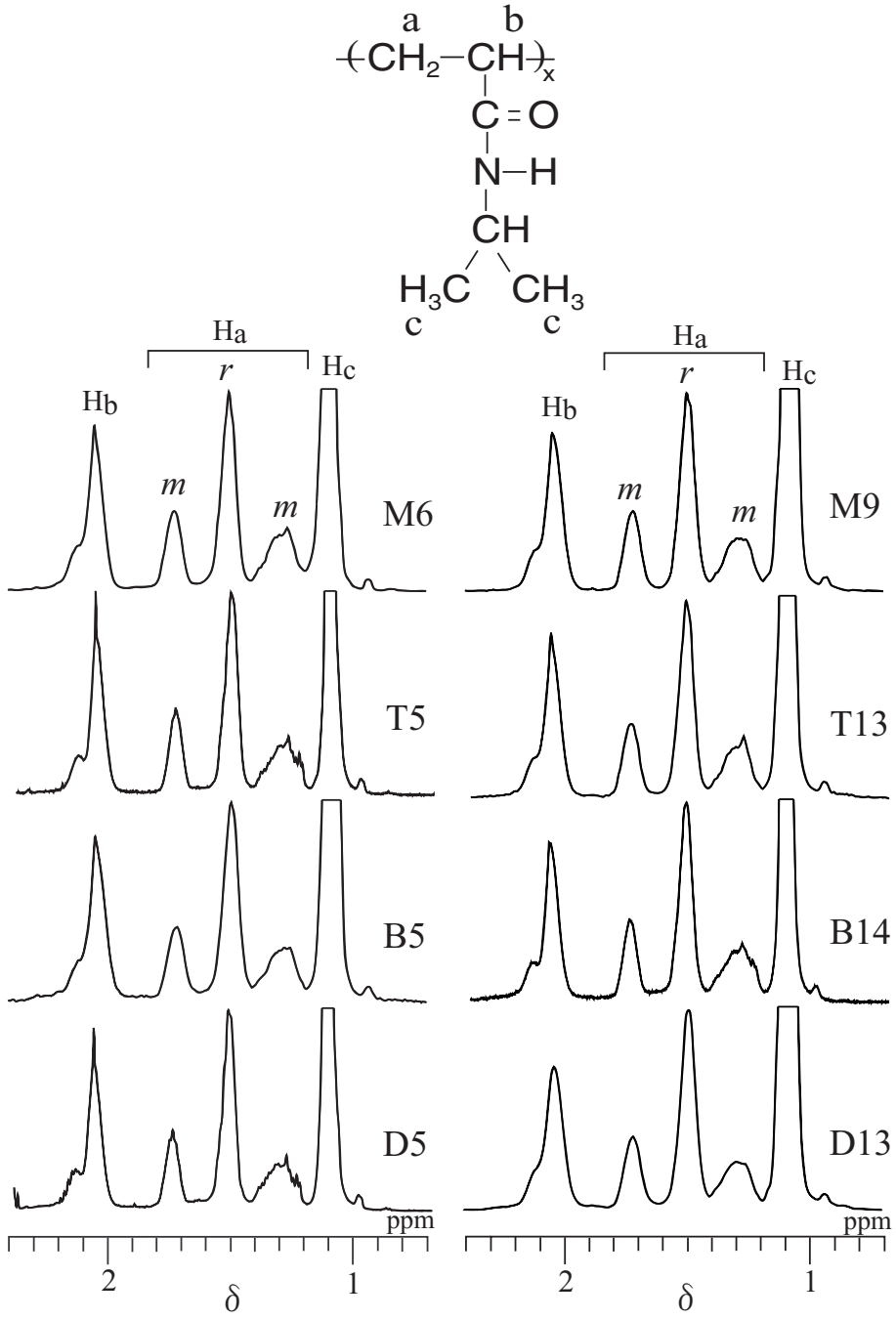

Figure 2.1. ^{1}H NMR spectra of the methylene (a) and methine (b) protons in the main chain and the methyl protons (c) in the side group for all the PNIPA samples.

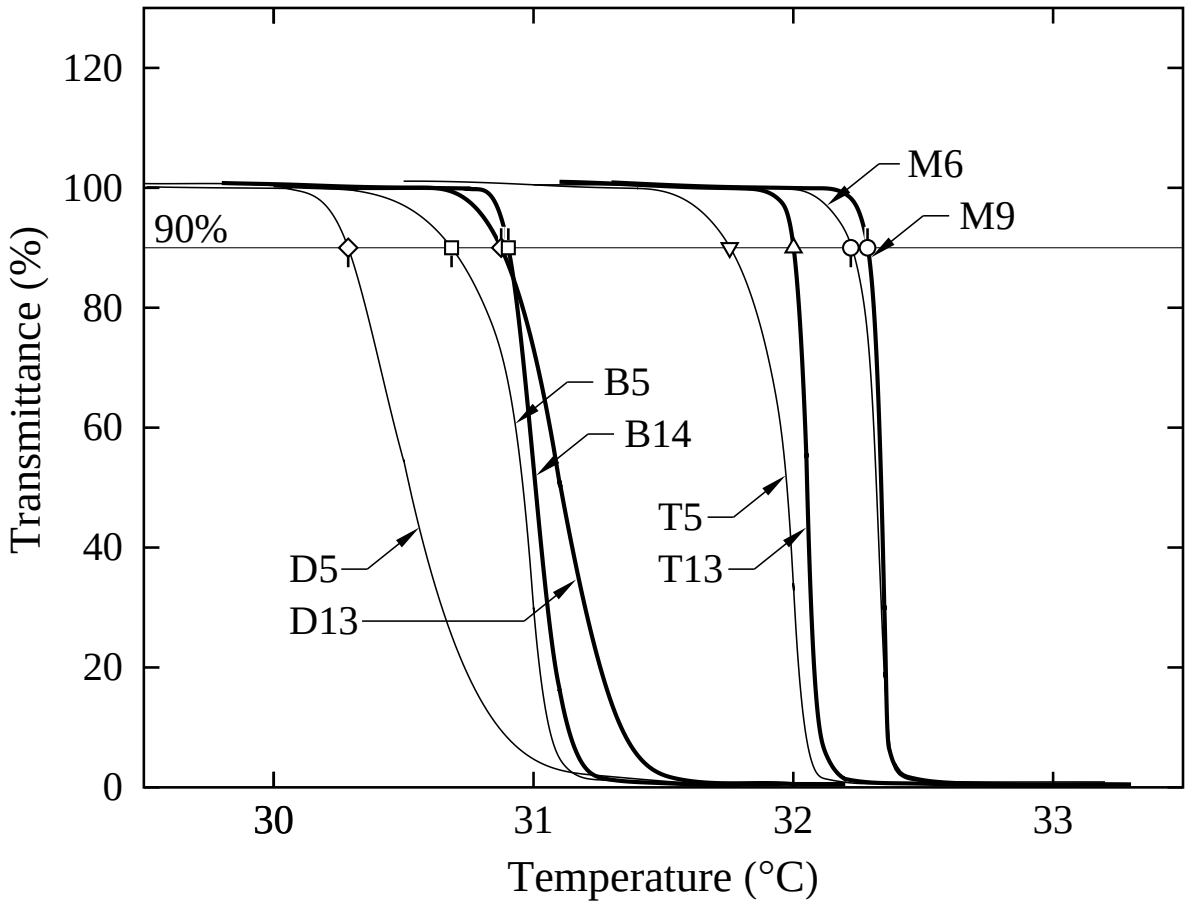

Figure 2.2. Temperature dependence of the transmittance of light passing through aqueous solutions of the PNIPA samples M6, M9, T5, T13, B5, B14, D5, and D13, at $w = 5.04$, 4.93, 5.04, 5.07, 4.96, 5.09, 4.94, and 5.02%, respectively, the symbols ⚲, ⚲, ▽, △, ⚲, ⚲, ⚲, and ⚲ representing the respective cloud points (see the text).

Table 2.2. Cloud Points in Aqueous Poly(*N*-isopropylacrylamide) Solutions

M6		M9		T5		T13		B5		B14		D5		D13	
w (%)	Temp. (°C)	w (%)	Temp. (°C)	w (%)	Temp. (°C)	w (%)	Temp. (°C)	w (%)	Temp. (°C)	w (%)	Temp. (°C)	w (%)	Temp. (°C)	w (%)	Temp. (°C)
0.49	32.9_1	0.51	32.8_0	0.50	32.7_1	0.52	32.5_4	0.50	31.6_2	0.47	31.5_2	0.49	31.7_4	0.58	31.5_7
0.98	32.7_4	1.02	32.6_9	0.99	32.3_8	1.02	32.4_0	1.01	31.3_2	0.91	31.3_8	0.99	31.3_0	1.14	31.3_6
1.91	32.5_7	2.01	32.5_2	2.00	32.0_9	2.01	32.2_5	2.02	31.0_9	1.93	31.1_9	1.99	30.8_8	2.33	31.1_6
3.00	32.4_4	2.98	32.4_3	3.06	31.9_6	3.04	32.1_7	2.93	31.0_1	3.05	31.0_8	2.97	30.6_8	3.04	31.0_7
3.93	32.3_4	4.03	32.3_6	4.01	31.8_5	4.05	32.1_0	3.98	30.8_1	4.05	30.9_9	3.97	30.4_0	4.45	30.9_1
5.04	32.2_3	4.93	32.2_9	5.04	31.7_4	5.07	32.0_0	4.96	30.6_9	5.09	30.9_1	4.94	30.2_8	5.02	30.8_9
7.02	32.0_9	7.39	32.1_7	7.50	31.5_5	7.43	31.8_7	7.52	30.4_8	7.59	30.7_8	7.47	30.2_6	7.03	30.7_3
9.03	31.9_5	8.57	32.1_0	9.46	31.4_4	8.47	31.8_3	9.71	30.3_5	9.51	30.6_7	9.32	30.0_9	9.17	30.5_9

Although there still remain some issues concerning the experimental determination of the cloud point, it is clearly seen that the cloud points for the samples M6, M9, T5, and T13 are definitely higher than those for the samples B5, B14, D5, and D13 in spite of the fact that all the samples have the same f_r and the same end group and that all the test solutions in Figure 2.2 are at almost the same concentration. Although the cloud point in general depends on M_w of the sample used, the above-mentioned difference in the cloud point is larger than that between the two samples of each kind (M, T, B, and D) having different M_w.

In Table 2.2 are given the cloud points so determined for aqueous solutions of all the eight PNIPA samples at various w. Figure 2.3 shows plots of the cloud point against w for the aqueous PNIPA solutions. The unfilled symbols represent the present data for the PNIPA samples M6 (○), M9 (◌̇), T5 (▽), T13 (△), B5 (□̣), B14 (□̇), D5 (◇̣), and D13 (◇̇), each solid curve connecting smoothly the data points for the same sample. The filled symbols represent the literature data for PNIPA samples synthesized by radical polymerization by the use of AIBN as an initiator in various solvent conditions, *i.e.*, the data by Fujishige *et al.*[2] for the sample with the molecular weight $M = 8.40 \times 10^6$ synthesized in a benzene/acetone mixture at 60 °C (◆), which have been evaluated from their transmittance data in the manner mentioned above, those by Boutris *et al.*[4] for the sample with $M_n = 9.0 \times 10^3$ synthesized in benzene at 50 °C (■), those by Tong *et al.*[5,6] for the samples with $M_w = 4.94 \times 10^4$ (▼) and 1.01×10^5 (▲) synthesized in *tert*-butanol at 55 °C, those by Afroze *et al.*[7] for the sample with $M_w = 1.0 \times 10^4$ synthesized in tetrahydrofuran at 50 °C (●), and those by Furyk *et al.*[9] for the samples with $M_w = 5.58 \times 10^4$ (●̣) and 4.75×10^5 (●̇) synthesized in methanol. The symbol ◑ represents the literature data for the PNIPA samples with $M_w = 6.15 \times 10^5$ synthesized by aqueous redox polymerization at 25 °C by de Azevedo *et al.*[8] Each dashed curve connects smoothly the literature data points for the same sample.

Considering the ambiguity in the determination of the cloud point, the present data for T5 and T13 are consistent with the corresponding literature ones by Tong *et al.*[5,6] but the present data for M6 and M9 and those for B5 and B14 are appreciably different from the corresponding literature ones by Furyk *et al.*[9] and Boutris *et al.*,[4] respectively. The difference between the present data for M6 and M9 and those by Furyk *et al.* may be regarded as arising from the fact that the instrument used by them to determine the cloud point is a newly-designed one,[15] which measures intensity of light scattered from solutions contained in rectangular capillary tubes under a temperature gradient, and completely different from those used by the others and us. The cause of the difference between the present data for M5 and M14 and those by Boutris *et al.* is not clear. As for the literature data by Fujishige *et al.*,[2] Afroze *et al.*,[7] and de Azevedo *et al.*,[8] we have no corresponding

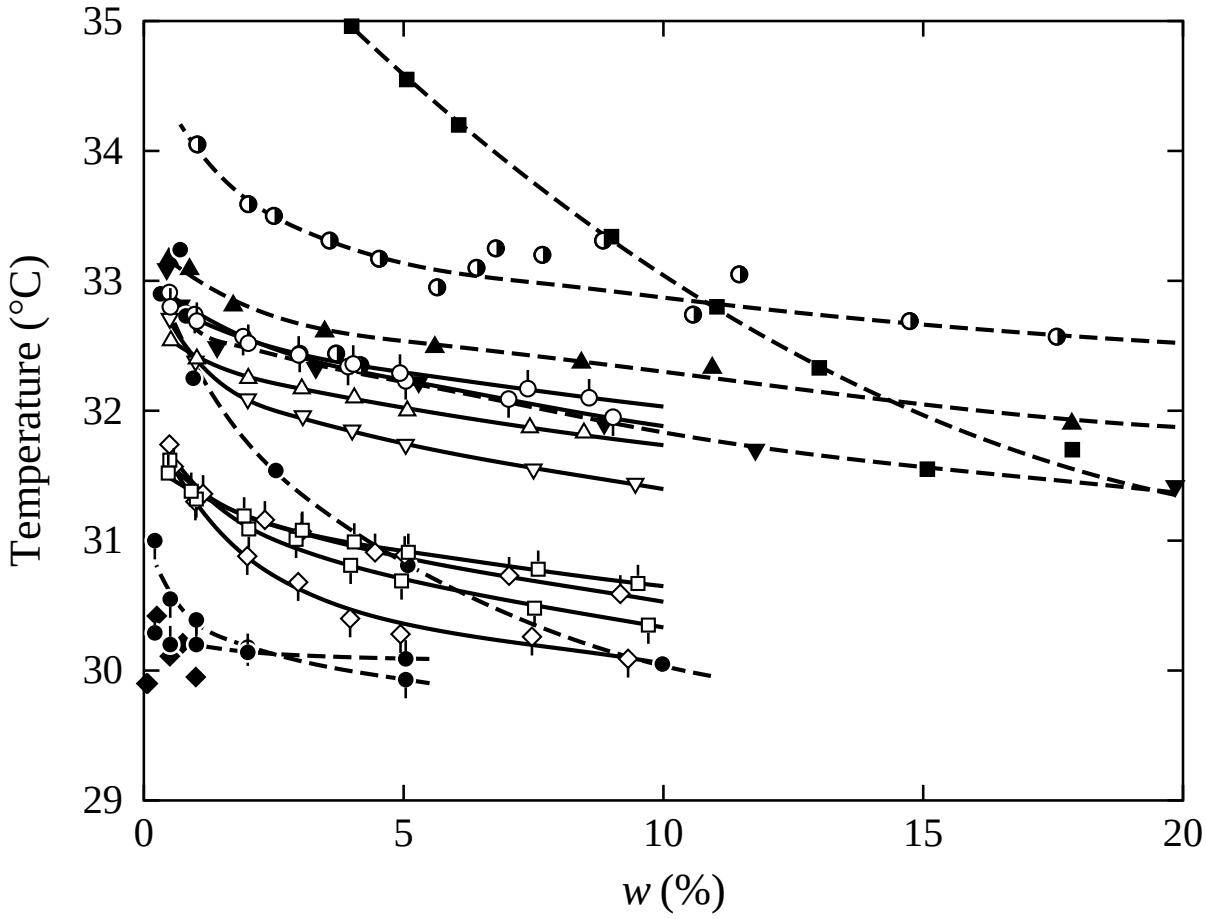

Figure 2.3. Cloud-point curves for aqueous solutions of PNIPA. The unfilled symbols represent the present data for the samples M6 (○), M9 (○), T5 (▽), T13 (△), B5 (□), B14 (□), D5 (◇), and D13 (◇) and the filled and half-filled symbols the literature data by Fujishige *et al.*[2] for the sample with $M = 8.40 \times 10^6$ (◆), by Boutris *et al.*[4] for the sample with $M_n = 9.0 \times 10^3$ (■), by Tong *et al.*[5,6] for the samples with $M_w = 4.94 \times 10^4$ (▼) and 1.01×10^5 (▲), by Afroze *et al.*[7] for the sample with $M_w = 1.0 \times 10^4$ (●), by de Azevedo *et al.*[8] for the sample with $M_w = 6.15 \times 10^5$ (◑), and by Furyk *et al.*[9] for the samples with $M_w = 5.58 \times 10^4$ (●) and 4.75×10^5 (●). The solid and dashed curves connect smoothly the present and literature data points, respectively.

sample to be compared because the polymerization solvents and/or the initiators used by them are different from ours.

As first pointed out by Tong *et al.*,[5] the cloud point is lower for the sample with smaller M_w in the range of $1 \lesssim w \lesssim 10\%$ for each pair of samples synthesized in the same solvent, although it is not conclusive because of the above-mentioned ambiguity in the determination of the cloud point. If such dependence of the cloud point on M_w is true, it is opposite to that of the literature data for the aqueous POE solutions,[16,17] the latter dependency being easy to understand on the basis of the conventional polymer solution thermodynamics.[18] Considering the recent results for aqueous solutions of block copolymers having hydrophobic end parts,[9,19–22] it may be regarded as arising from interactions between hydrophobic chain end groups.

It is more important to note that the cloud points for the samples B5, B14, D5, and D13 are definitely lower than those for the samples M6, M9, T5, and T13. Recently, Gao and Frisken[23,24] have carried out aqueous redox polymerization of PNIPA at various temperatures ranging from 40 to 90 °C and then found that gel particles of PNIPA have been formed by interchain self-cross-linking (or branching) through the chain transfer reaction during and after the polymerization. Their result implies that the quality (good or poor) of the solvent used for radical polymerization should probably affect the primary structure of resultant PNIPA, *i.e.*, the poorer the solvent is, the higher degree of branching the resultant PNIPA should have. The samples B5 and B14 therefore seem to have higher degree of branching than the samples M6, M9, T5, and T13, since benzene is a poor solvent for PNIPA, while methanol and *tert*-butanol are the good. The decrease in the cloud point for the samples B5 and B14 might be caused by increase in the number of the hydrophobic end groups associated with the increase in the degree of branching. As for the samples D5 and D13, we have no plausible reason for their lower cloud point.

2.4 Concluding Remarks

The cloud point was determined for aqueous solutions of the four kinds of PNIPA samples synthesized by radical polymerization in methanol, *tert*-butanol, benzene, and 1,4-dioxane by the use of AIBN as an initiator. It has then been found that the cloud points for the samples synthesized in benzene and 1,4-dioxane are definitely lower than those for the samples synthesized in methanol and *tert*-butanol, although all the samples have almost the same stereochemical composition and the same end group. On the basis of the recent experimental results obtained by Gao and Frisken,[23,24] we have conjectured that the PNIPA samples synthesized in the different kinds of solvents should probably have different primary structures, *i.e.*, the degree of branching, which might mainly be

caused by the difference in the quality (good or poor) of the solvent used for radical polymerization. In order to confirm such a conjecture, it is desirable to examine the primary structure of PNIPA synthesized by radical polymerization in some solvents having different quality on the basis of, for example, its dilute solution properties.

References

1. M. Heskins and J. E. Guillet, *J. Macromol. Sci. Chem.*, **A2**, 1441 (1968).
2. S. Fujishige, K. Kubota, and I. Ando, *J. Phys. Chem.*, **93**, 3311 (1989).
3. H. G. Schild and D. A. Tirrell, *J. Phys. Chem.*, **94**, 4352 (1990).
4. C. Boutris, E. G. Chatzi, and C. Kiparissides, *Polymer*, **38**, 2567 (1997).
5. Z. Tong, F. Zeng, X. Zheng, and T. Sato, *Macromolecules*, **32**, 4488 (1999).
6. F. Zeng, Ph. D. Thesis, South China University of Technology, 1997.
7. F. Afroze, E. Nies, and H. Berghmans, *J. Mol. Struct.*, **554**, 55 (2000).
8. R. G. de Azevedo, L. P. N. Rebelo, A. M. Ramos, J. Szydlowski, H. C. de Sousa, and J. Klein, *Fluid Phase Equilibria*, **185**, 189 (2001).
9. S. Furyk, Y. Zhang, D. Ortiz-Acosta, P. S. Cremer, and D. E. Bergbreiter, *J. Polym. Sci., Polym. Chem. Ed.*, **44**, 1492 (2006).
10. B. Ray, Y. Okamoto, M. Kamigaito, M. Sawamoto, K. Seno, S. Kanaoka, and S.Aoshima, *Polym. J.*, **37**, 234 (2005).
11. Gj. Deželić and J. Vavra, *Croat. Chem. Acta*, **38**, 35 (1966).
12. G. C. Berry, *J. Chem. Phys.*, **44**, 4550 (1966).
13. B. L. Johnson and J. Smith, In *Light Scattering from Polymer Solutions*; M. B. Huglin, Ed.; Academic Press: London, 1972; Chapter 2.
14. Y. Isobe, D. Fujioka, S. Habaue, and Y. Okamoto, *J. Am. Chem. Soc.*, **123**, 7180 (2001) and its supporting information.
15. H. Mao, C. Li, Y. Zhang, D. E. Bergbreiter, and P. S. Cremer, *J. Am. Chem. Soc.*, **125**, 2850 (2003).
16. G. N. Malcolm and J. S. Rowlinson, *Trans. Faraday Soc.*, **53**, 921 (1957).
17. S. Saeki, N. Kuwahara, M. Nakata, and M. Kaneko, *Polymer*, **17**, 685 (1976).
18. P. J. Flory, "Principles of Polymer Chemistry," Cornell Univ. Press, Ithaca, N.Y., 1953.
19. J. E. Chung, M. Yokoyama, K. Suzuki, T. Aoyagi, Y. Sakurai, and T. Okano, *Colloids Surf. B*, **9**, 37 (1997).
20. J. E. Chung, M. Yokoyama, T. Aoyagi, Y. Sakurai, and T. Okano, *J. Controlled Release*, **53**, 119 (1998).

21. P. Kujawa, F. Segui, S. Shaban, C. Diab, Y. Okada, F. Tanaka, and F. M. Winnik, *Macromolecules*, **39**, 341 (2006).
22. Q. Duan, A. Narumi, Y. Miura, X. Shen, S. Sato, T. Satoh, and T. Kakuchi, *Polym. J.*, **38**, 306 (2006).
23. J. Gao and B. J. Frisken, *Langmuir*, **19**, 5212 (2003).
24. J. Gao and B. J. Frisken, *Langmuir*, **19**, 5217 (2003).

3 Primary Structure of Poly(*N*-isopropylacrylamide) Synthesized by Radical Polymerization. Effects of Polymerization Solvents

3.1 Introduction

In Chapter 2, we have reported results for the cloud point in aqueous solutions of four kinds of poly(*N*-isopropylacrylamide) (PNIPA) samples synthesized by radical polymerization in *tert*-butanol, methanol, benzene, and 1,4-dioxane by the use of azobis(isobutyronitrile) (AIBN) as an initiator.[1] It has been shown that the cloud point is definitely lower for the samples synthesized in benzene and 1,4-dioxane than for those synthesized in *tert*-butanol and methanol, although all the samples have almost the same stereochemical composition and the same end group. It has then been conjectured that the difference in the cloud point may be regarded as arising from the difference in the primary structure, *i.e.*, the number of branch points, between the samples synthesized in the solvents of different quality (good or poor). In this chapter, we actually perform a detailed examination of the primary structure of the PNIPA samples synthesized in *tert*-butanol (good solvent) and benzene (poor or nonsolvent) in order to confirm the conjecture.

Previously, we have not been able to verify the existence of branch points in the PNIPA samples by means of ^{1}H NMR[1] (Chapter 2). It may be considered that the number of branch points, which form through side-chain reactions such as the chain transfer during the radical polymerization, is not large enough to be detected by ^{1}H or ^{13}C NMR or by other spectroscopic methods, since the intensity of such a spectroscopic signal is in principle proportional to the number of atoms which belong to the branch points. On the other hand, the average dimension of a polymer chain represented by its mean-square radius of gyration $\langle S^2 \rangle$ and/or the intrinsic viscosity $[\eta]$ is considered to be sensitive to its primary structure and is expected to be useful to detect branch points in it even if they are only a few. In this chapter, therefore, we determine $\langle S^2 \rangle$ and the second virial coefficient A_2 by light scattering (LS) measurements and $[\eta]$ by viscosity measurements and then examine the difference in the average chain dimension between the PNIPA

samples synthesized in *tert*-butanol and benzene.

3.2 Experimental

3.2.1 Materials

Two kinds of (original) PNIPA samples were synthesized by radical polymerization in *tert*-butanol and benzene by the use of AIBN as an initiator. In each solvent, *N*-isopropylacrylamide (*ca.* 20 g), which had been recrystallized three times from a 8/2 mixture of *n*-hexane and benzene and then dried in a vacuum for 12 h, were polymerized in the solvent (*ca.* 150 mL) with AIBN (*ca.* 1 mol%) under dry nitrogen at 60 °C for 30 h, the conversion being almost 100%. The original samples so synthesized were purified by reprecipitation from acetone solutions into *n*-hexane and then separated into fractions of narrow molecular weight distribution by fractional precipitation using acetone as a solvent and *n*-hexane as a precipitant, or by a column elution method with a mixture 6/4 of *n*-hexane and acetone as an eluent. The test samples so prepared were dissolved in 1,4-dioxane, then filtered through a Teflon membrane of pore size 1.0 μm, and finally freeze-dried from their 1,4-dioxane solutions. They were dried in a vacuum at *ca.* 80 °C for *ca.* 12 h just prior to use.

In the first and fourth columns of Table 3.1 are given the codes of all the 17 samples used in this work, the first letters T and B in the codes indicating the solvents used for radical polymerization, *i.e.*, *tert*-butanol and benzene, respectively. We note that the samples T5, T13, B5, and B14 are the same as those used in the previous study[1] (Chapter 2). In the second and fifth columns of the table are given the values of the ratio of the weight-average molecular weight M_{w} to the number-average molecular weight M_{n}, which were determined from analytical gel permeation chromatography (GPC) in the same manner as Chapter 2 using tetrahydrofuran as an eluent and 12 standard polystyrene (PS) samples (Tosoh, $M_{\mathrm{w}} = 2.8 \times 10^3$—$8.4 \times 10^6$, $M_{\mathrm{w}}/M_{\mathrm{n}} = 1.02$—$1.17$) as reference standards. In the table are also given the values of the fraction f_{r} of racemo diads for the samples T5, T13, T220, B5, B14, and B270 in the third and sixth columns, which were determined from ^{1}H NMR spectra in the same manner as Chapter 2 on the basis of the assignments of the ^{1}H signals proposed by Isobe *et al.*[2] Each of the two series of samples Tx and Bx came from one original sample, so that all the samples listed in the Table 3.1 should have almost the same stereochemical composition.

The solvent methanol used for LS and viscosity measurements was purified by distillation after refluxing over calcium hydride for *ca.* 6 h. The solvents tetrahydrofuran used for analytical GPC and deuterated dimethyl sulfoxide used for NMR spectroscopy were of reagent grade.

Table 3.1. Poly(*N*-isopropylacrylamide) samples synthesized in *tert*-butanol and benzene

in *tert*-butanol			in benzene		
sample	M_w/M_n	f_r	sample	M_w/M_n	f_r
T5	1.14	0.52	B5	1.17	0.52
T7	1.11		B11	1.22	
T13	1.23	0.52	B14	1.14	0.51
T23	1.18		B20	1.18	
T38	1.12		B62	1.22	
T54	1.16		B130	1.21	
T96	1.19		B170	1.24	
T120	1.23		B270	1.26	0.52
T220	1.20	0.52			

3.2.2 Light Scattering

LS measurements were carried out to determine M_w and A_2 for all the 17 samples and $\langle S^2 \rangle$ for 13 samples with $M_w \gtrsim 1.3 \times 10^5$, in methanol at 25.0 °C. A Fica 50 light-scattering photometer was used for all the measurements with vertically polarized incident light of wavelength $\lambda_0 = 436$ nm. For a calibration of the apparatus, the intensity of light scattered from pure benzene was measured at 25.0 °C at a scattering angle of 90°, where the Rayleigh ratio $R_{Uu}(90°)$ of pure benzene was taken as 46.5×10^{-6} cm^{-1}.[3] The depolarization ratio ρ_u of pure benzene at 25.0 °C was determined to be 0.41 ± 0.01. Scattered intensity was measured at seven or eight different concentrations and at scattering angles θ ranging from 15.0 to 142.5°, and then converted to the excess unpolarized (Uv) components ΔR_{Uv} of the reduced scattered intensity by the use of the scattered intensity from the solvent methanol. The data obtained were treated by using the Berry square-root plot.[4] For all the samples, corrections for the optical anisotropy were unnecessary since the degree of depolarization was negligibly small.

The most concentrated solution of each sample was prepared gravimetrically and made homogeneous by continuous stirring at room temperature for 1-3 days. It was optically purified by filtration through a Teflon membrane of pore size 1.0, 0.45, or 0.10 μm. The solutions of lower concentrations were obtained by successive dilution. The weight concentrations of the test solutions were converted to the polymer mass concentrations c by the use of the densities of the respective solutions calculated with the partial specific volumes v_2 of the samples and with the density ρ_0 of the solvent methanol. The values of v_2 in methanol at 25.0 °C were determined to be 0.903 cm^3/g for all the samples independently of the kinds of solvents used for radical polymerization and M_w, by the use of a pycnometer of the Lipkin–Davison type having a volume of 10 cm^3. For the value of ρ_0 of methanol at 25.0 °C, we used the literature value 0.7866 g/cm^3.[5]

The refractive index increment $\partial n/\partial c$ was measured at the wavelength of 436 nm by the use of a Shimadzu differential refractometer DR-1. The values of $\partial n/\partial c$ in methanol at 25.0 °C were determined to be 0.184_4, 0.183_0, and 0.183_7 cm^3/g for the samples T5, T7, and T13, respectively, 0.185_4 cm^3/g for the samples T23—T220 independently of M_w, 0.182_2 and 0.183_8 cm^3/g for the samples B5 and B11, respectively, and 0.185_7 cm^3/g for the samples B14—B270 independently of M_w. For the refractive index n_0 of methanol at 25.0 °C at the wavelength of 436 nm, we used the literature value 1.3337.[5]

3.2.3 Viscosity

Viscosity measurements were carried out for all the 17 samples in methanol at 25.0 °C by the use of a conventional capillary viscometer of the Ubbelohde type. The flow time was

measured to a precision of 0.1 s, keeping the difference between those of the solvent and solution larger than 20 s. The test solutions were maintained at a constant temperature within ±0.005 °C during the measurements.

The most concentrated solution of each sample was prepared in the same manner as in the case of the LS measurements. The solutions of lower concentrations were obtained by successive dilution. The polymer mass concentrations c were calculated from the weight fractions with the densities of the solutions. Density corrections were also made in the calculations of the relative viscosity η_r from the flow times of the solution and solvent. The data obtained for the specific viscosity η_{sp} and η_r in the range of $\eta_r < 1.8$ were treated as usual by the Huggins (η_{sp}/c vs c) and Fuoss–Mead ($\ln \eta_r/c$ vs c) plots, respectively, to determine $[\eta]$ and the Huggins coefficient k'. (Note that the two plots have the same intercept.)

3.3 Results and Discussion

The values of M_w, $\langle S^2 \rangle$, and A_2 determined from LS measurements and those of $[\eta]$ and k' from viscosity measurements for the PNIPA samples in methanol at 25.0 °C are given in the second through sixth columns, respectively, in Table 3.2. In the table, the values of $\langle S^2 \rangle$ for the samples T5, T7, B5, and B11 with smaller M_w have been omitted because the slopes of the Berry square-root plots against the square of the magnitude of the scattering vector for those samples are not sufficiently large to evaluate $\langle S^2 \rangle$ accurately. The values of A_2 are of order 10^{-4} cm^{3}mol/g^2 and those of k' are in the range of $0.3 \lesssim k' \lesssim 0.4$, indicating that methanol at 25.0 °C is a good solvent for PNIPA.

3.3.1 Mean-Square Radius of Gyration

Figure 3.1 shows double-logarithmic plots of $\langle S^2 \rangle$ (in Å^2) against M_w for PNIPA in methanol at 25.0 °C. The circles and triangles represent the values for the PNIPA samples synthesized in *tert*-butanol and benzene, respectively. The solid curve connects smoothly the data points for the samples synthesized in each solvent. It is seen from the figure that the data points for the samples synthesized in benzene deviate downward from those synthesized in *tert*-butanol in the whole range of M_w examined, and the deviation increases with increasing M_w. The slopes of the data points in the range of $M_w \gtrsim 10^6$ are 1.1_2 and 0.9_0 for the samples synthesized in *tert*-butanol and benzene, respectively. Note that the former value 1.1_2 is somewhat smaller than 1.2 for linear flexible polymers with very large M_w in good solvents and further that the latter value 0.9_0 is even smaller than unity for unperturbed linear flexible polymers. It implies that the primary structure of PNIPA synthesized by radical polymerization is not linear.

Table 3.2. Results of LS and viscosity measurements for poly(*N*-isopropylacrylamide) in methanol at 25.0°C

sample	M_w	$10^{-4}\langle S^2\rangle$ (Å^2)	$10^4 A_2$ (cm^{3}mol/g^2)	$[\eta]$ (dL/g)	k'	Ψ	$10^{-23}\Phi$ (mol^{-1})
			samples synthesized in *tert*-butanol				
T5	5.17×10^4		6.05	0.308	0.40		
T7	7.19×10^4		5.35	0.389	0.39		
T13	1.31×10^5	1.8_7	4.71	0.606	0.36	0.23_7	2.1_2
T23	2.27×10^5	3.3_4	3.96	0.926	0.38	0.24_9	2.3_4
T38	3.76×10^5	6.1_2	3.58	1.27	0.36	0.25_0	2.1_4
T54	5.35×10^5	9.2_9	3.25	1.73	0.35	0.24_5	2.2_3
T96	9.63×10^5	$17._4$	2.90	2.47	0.36	0.27_7	2.2_4
T120	1.16×10^6	$22._6$	2.76	2.84	0.35	0.25_7	2.0_8
T220	2.20×10^6	$45._5$	2.39	4.33	0.39	0.28_1	2.1_1
			samples synthesized in benzene				
B5	4.65×10^4		5.73	0.275	0.42		
B11	1.11×10^5		4.48	0.484	0.39		
B14	1.44×10^5	1.9_3	4.31	0.591	0.40	0.25_1	2.1_7
B20	1.97×10^5	2.6_3	3.94	0.683	0.39	0.26_8	2.1_5
B62	6.21×10^5	8.9_8	2.88	1.40	0.39	0.30_8	2.2_0
B130	1.30×10^6	$17._7$	2.34	2.17	0.38	0.39_5	2.5_7
B170	1.72×10^6	$22._4$	2.02	2.61	0.39	0.42_4	2.8_9
B270	2.69×10^6	$34._2$	1.79	3.17	0.40	0.48_4	2.9_0

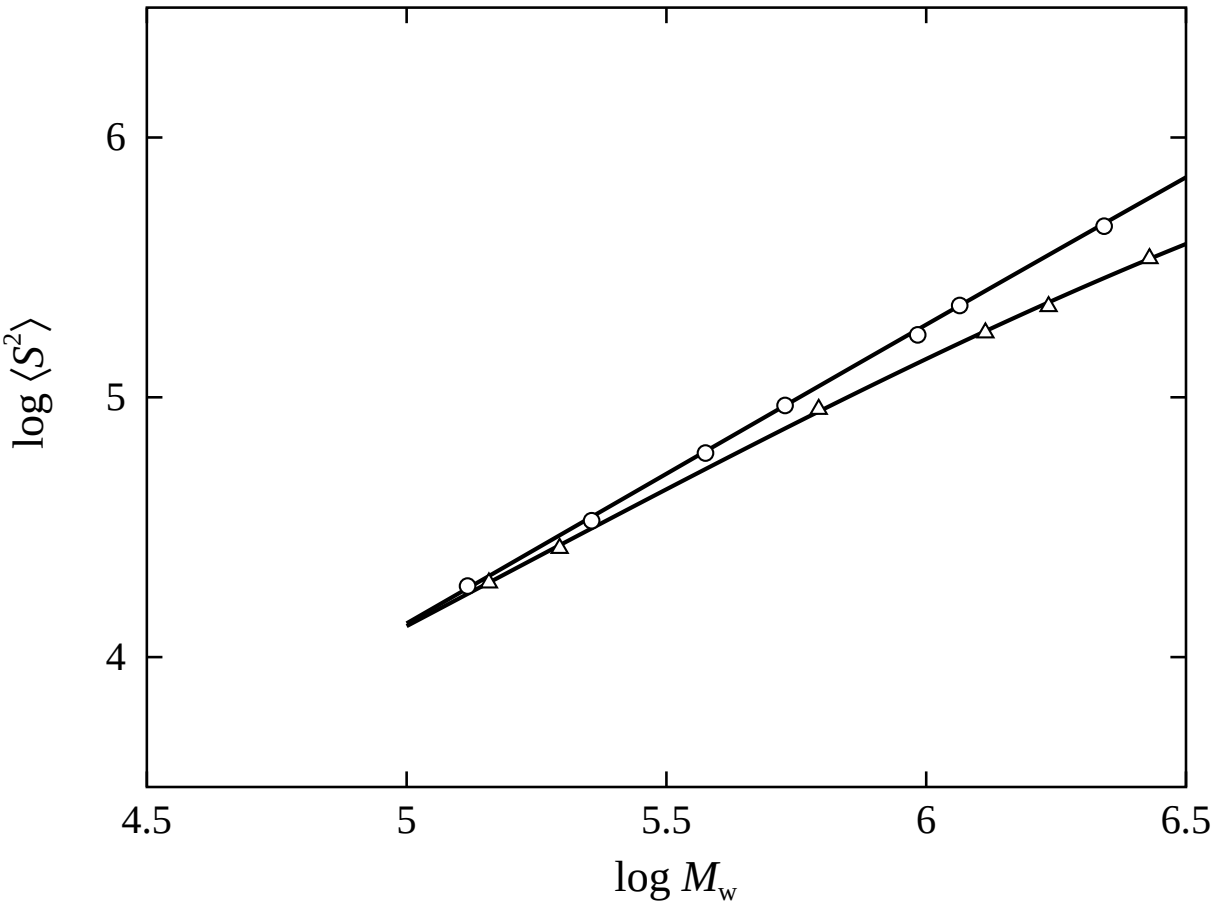

Figure 3.1. Double-logarithmic plots of $\langle S^2 \rangle$ (in Å^2) against M_w for PNIPA in methanol at 25.0°C: (○) samples synthesized in *tert*-butanol; (△) samples synthesized in benzene. The solid curve connects smoothly the data points for the samples synthesized in each solvent.

The average dimension of a given polymer chain in dilute solution may in general be affected by chain stiffness and local chain conformation[6] which are mainly determined by the chemical structure and stereochemical composition of the chain, by the intramolecular excluded-volume effect[6,7] which is determined by interactions between polymer segments and solvent molecules, and by the primary structure of the chain.[7] The stereochemical compositions of all the PNIPA samples used in this chapter have been confirmed to be almost identical with each other, as already mentioned in the preceding section. The difference in $\langle S^2 \rangle$ between the two kinds of samples, both having the same chemical structure and stereochemical composition and both measured in the same solvent condition, therefore, is considered to be caused by the difference in the primary structure, *i.e.*, the number of branch points. Then the number of branch points in the PNIPA sample synthesized in benzene seems larger than that in the sample synthesized in *tert*-butanol, since in general the larger the number of branch points is, the smaller the average chain dimension is. Further, the difference in the number of branch points between the two kinds of samples seems to increase with increasing M_w.

3.3.2 Second Virial Coefficient

Figure 3.2 shows double-logarithmic plots of A_2 (in cm^3mol/g^2) against M_w for PNIPA in methanol at 25.0 °C. The unfilled symbols and the solid curves have the same meaning as those in Figure 3.1. As in the case of $\langle S^2 \rangle$ shown in Figure 3.1, the data points for the samples synthesized in benzene deviate downward from those synthesized in *tert*-butanol in the whole range of M_w examined, and the deviation increases with increasing M_w. It indicates that the effective volume V_E excluded to one polymer chain by the presence of another, which may be defined by

$$A_2 = 4N_A V_E / {M_w}^2 \tag{3.1}$$

with N_A the Avogadro constant, is smaller for the former samples. The slopes of the data points in the range of $M_w \gtrsim 10^6$ are -0.2_3 and -0.3_3 for the samples synthesized in *tert*-butanol and benzene, respectively, which are somewhat less than -0.2 for linear flexible polymers with very large M_w in good solvents, implying that the distribution of segments constituting a single polymer chain is more compact for the present PNIPA, especially for that synthesized in benzene, than for linear flexible polymers in good solvents.

For comparison, in Figure 3.2 are also plotted the literature data for PNIPA in methanol at 25.0 °C reported by Chiantore *et al.*[8] (■) by the use of samples synthesized in methanol at temperatures ranging from 50 to 70 °C with AIBN as an initiator. Although their values of A_2 are rather in good agreement with ours in the range of $M_w \lesssim 10^5$, the former values deviate upward from ours and seem almost independent

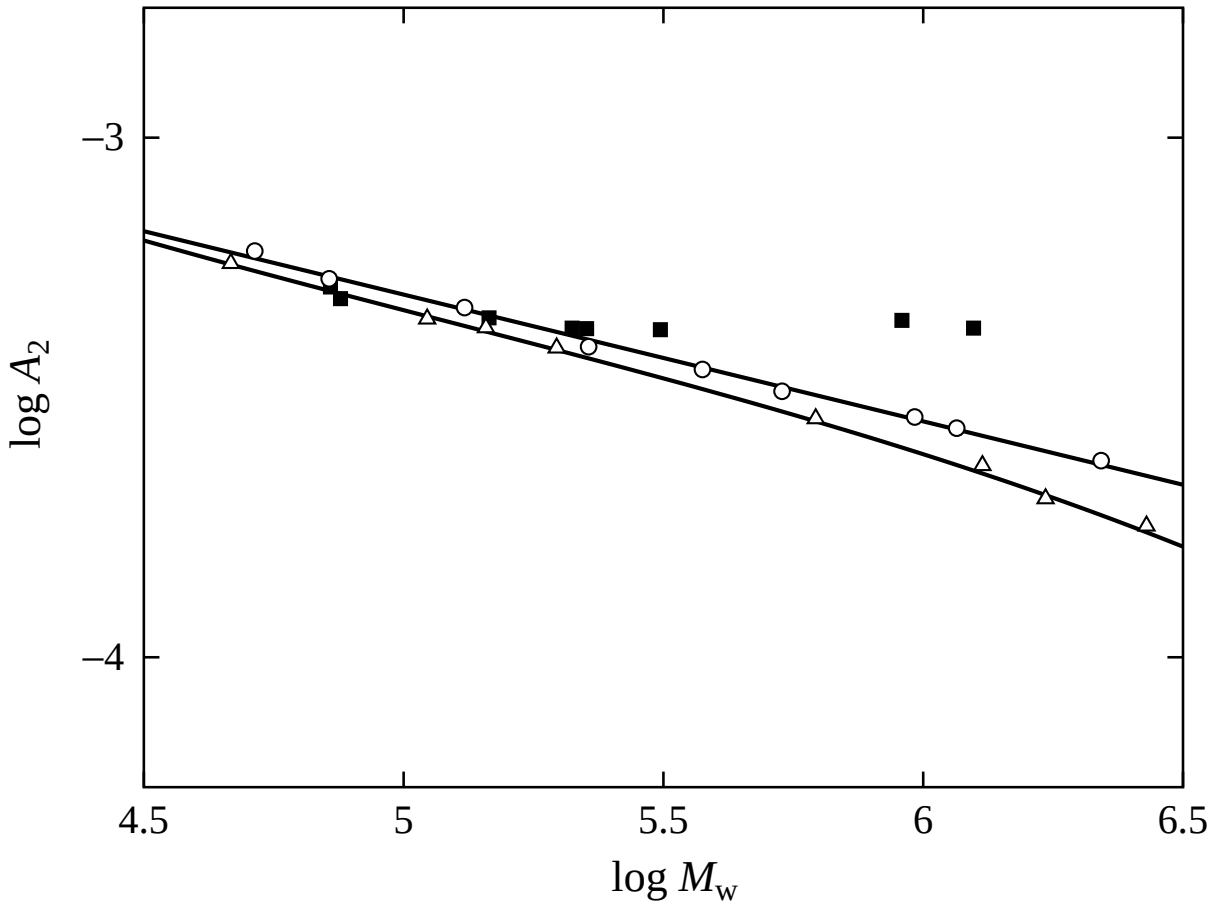

Figure 3.2. Double-logarithmic plots of A_2 (in cm^3mol/g^2) against M_w for PNIPA in methanol at 25.0°C: (■) literature data by Chiantore *et al.*[8] The unfilled symbols and curves have the same meaning as those in Figure 3.1.

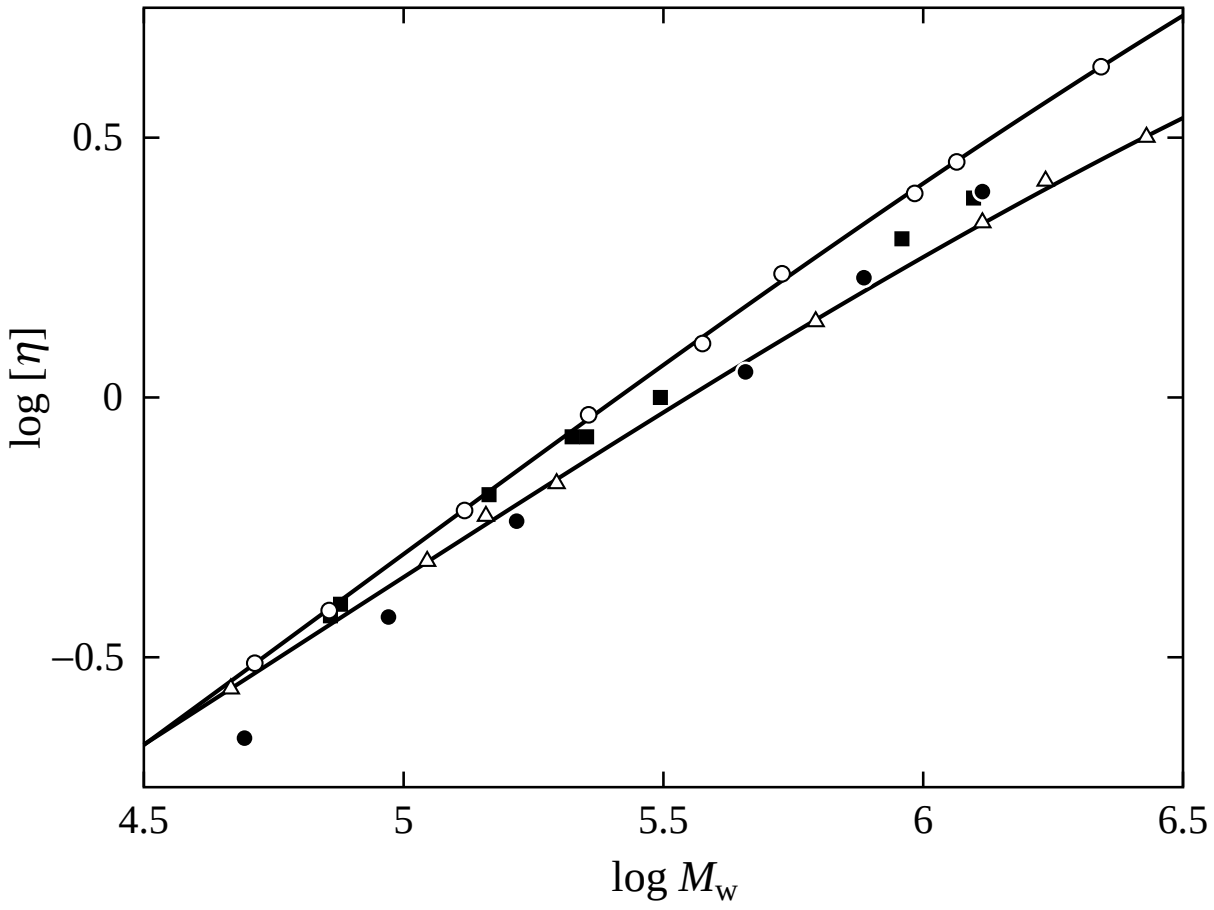

Figure 3.3. Double-logarithmic plots of $[\eta]$ (in dL/g) against M_w for PNIPA in methanol at 25.0°C: (■) literature data by Chiantore *et al.*;[8] (●) literature data by Zeng *et al.*[9] The unfilled symbols and curves have the same meaning as those in Figure 3.1.

of M_w. Such behavior of A_2 is usually observed for very stiff chains and is unusual for flexible polymers with very large M_w in good solvents.

3.3.3 Intrinsic Viscosity

Figure 3.3 shows double-logarithmic plots of $[\eta]$ (in dL/g) against M_w for PNIPA in methanol at 25.0 °C. The unfilled symbols and the solid curves have the same meaning as those in Figure 3.1. As in the cases of $\langle S^2 \rangle$ and A_2 shown in Figures 3.1 and 3.2, respectively, the data points for the samples synthesized in benzene deviate downward from those synthesized in *tert*-butanol in the whole range of M_w examined, and the deviation increases with increasing M_w. It indicates that the effective hydrodynamic (molar) volume, which may be defined by

$$V_H = 6^{-3/2} M_w [\eta] \tag{3.2}$$

is smaller for the former samples. The slopes of the data points in the range of $M_w \gtrsim 10^6$ are 0.6_7 and 0.5_1 for the samples synthesized in *tert*-butanol and benzene, respectively, which are smaller than 0.8 for linear flexible polymers with very large M_w in good solvents.

For comparison, in Figure 3.3 are also plotted the literature data for PNIPA in methanol at 25.0 °C reported by Chiantore *et al.*[8] (■) by the use of the same samples as those shown in Figure 3.2 and by Zeng *et al.*[9] (●) by the use of samples synthesized in *tert*-butanol at 55 °C with AIBN as an initiator. The data points by Chiantore *et al.* follow a straight line with a slope of 0.6_1 in the range of $M_w \gtrsim 10^5$, implying that their PNIPA should be flexible. Such behavior is inconsistent with that of A_2. The data points by Zeng *et al.* deviate downward from the present ones for the samples synthesized in *tert*-butanol (○). The reason for this difference is not clear.

3.3.4 Interpenetration Function

All the present experimental results for $\langle S^2 \rangle$, A_2, and $[\eta]$ shown above imply that the number of branch points in the PNIPA samples synthesized in benzene is larger than that in the samples synthesized in *tert*-butanol. The interpenetration function Ψ defined by

$$\Psi = \frac{V_E}{\pi^{3/2} \langle S^2 \rangle^{3/2}} \tag{3.3}$$

is known to be a quantity sensitive to the primary structure of a polymer chain,[6,7] which takes a value *ca.* 0.24 for linear flexible polymer chains with very large M in good solvents and takes a larger value if the segment density of the polymer chain under consideration in dilute solution is larger than that of the linear flexible chain. It is therefore interesting to examine the behavior of Ψ.

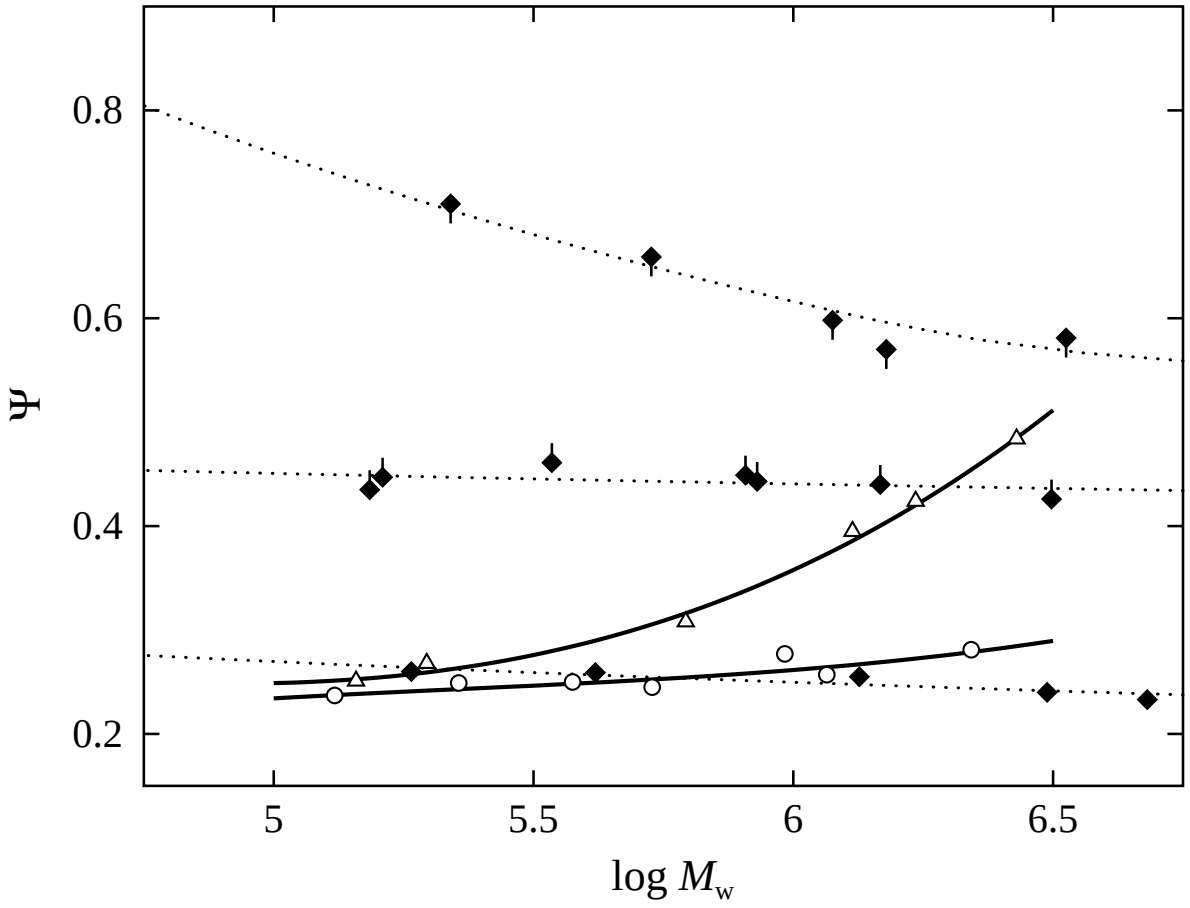

Figure 3.4. Plots of Ψ against log M_w. The unfilled symbols and solid curves have the same meaning as those in Figure 3.1. The filled symbols represent the literature data for PS in benzene at 25.0°C: (◆) linear PS;[10,11] (◆) 4-arm star PS;[12] (◆) 6-arm star PS.[13] The dotted curve connects smoothly the data points for each kind of PS.

In the seventh column of Table 3.2 are given the values of Ψ calculated from eq 3.3 with eq 3.1 along with the values of M_w, $\langle S^2 \rangle$, and A_2 given in the second through fourth columns, respectively, of the table. Figure 3.4 shows plots of Ψ against $\log M_w$ for PNIPA in methanol at 25.0 °C. The unfilled symbols and the solid curves have the same meaning as those in Figure 3.1. It is seen that Ψ for the samples synthesized in benzene remarkably increases with increasing M_w.

For comparison, in Figure 3.4 are also plotted the literature data for linear polystyrene (PS) (◆),[10,11] regular four-arm star PS (◆),[12] regular six-arm star PS (◆),[13] all measured in benzene at 25.0 °C. The dotted curve connects smoothly the data points for each kind of PS. It is seen that Ψ increases with increasing number of the arms. Note that the linear PS corresponds to the regular 2-arm star PS. For the PNIPA samples synthesized in benzene, Ψ is close to that for the linear PS in the range of $M_w \lesssim 3 \times 10^5$, but deviates upward from the latter as M_w is increased, and becomes even larger than that for the regular four-arm star PS. In contrast to this, Ψ for the PNIPA samples synthesized in *tert*-butanol becomes slightly larger than that for the linear PS as M_w is increased. The difference in the behavior of Ψ between the two kinds of samples confirms the above implication that the number of branch points in the PNIPA samples synthesized in benzene is larger than that in the samples synthesized in *tert*-butanol.

3.3.5 Flory–Fox Factor

The Flory–Fox factor Φ defined by

$$\Phi = \frac{V_H}{\langle S^2 \rangle^{3/2}} \tag{3.4}$$

is also sensitive to the primary structure of a given polymer chain, which takes a value *ca.* 2×10^{23} mol^{-1} for linear flexible polymer chains with very large M in good solvents and takes a larger value if the segment density of the polymer chain under consideration in dilute solution is larger than that of the linear flexible chain. In the eighth column of Table 3.2 are given the values of Φ calculated from eq 3.4 with eq 3.2 along with the values of M_w, $\langle S^2 \rangle$, and $[\eta]$ given in the second, third, and fifth columns, respectively, of the table.

Figure 3.5 shows plots of Φ (in mol^{-1}) against $\log M_w$ for PNIPA in methanol at 25.0 °C. All the symbols and curves in the figure have the same meaning as those in Figure 3.4. The difference in behavior of Φ between the two kinds of PNIPA samples is the same as that in the behavior of Ψ.

Finally, we make brief mention of the number of branch points in the PNIPA samples. Existence of branch points could not be detected by ^{1}H NMR even for the samples synthesized in benzene,[1] which are considered to have not a few branch points, while,

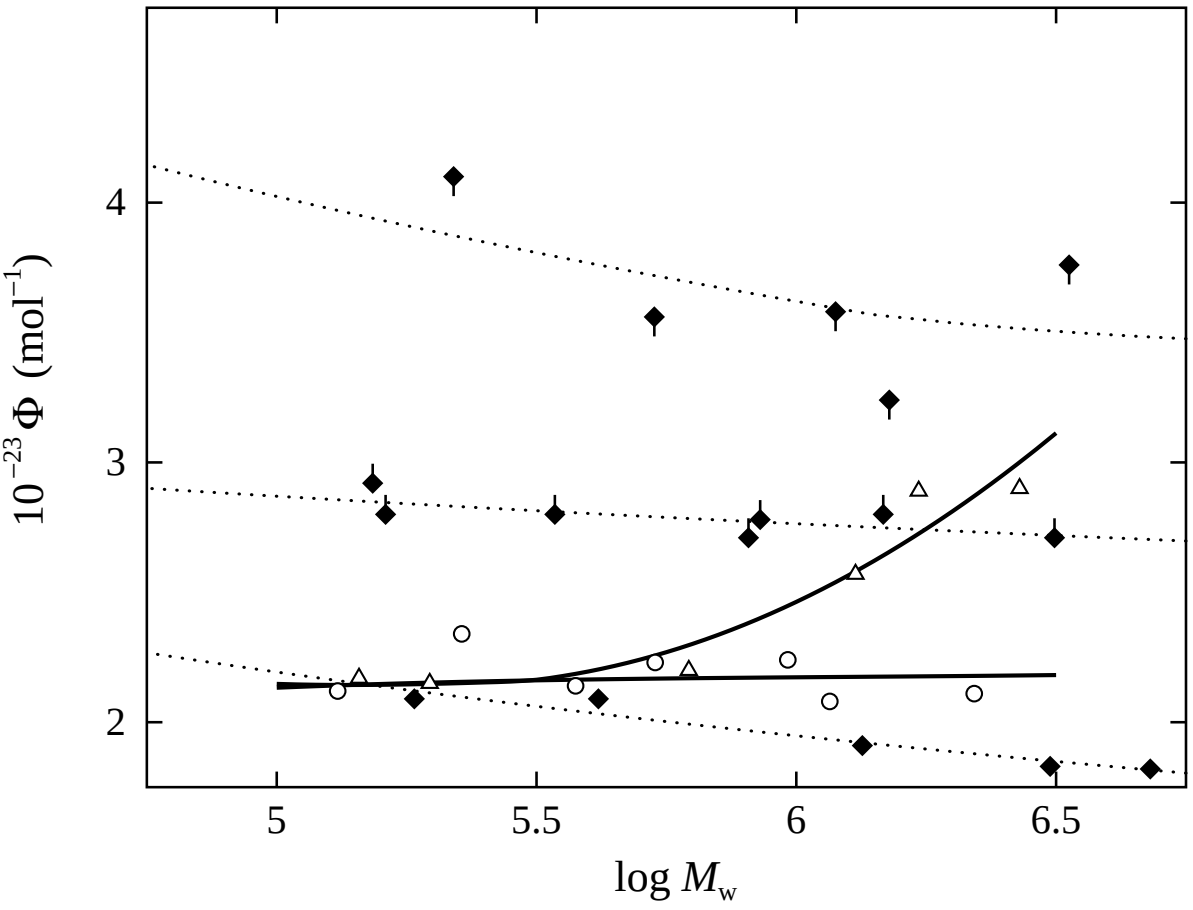

Figure 3.5. Plots of Φ (in mol^{-1}) against log M_w. The unfilled symbols and solid curves have the same meaning as those in Figure 3.1. The filled symbols and dotted curves have the same meaning as those in Figure 3.4.

as expected, it has been clearly verified in this chapter of the average chain dimension. Probability that a given proton belongs to one of the branch points in PNIPA chains should be smaller than 1%, *i.e.*, detectability of ^{1}H NMR spectroscopy.

3.4 Conclusion

We have determined $\langle S^2 \rangle$, A_2, and $[\eta]$ in methanol at 25.0 °C for the two kinds of PNIPA samples synthesized by radical polymerization in *tert*-butanol and benzene by the use of AIBN as an initiator. For all the three quantities, it has been found that the observed value for the latter PNIPA is smaller than that for the former and the difference increases with increasing M_w, indicating that the average chain dimension of the latter PNIPA is smaller than that of the former. Since the two kinds of PNIPA have the same stereochemical composition (and also the same chain end group), the difference in the average chain dimension may be regarded as arising from the difference in the primary structure, *i.e.*, the number of branch points. The average dimension of a given polymer chain in general decreases with increasing the number of branch points. It may then be concluded that the number of the branch points is larger in the latter PNIPA than in the former. It has also been found that the values of Ψ and Φ for the latter PNIPA are remarkably larger than the corresponding values for the linear PS, confirming the conclusion. Increase in the number of branch points is necessarily accompanied by increase in the number of hydrophobic end groups, which might be the reason for the difference in the cloud point between the two kinds of PNIPA.[1]

References

1. T. Kawaguchi, Y. Kojima, M. Osa, and T. Yoshizaki, *Polym. J.*, **40**, 455 (2008).
2. Y. Isobe, D. Fujioka, S. Habaue, and Y. Okamoto, *J. Am. Chem. Soc.*, **123**, 7180 (2001) and its supporting information.
3. Gj. Deželić and J. Vavra, *Croat. Chem. Acta*, **38**, 35 (1966).
4. G. C. Berry, *J. Chem. Phys.*, **44**, 4550 (1966).
5. B. L. Johnson and J. Smith, In *Light Scattering from Polymer Solutions*; M. B. Huglin, Ed.; Academic Press: London, 1972; Chapter 2.
6. H. Yamakawa, "Helical Wormlike Chains in Polymer Solutions," Springer, Berlin, 1997.
7. H. Yamakawa, "Modern Theory of Polymer Solutions," Harper & Row, New York, 1971. Its electronic edition is available on-line at the URL: `http://www.molsci.polym.kyoto-u.ac.jp/archives/redbook.pdf`

8. O. Chiantore, M. Guaita, and L. Trossarelli, *Makromol. Chem.*, **180**, 969 (1979).
9. F. Zeng, Z. Tong, and T. Sato, *Science in China, Series B*, **42**, 290 (1999).
10. Y. Miyaki, Y. Einaga, and H. Fujita, *Macromolecules*, **11**, 1180 (1978).
11. Y. Miyaki, Ph. D. Thesis, Osaka University, 1981.
12. M. Okumoto, Y. Nakamura, T. Norisuye, and A. Teramoto, *Macromolecules*, **31**, 1615 (1998).
13. M. Okumoto, Y. Iwamoto, Y. Nakamura, and T. Norisuye, *Polym. J.*, **32**, 422 (2000).

4 Characterization of Linear Poly(*N*-isopropylacrylamide) and Cloud Points in its Aqueous Solutions

4.1 Introduction

In Chapters 2 and 3, we have made a study of "phase" behavior of aqueous poly(*N*-isopropylacrylamide) (PNIPA) solutions, which we had conventionally considered to be a well-defined model solution of a polar polymer in a polar solvent and to show lower-critical-solution-temperature (LCST) miscibility behavior.[1] Contrary to our optimistic expectation, however, the cloud points determined for aqueous solutions of PNIPA samples synthesized by radical polymerization in *tert*-butanol and methanol by the use of azobis(isobutyronitrile) (AIBN) as an initiator have been found to be definitely higher than those of samples synthesized in benzene and 1,4-dioxane, although the four kinds of samples had almost the same weight-average molecular weight $M_{\rm w}$ and stereochemical composition specified by the fraction $f_{\rm r}$ of racemo diads.[2]

In order to investigate the causes of such difference in the cloud point, we have examined the average chain dimensions of the PNIPA samples synthesized in *tert*-butanol and benzene, in dilute methanol (good solvent) solution. The mean-square radius of gyration $\langle S^2 \rangle$, second virial coefficient A_2, and intrinsic viscosity $[\eta]$ have then been found to be larger for the former sample than for the latter, both having the same $M_{\rm w}$ and $f_{\rm r}$. It has been concluded that the PNIPA samples synthesized by radical polymerization have branch points and the number of them is smaller in the sample synthesized in *tert*-butanol (or methanol) than in the one synthesized in benzene (or 1,4-dioxane).[3] As a necessary continuation of the previous studies[2,3] (Chapters 2 and 3), we make a further study of the cloud point of the aqueous solutions of well-characterized linear PNIPA samples properly synthesized, *e.g.*, living anionic polymerization, in order to investigate the effect of the branch points on the cloud point.

As mentioned in Chapter 1, preparation of linear PNIPA by living anionic polymerization requires a comment. It is known that anionic polymerization of *N*-isopropylacrylamide (NIPA) is unfeasible because of acidity of its amide proton.[4,5] Recently, however, it has been shown that linear PNIPA may be synthesized by anionic polymerization of

"protected" NIPA whose amide proton is masked with a group properly chosen.[4–7] In this chapter, we adopt the Ishizone–Ito procedure by the use of NIPA masked with a methoxymethyl group along with diphenylmethylpotassium as an initiator,[5–7] which leads to a linear PNIPA sample having the same value of f_r ($\simeq 0.50$) as that of the previous samples synthesized by the radical polymerization ($f_r \simeq 0.52$).[2,3]

For the linear PNIPA samples so prepared, we first determine A_2 and $[\eta]$ in methanol (good solvent) and analyze them on the basis of the Kratky–Porod (KP) wormlike chain model.[8,9] We then determine the cloud points in aqueous solutions of the samples and compare the results so obtained with the previous ones for the PNIPA samples synthesized by radical polymerization.

4.2 Experimental

4.2.1 Material

Following the Ishizone–Ito procedure,[5–7] linear PNIPA samples were prepared by hydrolysis of methoxymethyl groups of poly(*N*-methoxymethyl-*N*-isopropylacrylamide) [poly(NMM-NIPA)] by the use of aqueous hydrochloric acid in 1,4-dioxane at room temperature for 10 h, where poly(NMM-NIPA) had been synthesized by living anionic polymerization of NMM-NIPA in tetrahydrofuran (THF) at -78°C under high vacuum conditions for 24 h by the use of diphenylmethylpotassium as an initiator in the presence of diethyl zinc. The monomer NMM-NIPA was synthesized by the reaction of NIPA with chloromethylmethyl ether in the presence of potassium *tert*-butoxide in dry diethyl ether under dry nitrogen at 0°C, where NIPA had been recrystallized three times from a 9/1 mixture of *n*-hexane and benzene and then dried in a vacuum for 12 h. The initiator diphenylmethylpotassium was synthesized by the reaction of diphenylmethane with potassium naphthalenide in dry THF under argon at room temperature, where potassium naphthalenide had been synthesized by the reaction of naphthalene with potassium. The polymerization of NMM-NIPA was terminated by adding methanol, so that the initiating and terminating chain ends of PNIPA are a diphenylmethyl group and a hydrogen atom, respectively.

Seven original samples so prepared were purified by reprecipitation from acetone solutions into *n*-hexane and then dialyzed seven times against pure water for 24 h by the use of a cellulose tube. By fractional precipitation using acetone as a solvent and *n*-hexane as a precipitant, each of the samples was separated into three fractions, the middle of them being used as a test sample. The seven test samples were freeze-dried from their 1,4-dioxane solutions after filtration through a Teflon membrane of pore size 1.0 μm.

Table 4.1. Values of M_w/M_n and f_r and results of LS and viscosity

sample	M_w/M_n[a]	f_r	M_w	$10^4 A_2$ ($cm^3\,mol/g^2$)	$[\eta]$ (dL/g)	k'
samples synthesized by living anionic polymerization						
L0.5	1.23	0.51	4.91×10^3	11.8	0.076_3	0.59
L0.6	1.12	0.49	5.47×10^3	11.5	0.080_6	0.59
L1	1.16	0.50	8.98×10^3	9.1_2	0.103	0.53
L2	1.12	0.51	2.21×10^4	7.1_5	0.175	0.47
L3	1.08	0.51	3.11×10^4	6.9_6	0.235	0.46
L6	1.09	0.51	5.64×10^4	5.8_4	0.367	0.39
L7	1.12	0.50	7.23×10^4	5.6_4	0.413	0.41
samples synthesized by radical polymerization in *tert*-butanol						
T1	1.29	0.52	1.23×10^4	8.5_5	0.125	0.54
T3	1.25	0.52	2.76×10^4	6.6_5	0.204	0.57
T4	1.29	0.52	4.23×10^4	6.1_1	0.280	0.42
samples synthesized by radical polymerization in benzene						
B3	1.26	0.52	2.90×10^4	6.5_9	0.206	0.43
B8	1.28	0.52	7.83×10^4	4.7_3	0.398	0.39

[a]The values of M_w/M_n were determined by analytical GPC using standard PS samples as reference standards.

Besides the above linear PNIPA samples, we also synthesized two PNIPA samples by radical polymerization with AIBN as an initiator, in the same manner as in the previous study[2] (Chapter 2). One sample was synthesized in *tert*-butanol and the other in benzene. We note that chain ends of the PNIPA samples are considered to be isobutyronitrile groups derived from AIBN, although detailed information could not be obtained. The samples so synthesized were purified and then separated into several fractions of narrow molecular-weight distribution, in the above-mentioned manners. Three and two fractions from the samples synthesized in *tert*-butanol and benzene, respectively, were used as test samples and were freeze-dried in the above-mentioned manner.

In the first column of Table 4.1 are given the codes of all the samples synthesized in this work. We use the letter L for the samples synthesized by living anionic polymerization and the letters T and B for those synthesized by radical polymerization in *tert*-butanol and benzene, respectively, and call the samples generally as L, T, and B samples, for convenience. In the second column of the table are also given the values of the ratio M_w/M_n of M_w to the number-average molecular weight M_n, which were determined from analytical gel permeation chromatography (GPC) in the same manner as before[2] using THF as an eluent and 12 standard polystyrene samples (Tosoh, $M_w = 2.8 \times 10^3$ — 8.4×10^6, $M_w/M_n = 1.02$ — 1.17) as reference standards.

The solvent methanol used for static light scattering and viscosity measurements was purified by distillation after refluxing over calcium hydride for *ca.* 6h. The solvent THF used for analytical GPC was of reagent grade with no stabilizer. The solvent deuterated dimethyl sulfoxide (DMSO) used for ^{1}H NMR spectroscopy was of reagent grade. The solvent water used for the determinations of the cloud point was highly purified through a Simpli Lab water purification system of Millipore Co., its resistivity being 18.2 MΩ·cm.

4.2.2 ^{1}H NMR

^{1}H NMR spectra for all the samples in deuterated DMSO at 170 °C were recorded on a JEOL EX-400 spectrometer at 399.8 MHz by the use of an rf pulse angle of 90° with a pulse repetition time of 8 s, where tetramethylsilane was added to each test solution as an internal standard.

4.2.3 Light Scattering

Light scattering (LS) measurements were carried out to determine M_w and the second virial coefficient A_2 for all the samples in methanol at 25.0 °C. A Fica 50 light-scattering photometer was used for all the measurements with vertically (v) polarized incident light of wavelength $\lambda_0 = 436$ nm. For a calibration of the apparatus, the intensity of light scattered

from pure benzene was measured at 25.0 °C at a scattering angle of 90°, where the Rayleigh ratio $R_{\mathrm{Uu}}(90°)$ of pure benzene was taken as 46.5×10^{-6} cm^{-1}.[10] The depolarization ratio ρ_{u} of pure benzene at 25.0 °C was determined to be 0.41 ± 0.01. Scattered intensity was measured at seven or eight different concentrations and at scattering angles θ ranging from 30.0 to 142.5°, and then converted to the excess unpolarized (Uv) components ΔR_{Uv} of the reduced scattered intensity by the use of the scattered intensity from the solvent methanol. The data obtained were treated by using the Berry square-root plot.[11] It was found that the corrections for the optical anisotropy were necessary to estimate true M_{w} and A_2 for samples with $M_{\mathrm{w}} \lesssim 8 \times 10^3$, and therefore the excess depolarized (HV) components ΔR_{Hv} of the reduced scattered intensity necessary for the corrections were also measured for them. As for samples with $M_{\mathrm{w}} \gtrsim 8 \times 10^3$, the corrections were unnecessary since effects of optical anisotropy were very small.

The most concentrated solution of each sample was prepared gravimetrically and made homogeneous by continuous stirring at room temperature for 1-3 days. It was optically purified by filtration through a Teflon membrane of pore size 0.10 μm. The solutions of lower concentrations were obtained by successive dilution. The weight concentrations of the test solutions were converted to the polymer mass concentrations c by the use of the densities of the respective solutions calculated with the partial specific volumes v_2 of the samples and with the density of the solvent methanol. The quantity v_2 was measured by using an oscillating U-tube density meter (Anton-Paar, DMA5000). The values of v_2 so determined in methanol at 25.0 °C are 0.893, 0.892, 0.904, 0.901, 0.901, 0.901, 0.901, 0.901, 0.902, 0.902, 0.892, and 0.903 cm^3/g for the samples L0.5, L0.6, L1, L2, L3, L6, L7, T1, T3, T4, B3, and B8, respectively. For the value of ρ_0 of methanol at 25.0 °C, we used the literature value 0.7866 g/cm^3.[12]

The refractive index increment $\partial n/\partial c$ was measured at the wavelength of 436 nm by the use of a Shimadzu differential refractometer DR-1. The values of $\partial n/\partial c$ in methanol at 25.0 °C were determined to be 0.188_9, 0.186_7, 0.187_6, 0.183_9, 0.184_1, 0.184_2, 0.184_3, 0.184_2, 0.183_6, 0.183_8, 0.184_1, and 0.184_9 cm^3/g for the samples L0.5, L0.6, L1, L2, L3, L6, L7, T1, T3, T4, B3, and B8, respectively. For the refractive index n_0 of methanol at 25.0 °C at the wavelength of 436 nm, we used the literature value 1.3337.[12]

4.2.4 Viscosity

Viscosity measurements were carried out for all the samples in methanol at 25.0 °C by the use of conventional capillary and four-bulb spiral capillary viscometers of the Ubbelohde type. The flow time was measured to a precision of 0.1 s, keeping the difference between

those of the solvent and solution larger than 20 s. The test solutions were maintained at a constant temperature within ±0.005°C during the measurements.

The most concentrated solution of each sample was prepared in the same manner as in the case of the LS measurements. The solutions of lower concentrations were obtained by successive dilution. The polymer mass concentrations c were calculated from the weight fractions with the densities of the solutions. Density corrections were also made in the calculations of the relative viscosity η_r from the flow times of the solution and solvent. The data obtained for the specific viscosity η_{sp} and η_r in the range of $\eta_r < 1.4$ were treated as usual by the Huggins (η_{sp}/c vs c) and Fuoss–Mead ($\ln \eta_r/c$ vs c) plots, respectively, to determine $[\eta]$ and the Huggins coefficient k'. (Note that the two plots have the same intercept.)

4.2.5 Transmittance of Light

The intensity of light passing through the aqueous solution of the five L samples at a given weight fraction w of the sample was monitored. All the measurements were carried out by the use of a self-made apparatus with incident light of wavelength 650 nm from a laser diode module, as described below. A cylindrical cell of outer diameter 10 mm containing a given test solution was immersed in a water bath, the test solution in the cell being stirred continuously.

In order to determine the cloud point of each solution, the temperature of the water bath was controlled to increase at the rate of *ca.* 1.5 °C/h. During continuous increase in temperature from 15 °C to 30 °C for the sample L0.6, from 17 °C to 32 °C for the sample L1, from 18 °C to 32 °C for the sample L2, from 20 °C to 33 °C for the sample L3, and from 26 °C to 34 °C for the sample L7, the intensity of light passing through the cell was monitored by a photodiode. The output of the photodiode along with the solution temperature measured simultaneously by the use of a platinum resistance thermometer combined with a programmable digital multimeter (Yokokawa 7555) was recorded on a personal computer at intervals of 10 s. Then, the (relative) transmittance as defined as the ratio of the intensity of light through a test solution at a temperature to that at a lower temperature at which the test solution may be regarded as transparent was determined as a function of temperature. The measurements were carried out at 8 different concentrations in the range of $0.5 \lesssim w \lesssim 10$ % for each sample. The most concentrated solution of each sample was prepared gravimetrically and made homogeneous by continuous stirring for 2 d at *ca.* 5 °C. The solutions of lower concentrations were obtained by successive dilution at *ca.* 5 °C.

4.3 Results

4.3.1 Stereochemical Composition

Figure 4.1 shows ^{1}H NMR spectra for the samples L0.5 and L7 (synthesized by living anionic polymerization) over the whole range of the chemical shift δ (in units of ppm) in which all the signals from PNIPA, *i.e.*, the methylene (a) and methine (b) protons in the main chain and the amide (c), methine (d), and methyl (e) protons in the side group, are included. According to Isobe *et al.*,[13] the three signals from the a protons in the range of $1.2 \lesssim \delta \lesssim 1.8$ may be assigned to those in the meso (m), racemo (r), and m diads, respectively, from the right to the left, as shown in the spectrum for L0.5. At $\delta \simeq 7.2$, the signals from the phenyl groups at the initiating end may be definitely observed ($*$) for L0.5, while those for L7 are very weak.

In the third column of Table 4.1 are given the values of f_r determined from the relative intensities of the three signals from the a protons. It is seen from the values of f_r that all the PNIPA samples synthesized in this work have almost the same stereochemical composition irrespective of the polymerization method, *i.e.*, living anionic or radical polymerization.

4.3.2 Second Virial Coefficient in Methanol at 25 °C

The values of M_w and A_2 determined from LS measurements in methanol at 25.0 °C are given in the fourth and fifth columns, respectively, of Table 4.1, where the corrections for the optical anisotropy to M_w and A_2 were made for the samples L0.5 and L0.6 following the standard procedure,[14–18] as done in previous studies.[19,20] We omit here the details of the corrections and only note that the values of the optical anisotropy factor δ determined from ΔR_{Uv} and ΔR_{Hv} are $9.9_3 \times 10^{-3}$ and $6.7_5 \times 10^{-3}$ for L0.5 and L0.6, respectively. From the relative intensities of the ^{1}H NMR signals from the phenyl groups at the initiating end of the L samples (see Figure 4.1), we have been able to estimate M_n of L0.5 and L0.6 to be 4.2×10^3 and 4.7×10^3, respectively, which are rather in good agreement with the M_n values 4.0×10^3 and 4.9×10^3 estimated for L0.5 and L0.6, respectively, from the values of M_w and M_w/M_n given in Table 4.1. For the other L samples, the intensities of the ^{1}H NMR signals from the terminal group are not strong enough to estimate M_n accurately. The values of A_2 are of order $10^{-3} - 10^{-4}$ cm^3 mol/g^2 for all the samples, indicating that methanol at 25.0 °C is a good solvent for them irrespective of the polymerization method.

Figure 4.2 shows double-logarithmic plots of A_2 (in cm^{3}mol/g^2) against M_w for PNIPA in methanol at 25.0 °C. The circles, triangles, and squares represent the values for the L, T, and B samples, respectively, and the solid curve connects smoothly the data points for the respective samples. We note that there are also plotted the data points for the

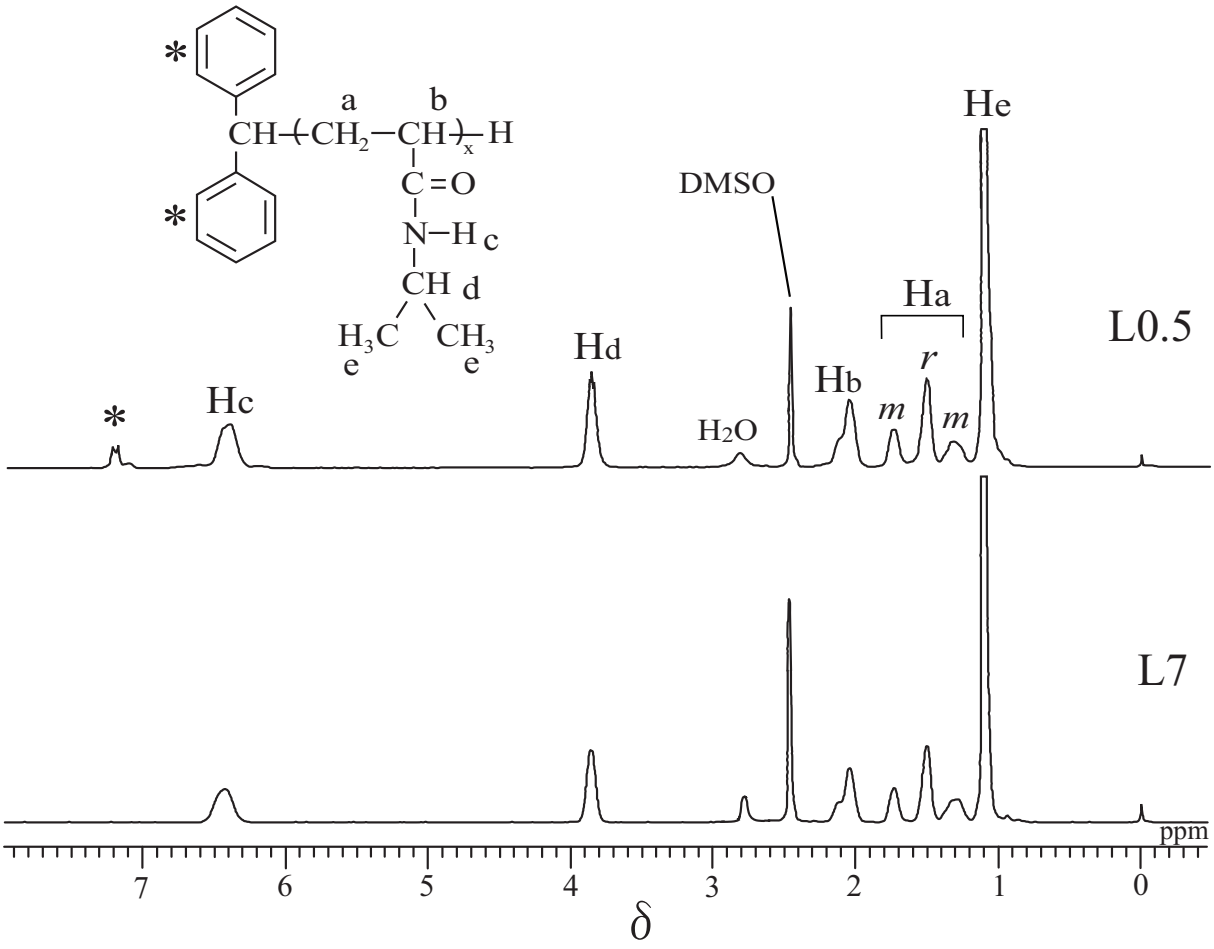

Figure 4.1. ^{1}H NMR spectra for the PNIPA samples L0.5 and L7. The signal indicated by the asterisk may be assigned to the phenyl protons at the initiating end of the PNIPA samples.

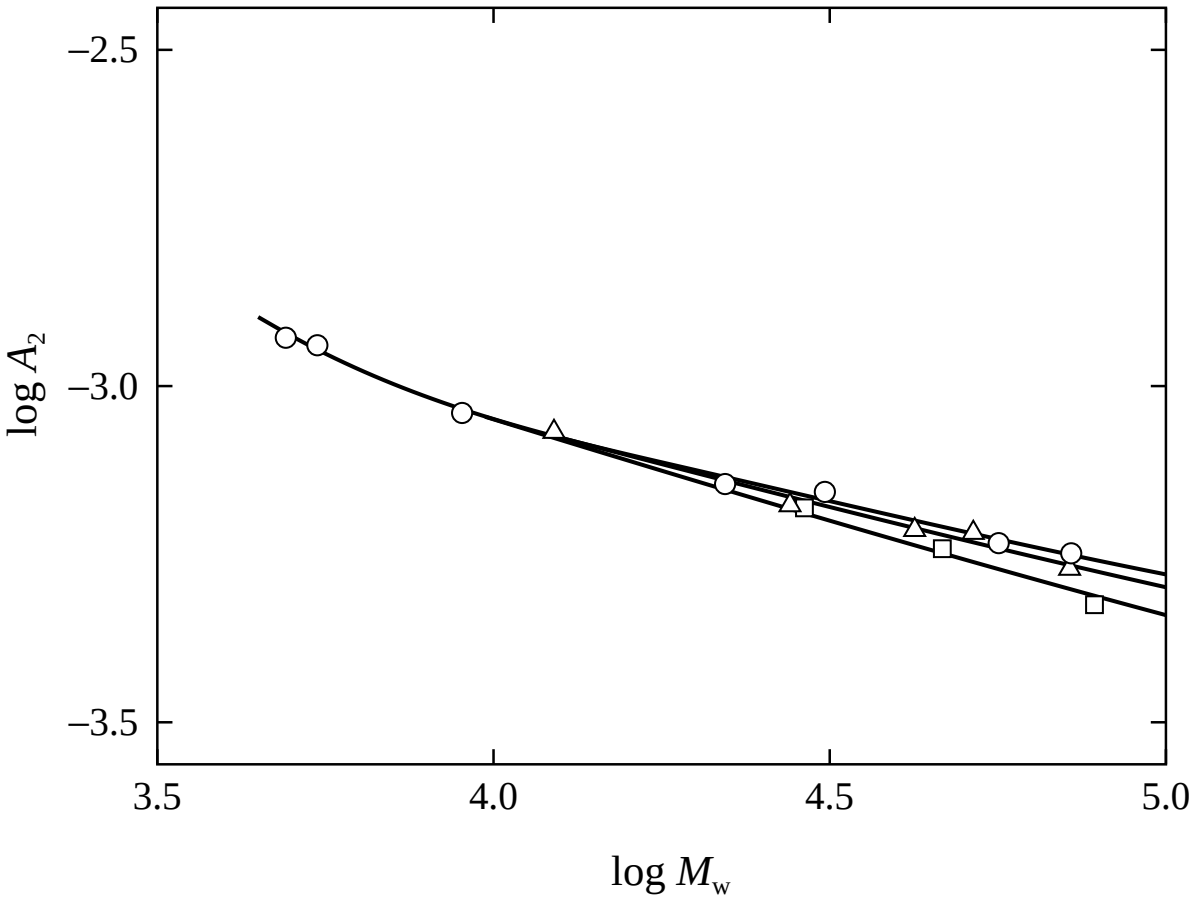

Figure 4.2. Double-logarithmic plots of A_2 (in $cm^3\,mol/g^2$) against M_w for PNIPA in methanol at 25.0 °C: (○) L samples; (△) T samples; (□) B samples. The solid curve connects smoothly the data points for the respective samples.

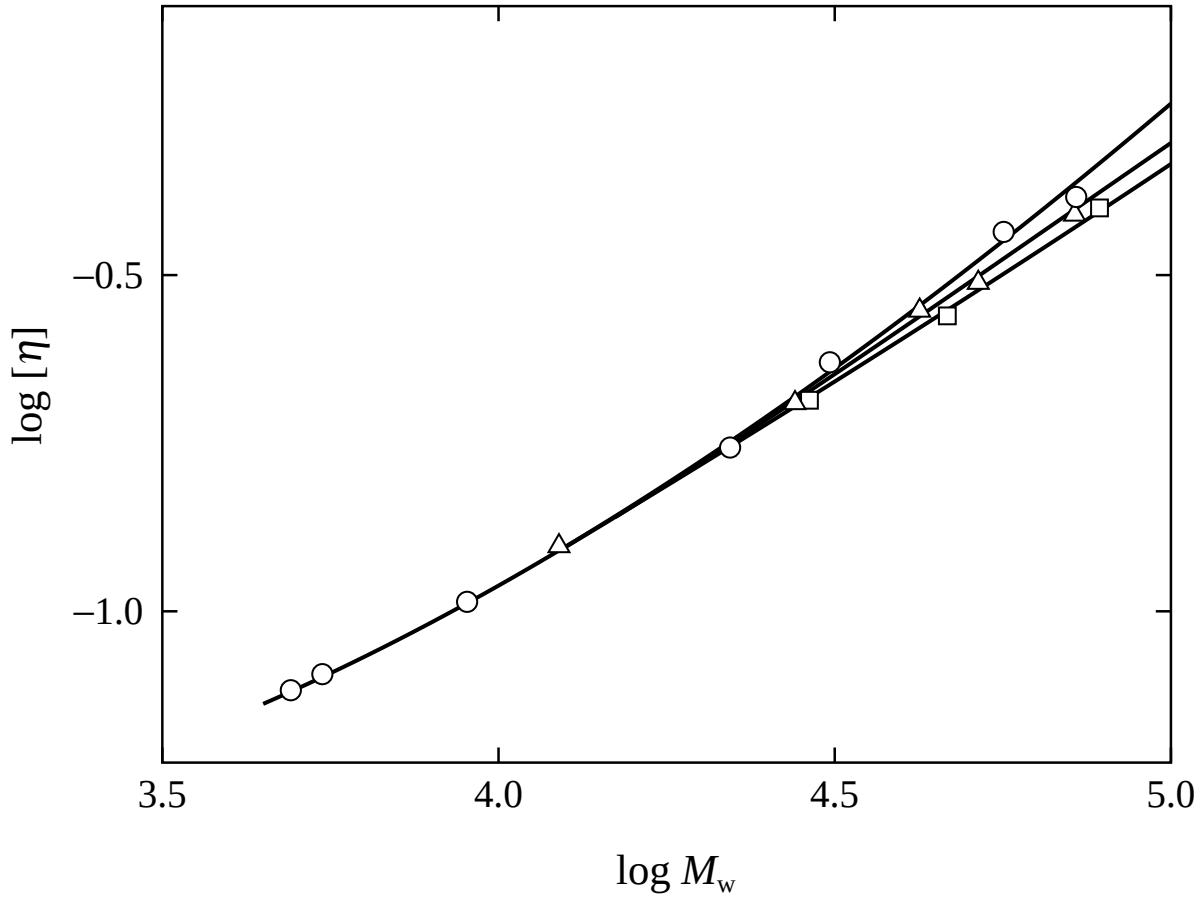

Figure 4.3. Double-logarithmic plots of $[\eta]$ (in dL/g) against M_w for PNIPA in methanol at 25.0 °C. The symbols and curves have the same meaning as those in Figure 4.2.

samples T5 ($M_w = 5.17 \times 10^4$), T7 (7.19×10^4), and B5 (4.65×10^4) which have been reproduced from Figure 3.2 (see also Table 3.2). It is seen that the data points for the three kinds of samples agree well with each other in the range of small M_w ($\lesssim 3 \times 10^4$) and the data points for the T and B samples deviate downward progressively from those for the L samples with increasing M_w ($\gtrsim 3 \times 10^4$), the value of A_2 for the B sample being the smallest at a given M_w.

It has been shown in the previous study[3] (Chapter 3) that the PNIPA samples synthesized by radical polymerization have a small number of branch points, which is larger for the B sample than for the T one at a given M_w. The quantity A_2 is proportional to an effective volume excluded to one polymer chain by the presence of another, and it may be considered to decrease with increasing the number of branch points. The above result that A_2 for the L sample having no branch point is the largest of all at a given M_w is therefore consistent with the previous conclusion.[3]

As is well known, effects of chain ends on A_2 become remarkably large in the range of small M_w, including oligomers.[9,21–26] The slope of the plots in the range of $M_w \lesssim 10^4$, where the A_2 values for the L, T, and B samples agree with each other, is *ca.* -0.34 and is appreciably steeper than the asymptotic value -0.2 for linear flexible polymers with very large M_w. This is due to the effects of chain ends. The agreement between the A_2 values in the range of small M_w implies that the number of the branch points in the T and B samples is negligibly small if any and the difference in the end group does not appreciably affect A_2 in methanol at 25.0 °C.

4.3.3 Intrinsic Viscosity in Methanol at 25 °C

The values of $[\eta]$ and k' determined from viscosity measurements in methanol at 25.0 °C are given in the sixth and seventh columns, respectively, of Table 4.1. Figure 4.3 shows double-logarithmic plots of $[\eta]$ (in dL/g) against M_w for PNIPA in methanol at 25.0 °C. The symbols and curves have the same meaning as those in Figure 4.2. We note that there are also plotted the data points for the samples T5, T7, and B5 which have been reproduced from Figure 3.3 (see also Table 3.2). As in the case of A_2 shown in Figure 4.2, the data points for the three kinds of samples agree well with each other in the range of small M_w ($\lesssim 3 \times 10^4$) and the data points for the T and B samples deviate downward progressively from those for the L samples with increasing M_w ($\gtrsim 3 \times 10^4$), the value of $[\eta]$ for the B sample being the smallest at a given M_w. Since $[\eta]$ proportional to the hydrodynamic volume is considered to decrease with increasing the number of branch points, the above result for $[\eta]$ is consistent with that for A_2 in the previous subsection.

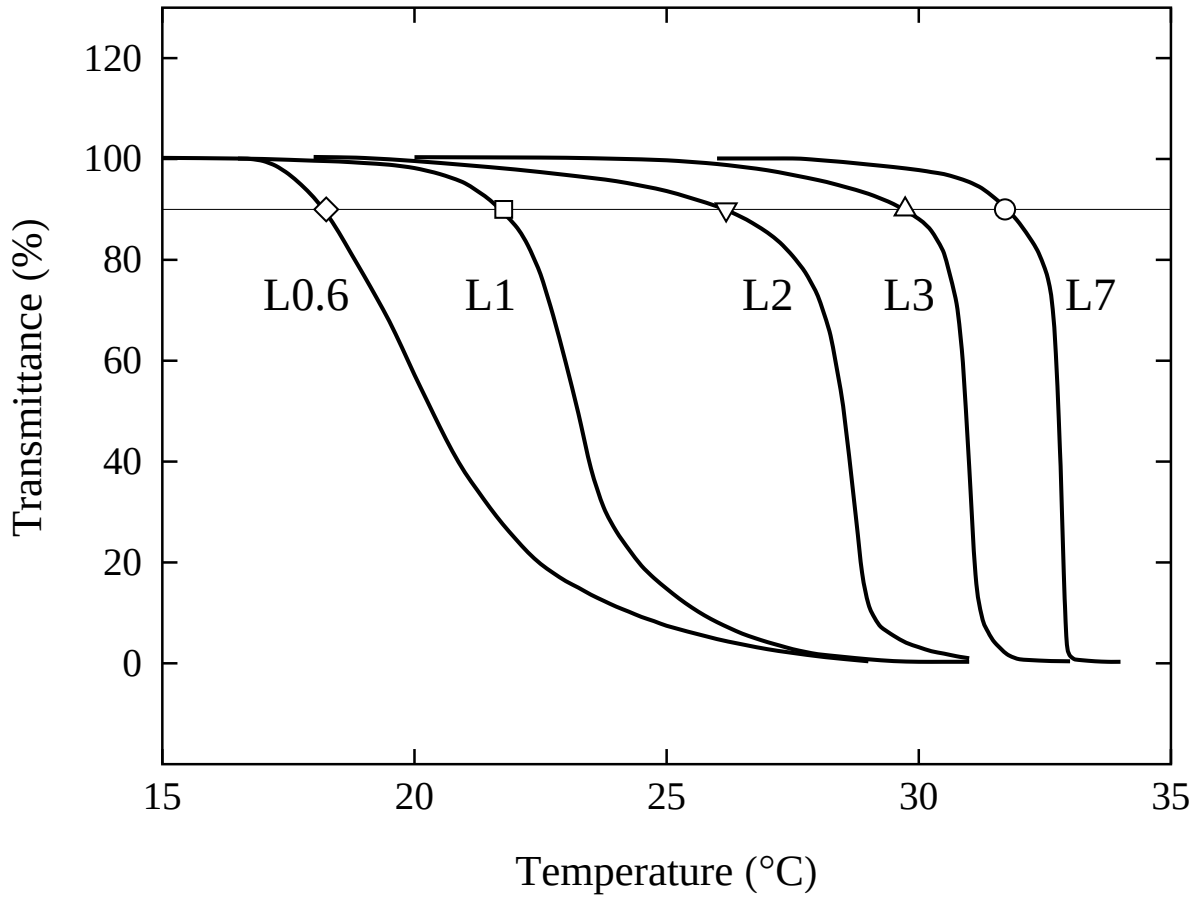

Figure 4.4. Temperature dependence of the transmittance of light passing through aqueous solutions of the PNIPA samples L0.6, L1, L2, L3, and L7 at w = 5.03, 4.97, 4.94, 4.93, and 4.94 %, respectively, the symbols ◇, □, ▽, △, and ○representing the respective cloud points (see the text).

Table 4.2. Cloud Points in Aqueous Solutions of Poly(*N*-isopropylacrylamide) Synthesized by Living Anionic Polymerization

L0.6		L1		L2		L3		L7	
w (%)	Temp. (°C)	w (%)	Temp. (°C)	w (%)	Temp. (°C)	w (%)	Temp. (°C)	w (%)	Temp. (°C)
0.50	24.5_5	0.51	24.8_0	0.49	28.6_6	0.50	30.7_3	0.50	32.9_6
1.00	21.8_5	1.00	23.3_1	0.99	28.0_5	0.98	30.5_8	1.00	32.7_7
2.00	19.3_5	2.01	22.3_4	2.00	27.0_5	1.99	30.2_9	2.00	32.4_9
3.04	18.3_5	3.06	21.9_6	3.01	26.3_0	2.99	30.2_4	2.98	32.0_4
3.85	18.2_5	4.07	21.8_2	4.03	26.2_7	3.94	30.0_3	4.01	31.8_6
5.03	18.2_5	4.97	21.7_8	4.94	26.1_8	4.93	29.7_3	4.94	31.6_9
7.45	17.7_5	6.93	21.7_7	7.16	25.1_2	7.15	29.6_0	6.95	31.6_6
9.07	17.6_5	8.48	21.4_8	8.38	24.6_0	8.25	29.2_5	9.11	31.6_0

The agreement between the $[\eta]$ values in the range of small M_w indicates that the number of the branch points in the T and B samples is negligibly small if any. The slope of the plot for each sample increases with increasing M_w because of the intramolecular excluded-volume effect.

4.3.4 Cloud Point in Aqueous Solutions

Figure 4.4 shows plots of the (relative) transmittance of light through the aqueous solutions of the PNIPA samples L0.6, L1, L2, L3, and L7 at the weight fraction w = 5.03, 4.97, 4.94, 4.93, and 4.94%, respectively, against temperature. Here, the (relative) transmittance is defined as the ratio of the intensity of light passing through a test solution at a temperature to that at a lower temperature at which the test solution may be regarded as transparent. We note that the shape of the transmittance curve for each solution is almost independent of the rate of increase in temperature if it is slower than 1.5 °C/h.

It is seen that the transmittance curve shifts toward the low-temperature side and the decrease in the transmittance becomes gentle, with decreasing M_w.

The cloud point is experimentally determined to be the temperature at which a given test solution just begins to be turbid, *i.e.*, its transmittance just starts to decrease from 100%, in the heating process. As seen from Figure 4.4, it is difficult to determine such a temperature unambiguously, so that we adopt the temperature at which the transmittance becomes 90% as the cloud point, for convenience, following the previous study[2] (Chapter 2). The symbols ◇, □, ▽, △, and ○ in Figure 4.4 represent the cloud points so determined for the samples L0.6, L1, L2, L3, and L7, respectively. The cloud points determined for the aqueous solutions of the samples L0.6, L1, L2, L3, and L7 at various w are given in Table 4.2.

4.4 Discussion

4.4.1 Chain Stiffness in Methanol at 25 °C

As far as we know, there has not yet been made polymer molecular characterization of PNIPA on the basis of its dilute solution properties, and therefore there is no available information about its chain stiffness. Since the PNIPA samples used so far in studies of their solutions are synthesized by radical polymerization and consequently have branched structures,[3] the stiffness of the PNIPA chain could not be correctly estimated from their solution properties. Fortunately, however, we were able to prepare the series of linear PNIPA samples, *i.e.*, L samples, by living anionic polymerization, and analyze the data for their A_2 and $[\eta]$ in order to estimate the stiffness.

As shown in previous studies of dilute solution properties of various vinyl polymer chains, they prefer to take locally curved or helical conformations, so that the helical wormlike (HW) chain is suitable for the analysis of their solution properties.[9,27] It is therefore desirable to analyze the present data for the L samples on the basis of the HW chain. Unfortunately, however, the range 5×10^3—7×10^4 of M_w of the L samples is not sufficiently wide to determine unambiguously all the HW model parameters from a comparison of the HW theory with the experimental data. Then we adopt the KP chain[8,9] as the second best model.

Before proceeding to make a comparison of theory with experiment, we briefly summarize the KP theory of A_2 and $[\eta]$. The KP chain is an elastic wire with bending energy immersed in a thermal bath, whose statistical behavior may be characterized by the stiffness parameter λ^{-1} having the dimension of length.[9] We note that the chain becomes stiff with increasing λ^{-1}, and the two limits of $\lambda^{-1} \to 0$ and ∞ correspond to the random coil and rigid rod, respectively. We also note that the HW chain is also an elastic wire with torsional energy in addition to the bending one and includes the KP chain as a special case. The total contour length L of the KP chain is related to the molecular weight M of a real polymer chain by

$$L = M/M_L \tag{4.1}$$

where M_L is the shift factor as defined as the molecular weight per unit contour length of the KP chain. The equilibrium conformational behavior of the KP chain without excluded volume may then be described by the two parameter λ^{-1} and M_L.

According to the Yamakawa theory,[9,21] A_2 of the KP chain may be written in the form,

$$A_2 = A_2^{(HW)} + A_2^{(E)} \tag{4.2}$$

where $A_2^{(HW)}$ is a part of A_2 without effects of chain ends and $A_2^{(E)}$ represents a contribution of the effects. We note that the superscript (HW) has been attached since the theory is originally formulated on the basis of the HW chain. In the theory, the excluded volume is incorporated by $n+1$ beads arrayed with spacing a between them along the KP chain contour, so that $L = na$. The $n-1$ intermediate beads are identical and the two end beads are different from the intermediate ones and also from each other in species. Identical excluded-volume interactions between intermediate beads are expressed in terms of the binary cluster integral β, which characterizes $A_2^{(HW)}$. In addition to β, two kinds of excess binary-cluster integrals β_1 and β_2 are introduced to express interactions between unlike (and like end) beads, β_1 being associated with one end bead and β_2 with two end beads, which characterize $A_2^{(E)}$.

The first term $A_2^{(\mathrm{HW})}$ on the right-hand side of eq 5.2 may be written in the form,

$$A_2^{(\mathrm{HW})} = \frac{N_\mathrm{A} B}{2{M_\mathrm{L}}^2}\, h\!\left(\frac{\tilde{\tilde{z}}}{\alpha_S^3(\tilde{z})}\right) \tag{4.3}$$

where N_A is the Avogadro constant, B is the excluded-volume strength defined by

$$B = \beta/a^2 \tag{4.4}$$

and h is the so-called h function that is the dimensionless function of the *intermolecular* scaled excluded-volume parameter $\tilde{\tilde{z}}$ divided by the cube of the gyration-radius expansion factor α_S as a function of the *intramolecular* scaled excluded-volume parameter $\tilde{z}$. The dimensionless quantities $\tilde{z}$ and $\tilde{\tilde{z}}$ are related to the (conventional) excluded-volume parameter z defined by

$$z = (3/2\pi)^{3/2}(\lambda B)(\lambda L)^{1/2} \tag{4.5}$$

by

$$\tilde{z} = \frac{3K(\lambda L)}{4} z \tag{4.6}$$

and

$$\tilde{\tilde{z}} = \frac{Q(\lambda L)}{2.865} z \tag{4.7}$$

respectively, where K and Q as functions of the reduced contour length λL represent effects of the chain stiffness on the intra- and intermolecular excluded-volume effects, respectively. Both the factors $3K/4$ and $Q/2.865$ become unity in the limit of $\lambda L \to \infty$ (random coil), so that $\tilde{z} = \tilde{\tilde{z}} = z$ and the above expression for $A_2^{(\mathrm{HW})}$ reduces to that of A_2 in the framework of the (conventional) two-parameter (TP) theory.[9,14] In the limit of $\lambda L \to 0$ (rigid rod), on the other hand, K and therefore $\tilde{z}$ (intramolecular excluded volume) vanishes. The h function is given by eq 8.110 of ref 9 (or eq 14 of ref 20), the Domb–Barrett equation[28] given by eq 8.57 of ref 9 (or eq 6 of ref 20) is adopted for α_S, and K and Q are given by eqs 8.46 and 8.102 of ref 9 (or eqs 8 and 17 of ref 20), respectively. We do not reproduce their explicit forms, for simplicity.

The second term $A_2^{(\mathrm{E})}$ on the right-hand side of eq 5.2 may be written in the form,

$$A_2^{(\mathrm{E})} = \frac{2N_\mathrm{A}\beta_1}{M_0}\,\frac{1}{M} + 2N_\mathrm{A}(\beta_2 - 2\beta_1)\frac{1}{M^2} \tag{4.8}$$

with M_0 the molecular weight of the bead. We note that $A_2^{(\mathrm{E})}$ rapidly decreases to 0 with increasing M and has been shown to be very small for $M \gtrsim 10^5$ for all the vinyl polymers examined so far.[9,22–25] It is seen from eqs 1—7 that the theoretical values of A_2 may be

calculated for a given polymer by the use of proper values of λ^{-1}, M_L, and λB along with β_1 and β_2.

As in the cases of other vinyl polymers, we adopt the touched-bead model as a hydrodynamic model,[9] in which N identical spherical beads of diameter d_b are arrayed with spacing d_b between them along the KP chain of total contour length $L = Nd_b$, its $[\eta]$ $(= [\eta]_0)$ without excluded volume may be written in the form,[9,29]

$$[\eta]_0 = \frac{1}{\lambda^2 M_L} f_{\eta,\mathrm{KP}}(\lambda L; \lambda d_b) \tag{4.9}$$

where $f_{\eta,\mathrm{KP}}$ as a function of λL and the reduced bead diameter λd_b is defined by

$$f_{\eta,\mathrm{KP}}(\lambda L; \lambda d_b) = \lambda^{-1} M_L [\eta]_{\mathrm{KP}} \tag{4.10}$$

with $[\eta]_{\mathrm{KP}}$ being given by eq 6.111 with eqs 6.113 and 6.117 of ref 9 (or eq 15 with eqs 17 and 22 of ref 29). We note that $[\eta]_{\mathrm{KP}}$ in refs 9 and 29 is written in units of $(\lambda^{-1})^3$ and the quantities L and d_b in those references means the reduced quantities λL and λd_b, respectively. We do not reproduce the explicit form of $[\eta]_{\mathrm{KP}}$, for simplicity.

In the framework of the quasi-two-parameter (QTP) scheme or the Yamakawa–Stockmayer–Shimada scheme[9,30–32] on the basis of the HW (or KP) chain, $[\eta]$ of the KP touched-bead model with excluded volume may be given by

$$[\eta] = [\eta]_0 \, \alpha_\eta^3(\tilde{z}) \tag{4.11}$$

where $[\eta]_0$ is given by eq 5.9 and α_η is the viscosity-radius expansion factor as a function of $\tilde{z}$ and may be given by the Barrett equation,[33] whose explicit form is not reproduced here, for simplicity. We note that all the expansion factors, including α_η, are functions only of $\tilde{z}$, in the QTP scheme. Then the theoretical values of $[\eta]$ may be calculated for a given polymer by the use of proper values of λ^{-1}, M_L, λB, and λd_b.

Now we are in a position to make a comparison of KP theories of A_2 and $[\eta]$ with the experimental data, from which we may in principle determine the values of λ^{-1}, M_L, λB, and λd_b along with β_1 and β_2 for linear PNIPA. As mentioned above, however, the range of M_w of the linear PNIPA samples is not wide enough to determine unambiguously all those parameters. Further, the double-logarithmic plots of A_2 and $[\eta]$ against M_w shown in Figures 4.2 and 3 ($\bigcirc$), respectively, do not have any characteristic features but are rather monotonous over the whole range of M_w examined. In order to reduce the number of the parameters to be determined, therefore, we assume the value of M_L to be 45 Å^{-1}, which has been calculated from the value 113 of the molecular weight of the repeat

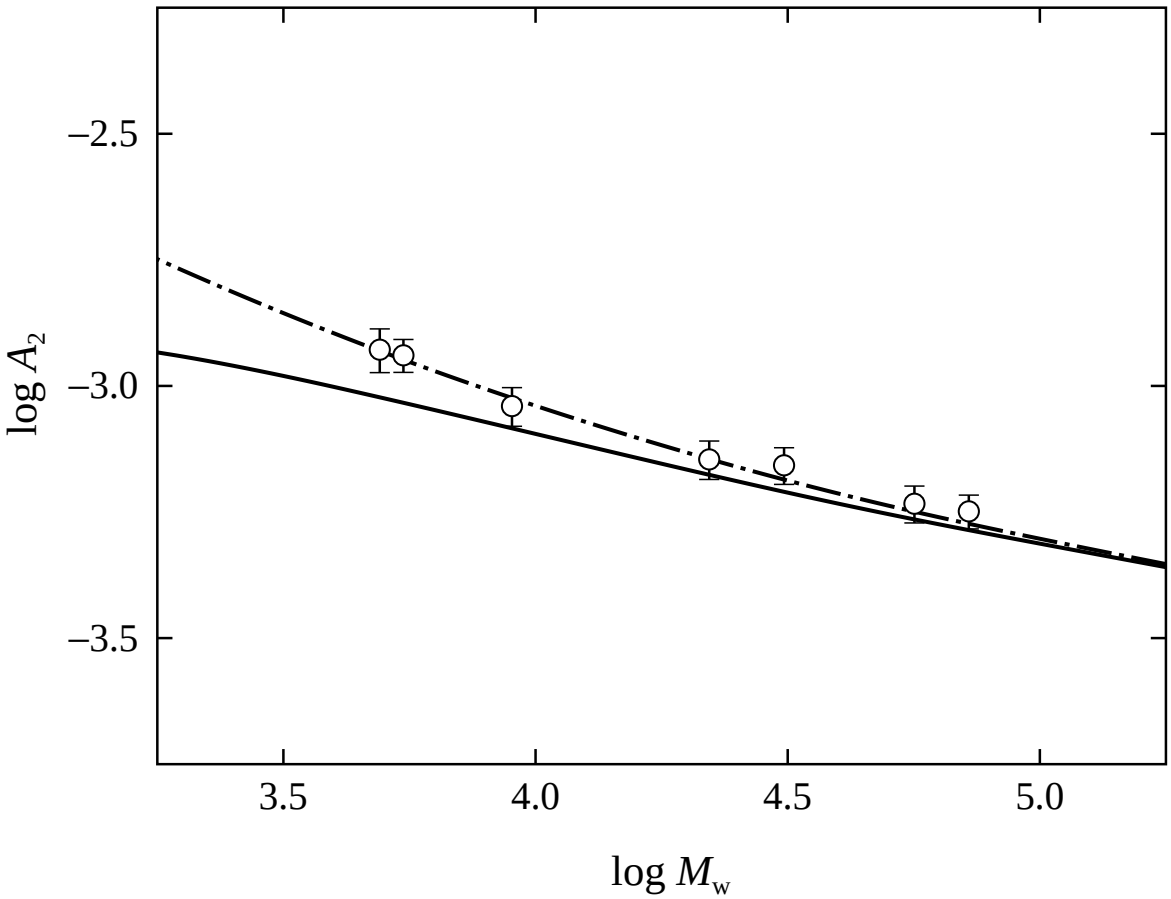

Figure 4.5. Double-logarithmic plots of A_2 (in $cm^3\,mol/g^2$) against M_w for the L samples in methanol at 25.0 °C. The solid curve represents the best-fit KP theory values without the effects of chain end and the dot-dashed curve represents those with the effects (see the text).

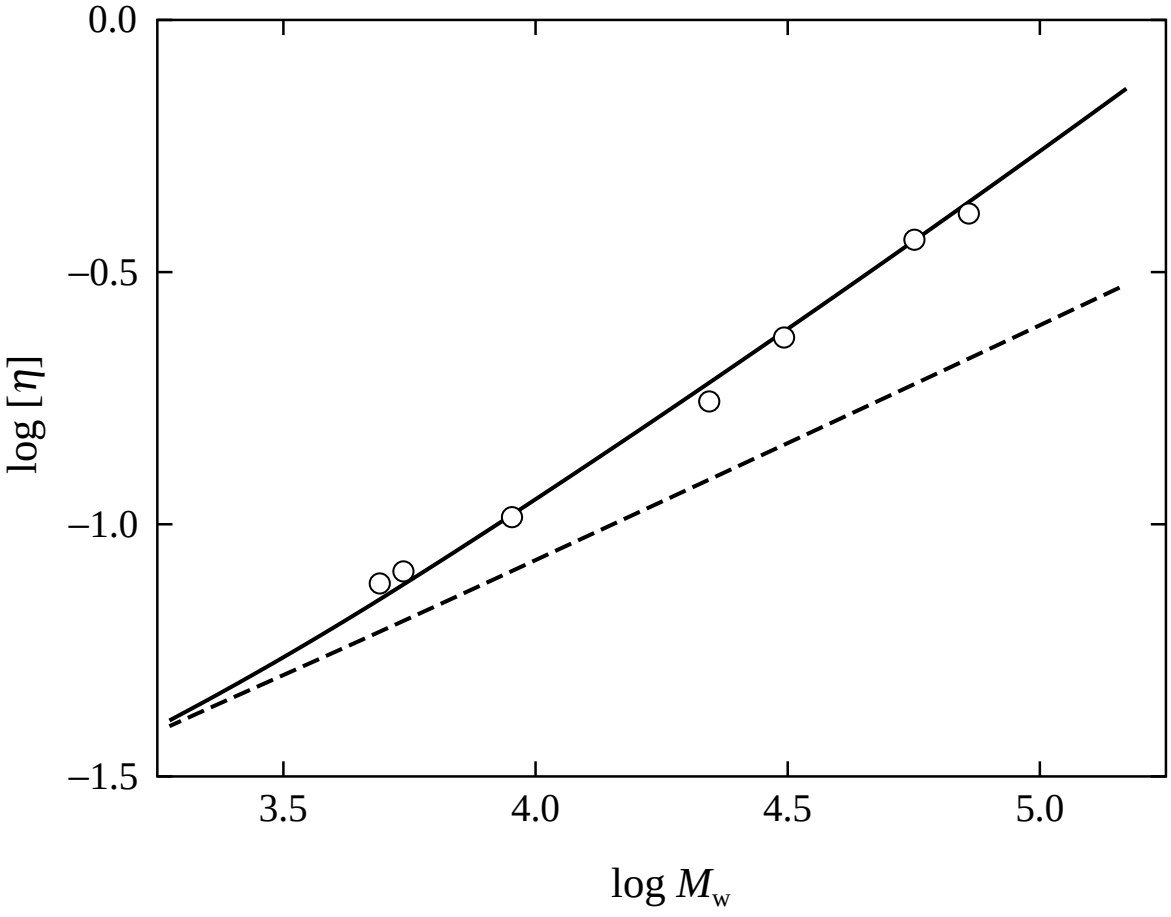

Figure 4.6. Double-logarithmic plots of $[\eta]$ (in dL/g) against M_w for the L samples in methanol at 25.0 °C. The solid curve represents the best-fit perturbed KP theory values and the dashed curve represents the corresponding unperturbed values (see the text).

unit and its length[34,35] 2.5 Å in the all-*trans* conformation. We then attempt to determine the three parameters λ^{-1}, λB, and λd_b from a simultaneous comparison of the KP theories of A_2 and $[\eta]$ with the experimental data. For A_2, the comparison is restricted to the range of $M_w \gtrsim 5 \times 10^4$ where the effects of chain ends is considered to be sufficiently small to neglect the contribution of $A_2^{(E)}$ on the right-hand side of eq 5.2. As for the data for A_2 in the range of $M_w \lesssim 5 \times 10^4$, we analyze them to evaluate β_1 and β_2 included in $A_2^{(E)}$ given by eq 4.8 by the use of the values of $A_2^{(HW)}$ calculated from eq 5.3 with the values of λ^{-1} and λB so determined.

Figures 4.5 and 6 show double-logarithmic plots of A_2 (in cm^3mol/g^2) and $[\eta]$ (in dL/g) against M_w for the L samples in methanol at 25.0 °C, where the solid curves represent the best-fit KP theory values of A_2 without the effects of chain ends, *i.e.*, $A_2^{(HW)}$, calculated from eq 5.3 with eqs 5.4—5.7 and those of $[\eta]$ calculated from eq 4.11 with eqs 5.9 and 4.10, respectively, with $\lambda^{-1} = 18$ Å, $\lambda B = 0.60$, and $\lambda d_b = 0.58$. We note that relative errors in the values of λ^{-1}, λB, and λd_b are estimated to be ±10%, ±15%, and ±12%, respectively, at most. The value 18 Å of λ^{-1} so determined is almost the same as the values $\lambda^{-1} = 20.6$—27.0 Å and 12.7—18.7 Å determined for atactic polystyrene (a-PS) with $f_r = 0.59$ in cyclohexane at 34.5 °C (Θ) and polyisobutylene (PIB) in isoamyl isovalerate at 25.0 °C (Θ),[9] respectively, indicating that PNIPA in methanol is as flexible as typical flexible polymers. The value $10._4$ Å of d_b evaluated from the above-mentioned values of λ^{-1} and λd_b seems reasonable.

In Figure 4.5, the experimental value deviates upward progressively from the $A_2^{(HW)}$ value (solid curve) as M_w is decreased from *ca.* 5×10^4 because of the effects of chain ends. The dot-dashed curve in the figure represents the value of A_2 calculated from eq 5.2 with the $A_2^{(HW)}$ value represented by the solid curve and the $A_2^{(E)}$ calculated from eq 4.8 with the values 100 and 210 $Å^3$ of β_1 and β_2, respectively, where we have taken the monomer unit of the PNIPA chain as a single bead ($M_0 = 113$). We note that the values of β_1 and β_2 for PNIPA in methanol at 25.0 °C are comparable to those obtained for other flexible polymers in good solvents.[22–25]

In Figure 4.6, the dashed curve represents the unperturbed value $[\eta]_0$ of $[\eta]$ calculated from eq 5.9 with eq 4.10 with the above-mentioned values of λ^{-1} and λd_b. It is seen that the experimental value deviates upward progressively from the $[\eta]_0$ value as M_w is increased because of the intramolecular excluded-volume effect.

It should be noted here that the PNIPA chain in aqueous solution might become stiffer than that in methanol due to the hydration of the solvent water. Unfortunately, however, it is difficult to carry out fine molecular characterization of the chain in aqueous solution in the same manner as above, since the cloud point in aqueous PNIPA solution remarkably decreases with decreasing temperature, as shown in the previous subsection.

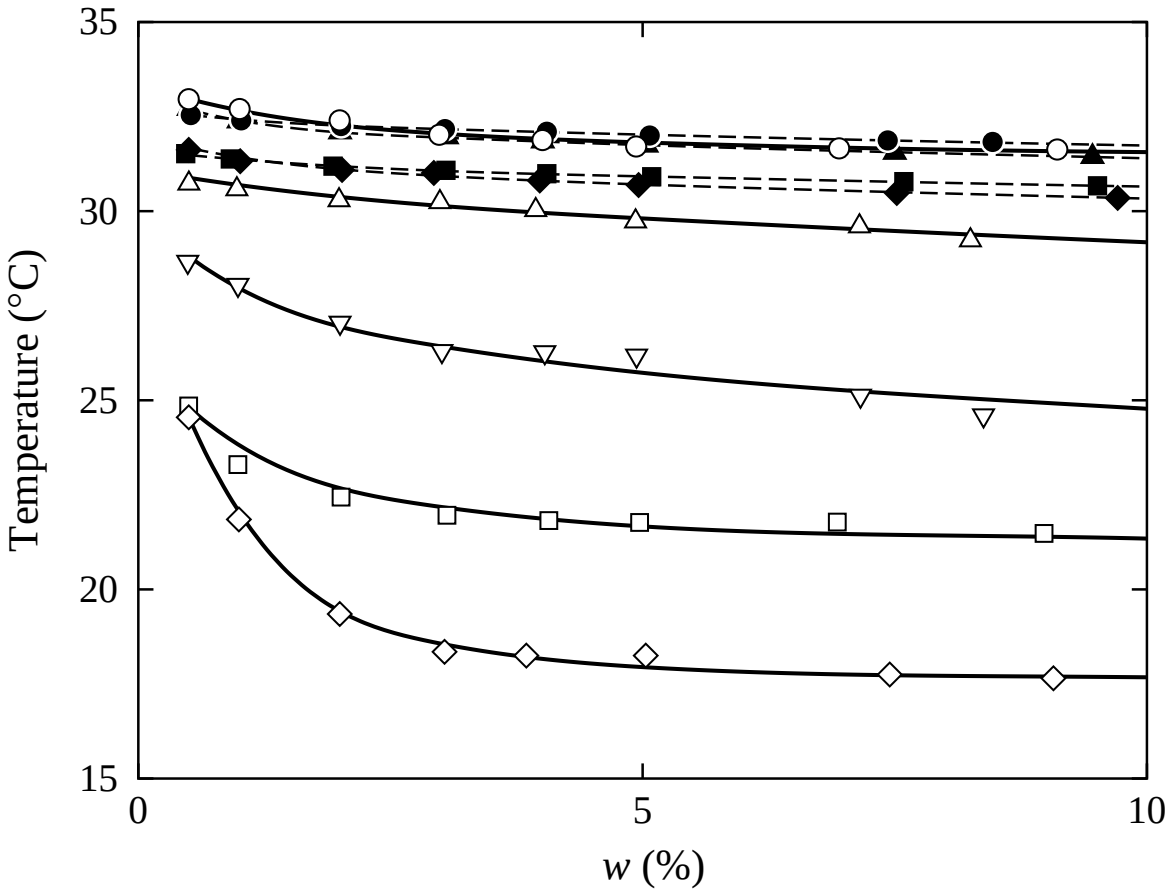

Figure 4.7. Cloud-point curves in aqueous PNIPA solutions. The unfilled symbols represent the cloud points in aqueous solutions of the L samples L0.6 (◇), L1 (□), L2 (▽), L3 (△), and L7 (○) and the filled symbols represent those of the T and B samples T5 (▲), T13 (●), B5 (◆), and B14 (■) which have been reproduced from Figure 2.3. The solid and dashed curves connect smoothly the cloud points of the L samples and the T and B samples, respectively.

4.4.2 Cloud-Point Curve in Aqueous Solutions

Figure 4.7 shows cloud-point curves in aqueous PNIPA solutions. The unfilled symbols represent the cloud points for the L samples L0.6 (◇), L1 (□), L2 (▽), L3 (△), and L7 (○), and the filled symbols represent those previously determined for the T and B samples T5 (▲) with $M_w = 5.17 \times 10^4$, T13 (●) with $M_w = 1.31 \times 10^5$, B5 (◆) with $M_w = 4.65 \times 10^4$, and B14 (■) with $M_w = 1.44 \times 10^5$, which have been reproduced from Figure 2.3. The solid and dashed curves connect smoothly the cloud points for the L samples and the T and B samples, respectively. We note that all the L, T, and B samples have almost the same values of f_r ($= 0.50 - 0.52$).

It is interesting to see that the cloud point in the aqueous solutions of the L samples decreases remarkably with decreasing M_w, especially in the range of rather large w ($\gtrsim 2\%$). Such behavior sharply contradicts the familiar conclusion derived from the polymer solution thermodynamics. It is known that amphiphilic A-B diblock[36,37] or A-B-A triblock[38] copolymers with the B block being PNIPA form aggregates and the cloud points in their aqueous solutions are lower than that in aqueous PNIPA solution. Further, it was pointed out by Ito and Ishizone[7] that the hydrophobic diphenylmethyl group at the initiating end of the L sample affects the cloud points in its aqueous solutions. For PNIPA samples synthesized by radical polymerization, it was also pointed out by Duan *et al.*[39] and by Furyk *et al.*[40] that the cloud points of their aqueous solutions become lower as hydrophobicity of the end group is increased. It may therefore be considered that the cloud point in aqueous solutions of the L samples is mainly governed by the diphenylmethyl group and decreases as its effect is relatively increased by decreasing M_w.

At first we expected that the cloud points in the aqueous solutions of the L samples without branch points would be higher than those for the T and B samples with branch points. As seen from Figure 4.7, however, the cloud point in the range of $w \gtrsim 3\%$ is still lower for L7 than for T13 due to the effect of the diphenylmethyl group whose hydrophobicity seems to be larger than that of the isobutyronitrile group at the ends of the T and B samples. In this connection, we may conjecture that the decrease in the cloud point with decreasing M_w and with increasing the number of branch points observed in Chapters 2 and 3 (and also shown by the filled symbols in Figure 4.7) for the aqueous solutions of the T and B samples is also caused by the hydrophobicity of the end group.

Considering the above-mentioned situation along with the fact that the transmittance curves shown in Figure 4.4 do not show sharp decrease as usually observed in common LCST miscibility behavior, there arises a doubt that the cloud point determined from the transmittance of the light through the aqueous PNIPA solutions does not necessarily correspond to the binodal point, at which the macroscopic phase separation occurs.

4.5 Concluding Remarks

We have determined A_2 and $[\eta]$ in methanol at 25.0 °C for the PNIPA samples synthesized by living anionic polymerization following the procedure of Ishizone and Ito,[5–7] which we call L samples, and also for those by radical polymerization in *tert*-butanol and benzene by the use of AIBN as an initiator, which we call T and B samples, respectively. Note that the L samples are linear while the T and B samples have a small number of branch points. It has been found for both A_2 and $[\eta]$ that their values for the three kinds of samples agree well with each other in the range of small M_w ($\lesssim 3 \times 10^4$) but deviate from each other as M_w is increased from 3×10^4, the value for the L sample being the largest and that for B sample the smallest. Such deviations may be regarded as arising from the difference in the primary structure of the samples, *i.e.*, the average chain dimension is the largest for the L sample having no branch point and the smallest for the B sample having the largest number of branch points. The number of the branch points in the T and B samples seems to become very small for $M_w \lesssim 3 \times 10^4$. From a simultaneous analysis of A_2 and $[\eta]$ for the L samples on the basis of the KP chain with excluded volume, the stiffness parameter λ^{-1} has been estimated to be 18 Å, which is almost the same as the values for typical flexible polymers, *e.g.*, a-PS and PIB.

For the L samples, the cloud point has also been determined in their aqueous solutions in the range of $0.5\% \lesssim w \lesssim 10\%$ by monitoring the transmittance of light through the solutions in the heating process. It has then been found that the cloud point decreases remarkably with decreasing M_w, especially in the range of $w \gtrsim 2\%$, because of the effects of the hydrophobic chain end groups of the L samples. It is more important to note that the transmittance curve for each solution does not show sharp decrease as usually observed in common LCST miscibility behavior. Such a result implies that the cloud point does not necessarily correspond to the binodal one as far as the aqueous PNIPA solutions are concerned.

References

1. H. G. Schild, *Prog. Polym. Sci.*, **17**, 163 (1992).
2. T. Kawaguchi, Y. Kojima, M. Osa, and T. Yoshizaki, *Polym. J.*, **40**, 455 (2008).
3. T. Kawaguchi, Y. Kojima, M. Osa, and T. Yoshizaki, *Polym. J.*, **40**, 528 (2008).
4. T. Kitayama, W. Shibuya, and K. Katsukawa, *Polym. J.*, **34**, 405 (2002).
5. T. Ishizone and M. Ito, *J. Polym. Sci., Polym. Chem. Ed.*, **40**, 4328 (2002).
6. M. Ito and T. Ishizone, *Designed Monomers and Polymers*, **7**, 11 (2004).
7. M. Ito and T. Ishizone, *J. Polym. Sci., Polym. Chem. Ed.*, **44**, 4832 (2006).

8. O. Kratky and G. Porod, *Recl. Trav. Chim. Pays-Bas*, **68**, 1106 (1949).
9. H. Yamakawa, "Helical Wormlike Chains in Polymer Solutions," Springer, Berlin, 1997.
10. Gj. Deželić and J. Vavra, *Croat. Chem. Acta*, **38**, 35 (1966).
11. G. C. Berry, *J. Chem. Phys.*, **44**, 4550 (1966).
12. B. L. Johnson and J. Smith, In *Light Scattering from Polymer Solutions*; M. B. Huglin, Ed.; Academic Press: London, 1972; Chapter 2.
13. Y. Isobe, D. Fujioka, S. Habaue, and Y. Okamoto, *J. Am. Chem. Soc.*, **123**, 7180 (2001) and its supporting information.
14. H. Yamakawa, "Modern Theory of Polymer Solutions," Harper & Row, New York, 1971. Its electronic edition is available on-line at the URL: `http://www.molsci.polym.kyoto-u.ac.jp/archives/redbook.pdf`
15. H. Utiyama and M. Kurata, *Bull. Inst. Chem. Res. Kyoto Univ.*, **42**, 128 (1964).
16. H. Utiyama, *J. Phys. Chem.*, **69**, 4138 (1965).
17. K. Nagai, *Polym. J.*, **3**, 67 (1972).
18. H. Yamakawa, M. Fujii, and J. Shimada, *J. Chem. Phys.*, **71**, 1611 (1979).
19. M. Nakatsuji, Y. Ogata, M. Osa, T. Yoshizaki, and H. Yamakawa, *Macromolecules*, **34**, 8512 (2001).
20. M. Nakatsuji, M. Hyakutake, M. Osa, and T. Yoshizaki, *Polym. J.*, **40**, 566 (2008).
21. H. Yamakawa, *Macromolecules*, **25**, 1912 (1992).
22. Y. Einaga, F. Abe, and H. Yamakawa, *Macromolecules*, **26**, 6243 (1993).
23. F. Abe, Y. Einaga, and H. Yamakawa, *Macromolecules*, **27**, 3262 (1994).
24. M. Kamijo, F. Abe, Y. Einaga, and H. Yamakawa, *Macromolecules*, **28**, 4159 (1995).
25. W. Tokuhara, M. Osa, T. Yoshizaki, and H. Yamakawa, *Macromolecules*, **36**, 5311 (2003).
26. T. Mizuno, K. Terao, Y. Nakamura, and T. Norisuye, *Macromolecules*, **38**, 5311 (2005).
27. M. Osa, T. Yoshizaki, and H. Yamakawa, *Macromolecules*, **33**, 4828 (2000).
28. C. Domb and A. J. Barrett, *Polymer*, **17**, 179 (1976).
29. T. Yoshizaki, I. Nitta, and H. Yamakawa, *Macromolecules*, **21**, 165 (1988).
30. H. Yamakawa and W. H. Stockmayer, *J. Chem. Phys.*, **57**, 2843 (1972).
31. H. Yamakawa and J. Shimada, *J. Chem. Phys.*, **83**, 2607 (1985).
32. J. Shimada and H. Yamakawa, *J. Chem. Phys.*, **85**, 591 (1986).
33. A. J. Barrett, *Macromolecules*, **17**, 1566 (1984).
34. K. Kubota, S. Fujishige, and I. Ando, *Polym. J.*, **22**, 15 (1990).
35. K. Kubota, K. Hamano, N. Kuwahara, S. Fujishige, and I. Ando, *Polym. J.*, **22**, 1051 (1990).

36. J. E. Chung, M. Yokoyama, K. Suzuki, T. Aoyagi, Y. Sakurai, and T. Okano, *Colloids Surf. B*, **9**, 37 (1997).
37. J. E. Chung, M. Yokoyama, T. Aoyagi, Y. Sakurai, and T. Okano, *J. Controlled Release*, **53**, 119 (1998).
38. P. Kujawa, F. Segui, S. Shaban, C. Diab, Y. Okada, F. Tanaka, and F. M. Winnik, *Macromolecules*, **39**, 341 (2006).
39. Q. Duan, A. Narumi, Y. Miura, X. Shen, S. Sato, T. Satoh, and T. Kakuchi, *Polym. J.*, **38**, 306 (2006).
40. S. Furyk, Y. Zhang, D. Ortiz-Acosta, P. S. Cremer, and D. E. Bergbreiter, *J. Polym. Sci., Polym. Chem. Ed.*, **44**, 1492 (2006).

5 Is a "Cloud-Point Curve" in Aqueous Poly(*N*-isopropylacrylamide) Solution the Binodal?

5.1 Introduction

As mentioned in Chapters 2, 3, and 4, we found that aqueous solution behavior of poly(*N*-isopropylacrylamide) (PNIPA) is not so simple as usually considered, as follows. (1) The cloud points in aqueous solutions of PNIPA samples synthesized by radical polymerization with azobis(isobutyronitrile) (AIBN) as an initiator are appreciably different from each other if the solvents used for the polymerization are different, even though the samples have the same weight-average molecular weight M_w and stereochemical composition specified by the fraction f_r of racemo diads.[1] (2) Those samples have branched structure and the number of branch points depends on the kind of solvent used for the radical polymerization.[2] (3) The cloud point in aqueous solutions of linear PNIPA samples synthesized by living anionic polymerization, which have a diphenylmethyl group at the initiating chain end, decreases remarkably with decreasing M_w in the range of $5 \times 10^3 \lesssim M_w \lesssim 7 \times 10^4$.[3] The implication is that the cloud point in aqueous PNIPA solutions is governed not only by the hydrogen bonds between PNIPA and surrounding water molecules but also by the end group and primary structure of PNIPA chains.

The above-mentioned cloud point has been determined as usual as a temperature at which the transmittance of light passing through aqueous PNIPA solutions becomes equal to a threshold value (*e.g.*, 90%). If the transmittance changes steeply with increasing (or decreasing) temperature, the determination is unambiguous and the cloud point so determined may be equated to the binodal point. Unfortunately, however, the situation is rather unclear in the solutions. Figure 5.1 reproduces the plots in Chapter 4 of the (relative) transmittance against temperature for the aqueous solutions of the above-mentioned linear PNIPA samples with $M_w = 5.47 \times 10^3$, 8.98×10^3, 2.21×10^4, 3.11×10^4, and 7.23×10^4, at almost the same concentration *ca.* 5 wt% and in a heating process at a rate of *ca.* 1.5 °C/h. It is important to see that the transmittance for each solution decreases rather gently with increasing temperature, which raises a question whether or not the decrease in the transmittance corresponds to the macroscopic phase separation.

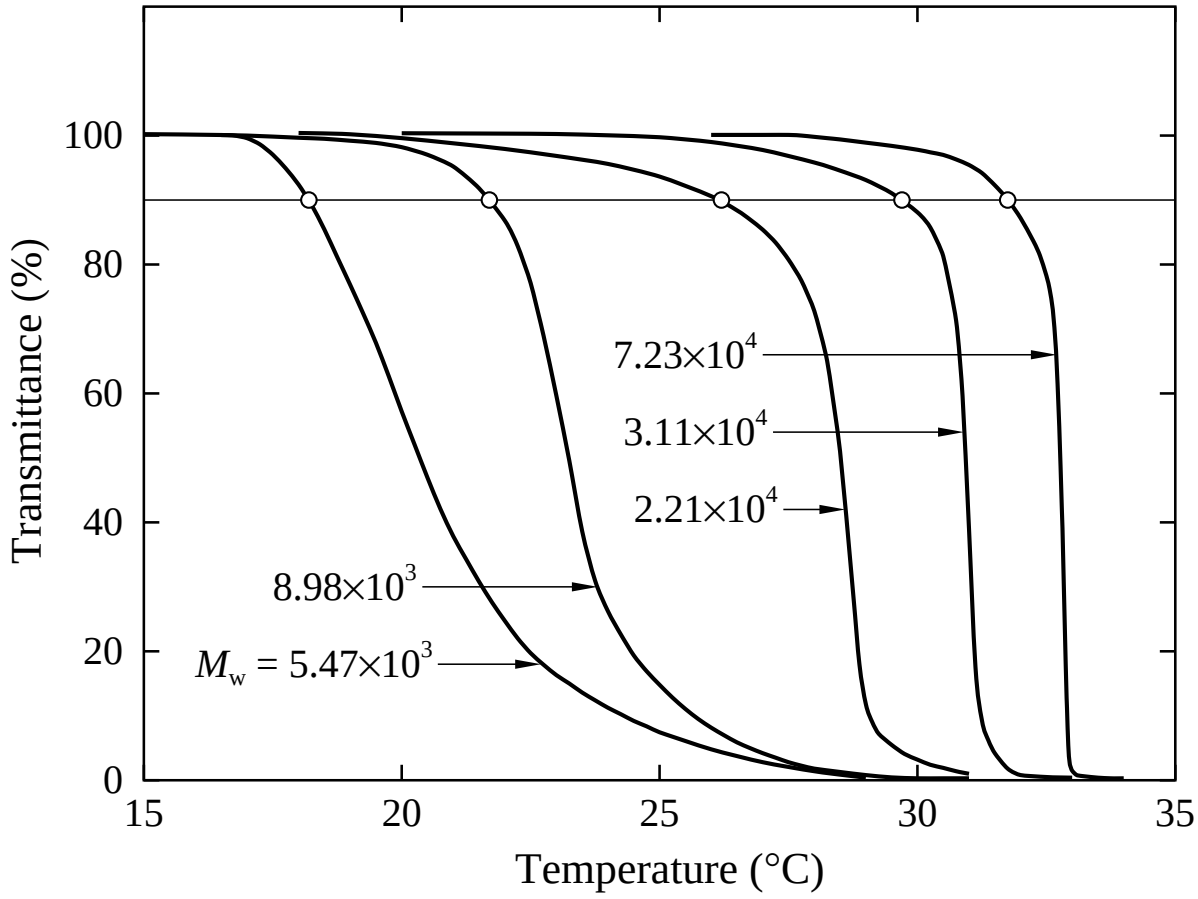

Figure 5.1. Temperature dependence of the transmittance of light passing through the aqueous solutions of the linear PNIPA samples with $M_w = 5.47\times10^3$, 8.98×10^3, 2.21×10^4, 3.11×10^4, and 7.23×10^4 at $w = 5.03$, 4.97, 4.94, 4.93, and 4.94%, respectively (Chapter 4). The horizontal line indicates the threshold value (90%) and the unfilled circle on each curve indicates the cloud point.

In this chapter, we make a rather detailed examination of an aqueous PNIPA solution in the vicinity of its cloud point in order to resolve the above question. If the decrease in the transmittance for the solution really reflects the macroscopic phase separation, it should continue to decrease to 0% accompanying spontaneous change in the solution, even though the solution temperature is fixed at a constant value slightly higher than the value at which the decrease begins. The first examination we carry out is therefore an observation of the transmittance under a series of changes in temperature different from the above-mentioned monotonous heating. If the decrease in the transmittance does not reflect the phase separation, it may be regarded as arising from formation of large aggregates of some kinds. Then we carry out static and dynamic light scattering (LS) measurements, as the second examination, of the solutions at some temperatures considerably lower than their cloud points in order to verify the existence of such aggregates.

5.2 Experimental

5.2.1 Materials

The two PNIPA samples L7 and T7 used in this work are fractions separated by fractional precipitation from original samples synthesized by living anionic polymerization in Chapter 4 following the procedure of Ishizone and Ito[4–6] and by radical polymerization in *tert*-butanol by the use of AIBN as an initiator in Chapters 2 and 3, respectively. The sample L7 is linear and its two chain ends are a diphenylmethyl group (initiating end) and a hydrogen atom (terminal end). On the other hand, the sample T7 has branched structure[2] and almost all its chain ends are considered to be isobutyronitrile groups derived from the initiator AIBN, although the detailed information could not be obtained. In the second, third, and fourth columns of Table 5.1 are reproduced from Chapters 3 and 4, the values of M_{w} determined from LS measurements in methanol at 25.0 °C, those of the ratio of M_{w} to the number-average molecular weight M_{n} determined from analytical gel permeation chromatography, and those of f_{r} determined from ^{1}H NMR, respectively, for the samples L7 and T7. It is seen from the f_{r} values that the two samples have almost the same stereochemical composition.

The atactic polystyrene (a-PS) sample F20 used in this Chapter is the standard one supplied by Tosoh Co., Ltd. The nominal values of its M_{w} and $M_{\mathrm{w}}/M_{\mathrm{n}}$ are 1.9×10^5 and 1.04, respectively, according to the supplier.

Water was highly purified through a Simpli Lab water purification system of Millipore Co., its resistivity being 18.2 MΩ·cm. Methanol and cyclohexane were purified by distillation after refluxing over calcium hydride and sodium, respectively, for *ca.* 6 h.

Table 5.1. Poly(*N*-isopropylacrylamide) Samples Synthesized by Living Anionic (L7) and Radical (T7) Polymerization[a]

sample	M_w	M_w/M_n	f_r
L7	7.23×10^4	1.12	0.50
T7	7.19×10^4	1.11	0.52

[a]All the values are reproduced from Chapters 3 and 4, where the values of M_w/M_n were determined by analytical GPC using standard PS samples as reference standards.

5.2.2 Transmittance of Light

The intensity of light passing through aqueous solutions of the sample L7 at the weight fraction $w = 1.01$ and 4.91% and of the sample T7 at $w = 0.98\%$ and also that through a cyclohexane solution of the a-PS sample F20 at $w = 3.14\%$ were monitored. All the measurements were carried out by the use of a self-made apparatus with incident light of wavelength 650 nm from a laser diode module. A cylindrical cell of outer diameter 10 mm containing a given test solution was immersed in a water bath, the test solution in the cell being stirred continuously.

In order to determine the cloud point of each aqueous PNIPA solution, the temperature of the water bath was controlled to increase at a rate of *ca.* 1.5 °C/h. During continuous increase in temperature from 26 °C to 35 °C, the intensity of light passing through the cell was monitored by a photodiode. The output of the photodiode along with the solution temperature measured simultaneously by the use of a platinum resistance thermometer combined with a programmable digital multimeter (Yokokawa 7555) was recorded on a personal computer at intervals of 10 s. Then, the (relative) transmittance as defined as the ratio of the intensity of light through a test solution at a temperature to that at a lower temperature at which the test solution may be regarded as transparent was determined as a function of temperature. Each solution was prepared gravimetrically and made homogeneous by continuous stirring for 2 days at *ca.* 5 °C.

As mentioned in Introduction, transmittance measurements were carried out for the aqueous solution of the sample L7 at 4.91% under the series of changes in temperature as follows: the temperature was first increased at the rate of *ca.* 1.5 °C/h from *ca.* 26 °C where the transmittance is *ca.* 100%, then kept at a constant value when the

transmittance became *ca.* 80%, and finally increased again at the rate of *ca.* 1.5 °C/h until the transmittance decreased to zero (*ca.* 35 °C) or decreased inversely at a rate of *ca.* −1.5 °C/h until the transmittance recovered to be *ca.* 100% (*ca.* 25 °C).

For comparison, a similar measurement was carried out for the cyclohexane solution of the a-PS sample F20 at $w = 3.14\%$ under the series of changes in temperature as follows: the temperature was first decreased at a rate of *ca.* −1.0 °C/h from *ca.* 27 °C where the transmittance is *ca.* 100%, then kept at a constant value when the transmittance became *ca.* 95%, and finally decreased again at the rate of *ca.* −1.0 °C/h until the transmittance decreased to zero (*ca.* 21 °C) or increased inversely at a rate of *ca.* 1.0 °C/h until the transmittance recovered to be *ca.* 100% (*ca.* 28 °C). Remember that the solution shows upper-critical-solution-temperature (UCST) miscibility behavior. The solution was prepared gravimetrically and made homogeneous by continuous stirring for 2 days at *ca.* 50 °C.

5.2.3 Static Light Scattering

Static LS measurements were carried out for the aqueous solutions of the sample L7 at $w = 0.103$ and 1.35% and of the sample T7 at $w = 0.102$ and 1.36%, each at 15.0, 20.0, and 25.0 °C, by the use of a Fica 50 light scattering photometer with vertically polarized incident light of wavelength $\lambda_0 = 436$ nm. For a calibration of the apparatus, the intensity of light scattered from pure benzene was measured at 25.0 °C at the scattering angle $\theta = 90°$, where the Rayleigh ratio $R_{\mathrm{Uu}}(90°)$ of pure benzene was taken as 46.5×10^{-6} cm^{-1}.[7] The depolarization ratio ρ_{u} of pure benzene at 25.0 °C was determined to be 0.41 ± 0.01 by the method of Rubingh and Yu.[8]

Each solution was prepared gravimetrically and made homogeneous by continuous stirring at *ca.* 5 °C for 2 days. Its weight concentration was converted to the polymer mass concentrations c by the use of its density calculated with the partial specific volume v_2 of the sample in water and with the density ρ_0 of water. The v_2 value was determined by the use of an oscillating U-tube density meter (Anton-Paar, DMA5000). The values of v_2 so determined in water at 15.0, 20.0, and 25.0 °C are 0.849, 0.854, and 0.858 cm^3/g, respectively, for the sample L7 and 0.861, 0.866, and 0.869 cm^3/g, respectively, for the sample T7. As for the values of ρ_0 of water, we used 0.99910, 0.99820, and 0.99704 g/cm^3 at 15.0, 20.0, and 25.0 °C, respectively.[9]

Each solution was poured into a cylindrical optical cell through a polyvinylidene fluoride membrane of pore size 0.10 μm in an atmosphere of *ca.* 5 °C. From the time the cell was immersed in thermo-controlled *p*-xylene in cylindrical quartz vessel set in the photometer, the excess unpolarized (Uv) components ΔR_{Uv} of the reduced scattered intensity at $\theta = 90°$ was recorded as a function of elapsed time t_{e} up to $t_{\mathrm{e}} \simeq 40$ h. At $t_{\mathrm{e}} \simeq 1$,

3, 6, 12, 24, and 36 h, ΔR_{Uv} was measured also at $\theta = 30.0$, 37.5, 45.0, 60.0, 75.0, 105.0, 120.0, 135.0, and 142.5° to examine the dependence of ΔR_{Uv} on θ.

For the values of the refractive index n_0 of water at $\lambda_0 = 436$ nm, we used 1.3401, 1.3396, and 1.3390 at 15.0, 20.0, and 25.0 °C, respectively, which were evaluated from $n_0 = 1.3390$ at 25.0 °C and the temperature coefficient $\mathrm{d}n_0/\mathrm{d}T = -1.1 \times 10^{-4}\mathrm{deg}^{-1}$.[10]

5.2.4 Dynamic Light Scattering

Dynamic LS measurements were carried out for methanol (good solvent) solutions of the samples L7 and T7 at 25.0 °C and also their aqueous solutions in the same solution conditions as those in the above-mentioned LS measurements. For the measurements, a Brookhaven Instrument model BI-200SM light scattering goniometer was used with vertically polarized incident light of $\lambda_0 = 532$ nm from a Spectra-Physics model Millenia Pro 2s Nd:YVO_4 laser. The photomultiplier tube used was EMI 9893B/350, whose output was processed by a Brookhaven Instrument model BI-9000AT Digital Correlator. (An electric shutter was attached to the original detector alignment in order to monitor the dark count automatically.)

The normalized autocorrelation function $g^{(2)}(t)$ of the scattered light intensity $I(t)$ at time t was measured for the methanol solutions at θ ranging from 20 to 50°. The time-averaged intensity $\bar{I}$ along with $g^{(2)}(t)$ were measured for the aqueous solutions at θ ranging from 20 to 120°. For a calibration of the apparatus, which is necessary for an evaluation of ΔR_{Uv} from $\bar{I}$ for each aqueous solution, $\bar{I}$ was measured also for pure toluene at 25.0 °C and at $\theta = 90°$, where $R_{\mathrm{Uv}}(90°)$ of pure toluene was taken as 27.4×10^{-6} cm^{-1}.[11]

The most concentrated solution of each sample in methanol was prepared gravimetrically and made homogeneous by continuous stirring at room temperature for 2 days. The methanol solutions of lower concentrations were obtained by successive dilution. The weight concentration of each methanol solution was converted to c by the use of its density calculated with $v_2 = 0.901$ and 0.903 cm^3/g for the samples L7 and T7, respectively, in methanol at 25.0 °C, which was determined by the use of the above-mentioned oscillating U-tube density meter, and with $\rho_0 = 0.7866$ $\mathrm{g/cm}^3$ of methanol at 25.0 °C.[10] Each methanol solution was poured into cylindrical optical cell through a Teflon membrane of pore size 0.10 μm in an atmosphere of room temperature. We note that the measurement for each methanol solution was started as soon as its temperature became 25.0 °C. As for the aqueous solutions, each solution was prepared in the same manner as in the case of the above-mentioned static LS and its $g^{(2)}(t)$ and $\bar{I}$ were measured at $t_{\mathrm{e}} \simeq 1$, 3, 6, 12, 24, and 36 h.

The value of n_0 of methanol at $\lambda_0 = 532$ nm and at 25.0 °C is 1.3289, which was estimated by a linear interpolation of the plot of n_0 against λ_0^{-2} with the literature values[10]

1.3337 and 1.3284 of n_0 of methanol at $\lambda_0 = 436$ and 546 nm, respectively, and at 25.0 °C. The value of n_0 of water at $\lambda_0 = 532$ nm and at 25.0 °C was similarly estimated to be 1.3345 from the literature values[10] 1.3390 and 1.3340 of n_0 of water at 25.0 °C and at $\lambda_0 = 436$ and 546 nm, respectively. The values of n_0 of water at $\lambda_0 = 532$ nm and at 15.0 and 20.0 °C are 1.3356 and 1.3350, respectively, which were evaluated from the above-mentioned n_0 value 1.3345 at 25.0 °C and $\mathrm{d}n_0/\mathrm{d}T = -1.1 \times 10^{-4}\mathrm{deg}^{-1}$.[10] We used the value 0.545 cP of the viscosity coefficient η_0 of methanol at 25.0 °C,[12] and those 1.138, 1.002, and 0.890 cP of η_0 of water at 15.0, 20.0, and 25.0 °C, respectively.[13]

For later use, the viscosity coefficient η was determined for the aqueous solutions of the sample L7 at $w = 1.35\%$ and the sample T7 at $w = 1.36\%$, both at 15.0, 20.0, and 25.0 °C, by the use of a capillary viscometer with the use of the above-mentioned values of η_0 of water at the respective temperatures. The values of η so determined are 1.997, 1.701, and 1.446 cP for the former solution at 15.0, 20.0, and 25.0 °C, respectively, and 2.034, 1.726, and 1.464 cP for the latter solution at 15.0, 20.0, and 25.0 °C, respectively.

5.3 Results

5.3.1 Transmittance

Figure 5.2 shows plots of the transmittance and the solution temperature against time for the aqueous solutions of the PNIPA sample L7 at $w = 4.91\%$ (a) and for the cyclohexane solution of the a-PS sample F20 at $w = 3.14\%$ (b). The heavy curves represent the values of the transmittance and the light line segments connect the values of the solution temperature. The kind of curve and line (solid or dashed) distinguishes patterns of change in temperature.

For the aqueous solution of the PNIPA sample L7 shown in Figure 5.2a, decrease in the transmittance slows down and it seems to approach a nonzero value (*ca.* 50%), from the time the solution temperature is fixed at 32.8 °C where the transmittance first becomes 80%. Then the transmittance decreases to 0% as the solution temperature is raised to *ca.* 35 °C or recovers to 100% as the temperature is lowered to *ca.* 25 °C. On the other hand, for the cyclohexane solution of the a-PS sample F20 shown in Figure 5.2b, which is a well-defined UCST system, the transmittance continues decreasing very steeply to zero even after the solution temperature is fixed at 23.0 °C where the transmittance first becomes 95%. The difference in the behavior of the transmittance between the two solutions clearly shown in Figure 5.2 indicates that the decrease in the transmittance in the aqueous PNIPA solution does not correspond to the macroscopic phase separation but arises from formation of large aggregates of some kinds.

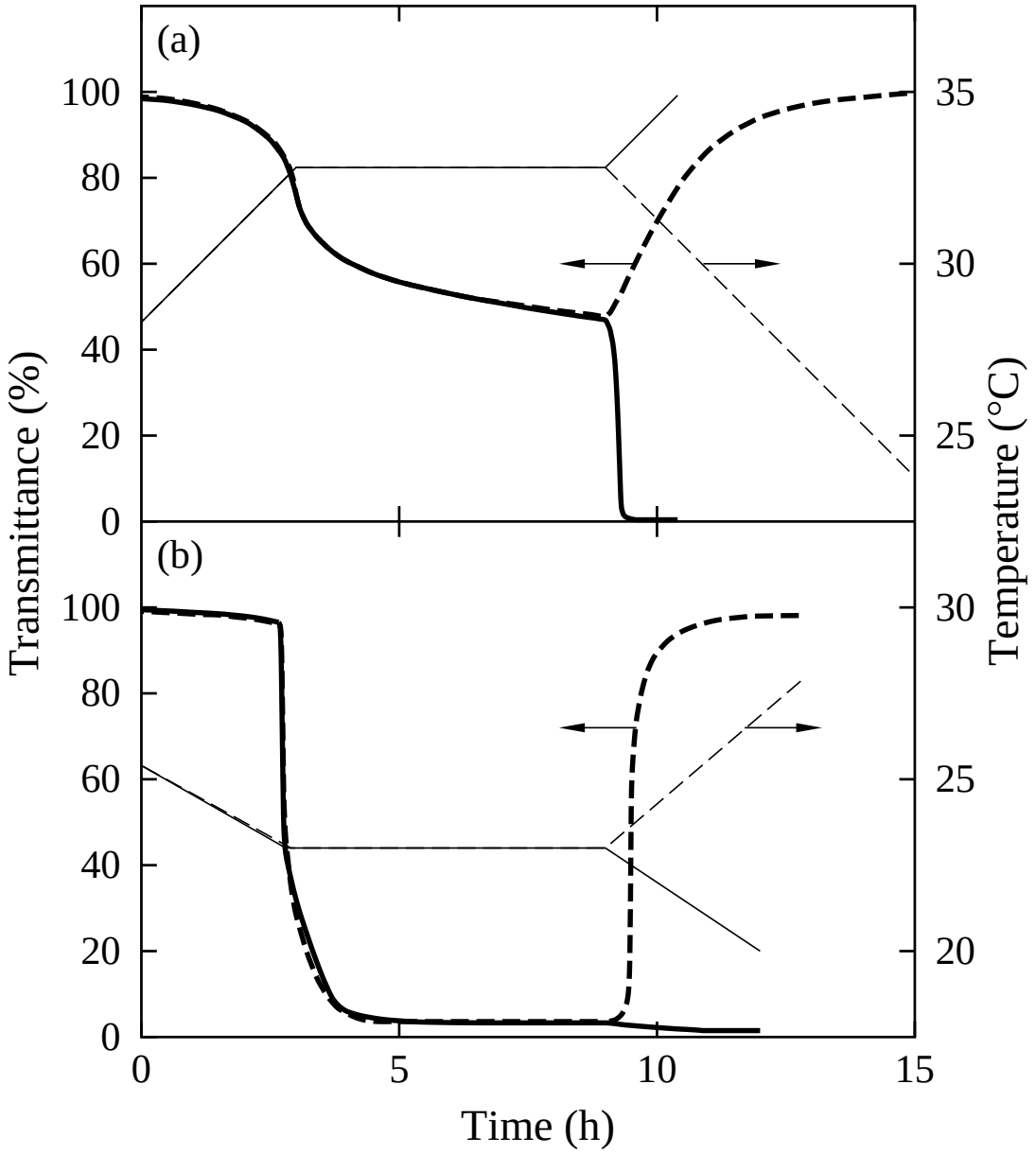

Figure 5.2. Plots of the transmittance and the solution temperature against time for the aqueous solution of the PNIPA sample L7 at $w = 4.91\%$ (a) and the cyclohexane solution of the a-PS sample F20 at $w = 3.14\%$ (b). The heavy curves represent the values of the transmittance and the light line segments connect the values of the solution temperature. The kind of curve and line (solid or dashed) distinguishes patterns of change in temperature.

5.3.2 Static Light Scattering

Figure 5.3 shows plots of $\Delta R_{\mathrm{Uv}}/c$ at $\theta = 90°$ against t_{e} for the four aqueous solutions of the sample L7 at $w = 0.103$ (a) and 1.35% (b) and of the sample T7 at $w = 0.102$ (c) and 1.36% (d), at 15.0, 20.0, and 25.0 °C. We note that the cloud points in the aqueous solutions of the sample L7 at $w = 1.01\%$ and of the sample T7 at $w = 0.98\%$ have been determined to be 32.9 and 32.4 °C, respectively, which are definitely higher than 25.0 °C. For all the solutions except that of the sample T7 at $w = 0.102\%$, $\Delta R_{\mathrm{Uv}}/c$ increases monotonically with increasing t_{e} over the whole range of t_{e} examined, and the increasing rate becomes large as the solution temperature is raised from 15 to 25 °C. The increase in $\Delta R_{\mathrm{Uv}}/c$ with increasing time and/or temperature implies that the average size (or molecular weight) or number of scatterers in the aqueous solutions increases with increasing time and/or temperature even at a temperature at which their transmittance is 100%.

The situation becomes more clear by examining the angular dependence of $\Delta R_{\mathrm{Uv}}/c$. Figure 5.4 shows the Berry square-root plots[14] of $(c/\Delta R_{\mathrm{Uv}})^{1/2}$ against k^2 in the range of θ from 30 to 142.5° for the same solutions as those in Figure 5.3, *i.e.*, the sample L7 at $w = 0.103$ (a) and 1.35% (b) and the sample T7 at $w = 0.102$ (c) and 1.36% (d), at 15.0, 20.0, and 25.0 °C, where the magnitude k of the scattering vector is related to θ as

$$k = \frac{4\pi n_0}{\lambda_0} \sin \frac{\theta}{2} \tag{5.1}$$

with λ_0 the wavelength of light in a vacuum. In the figure, the half-filled circles represent the experimental values with their direction distinguishing the values at $t_{\mathrm{e}} \simeq 1$ h (◓), 3 h (◔), 6 h (◑), 12 h (◕), 24 h (◒), and 36 h (◐) from top to bottom, and the solid curves connect smoothly the data points.

Corresponding to the monotonous increase in $\Delta R_{\mathrm{Uv}}/c$ with increasing t_{e} shown in Figure 5.3, for all the solutions except for that of the sample T7 at $w = 0.102\%$, the value of $(c/\Delta R_{\mathrm{Uv}})^{1/2}$ at a given k^2 decreases with increasing t_{e}. The slopes of the plots for the solution of the sample T7 at $w = 0.102\%$ are almost identical with zero, while those for the other solutions are definite and increase with decreasing k^2, implying that the average size of scatterers in the latter solutions is appreciably larger than that in the former solution and that the distribution of the sizes in each of the latter solutions is rather widespread. It is interesting to see for the solution of sample T7 at $w = 1.36\%$ that the initial slope becomes remarkably large with increasing t_{e}, especially at 25.0 °C. It means that there exist remarkably large scatterers although the number of them is not so large.

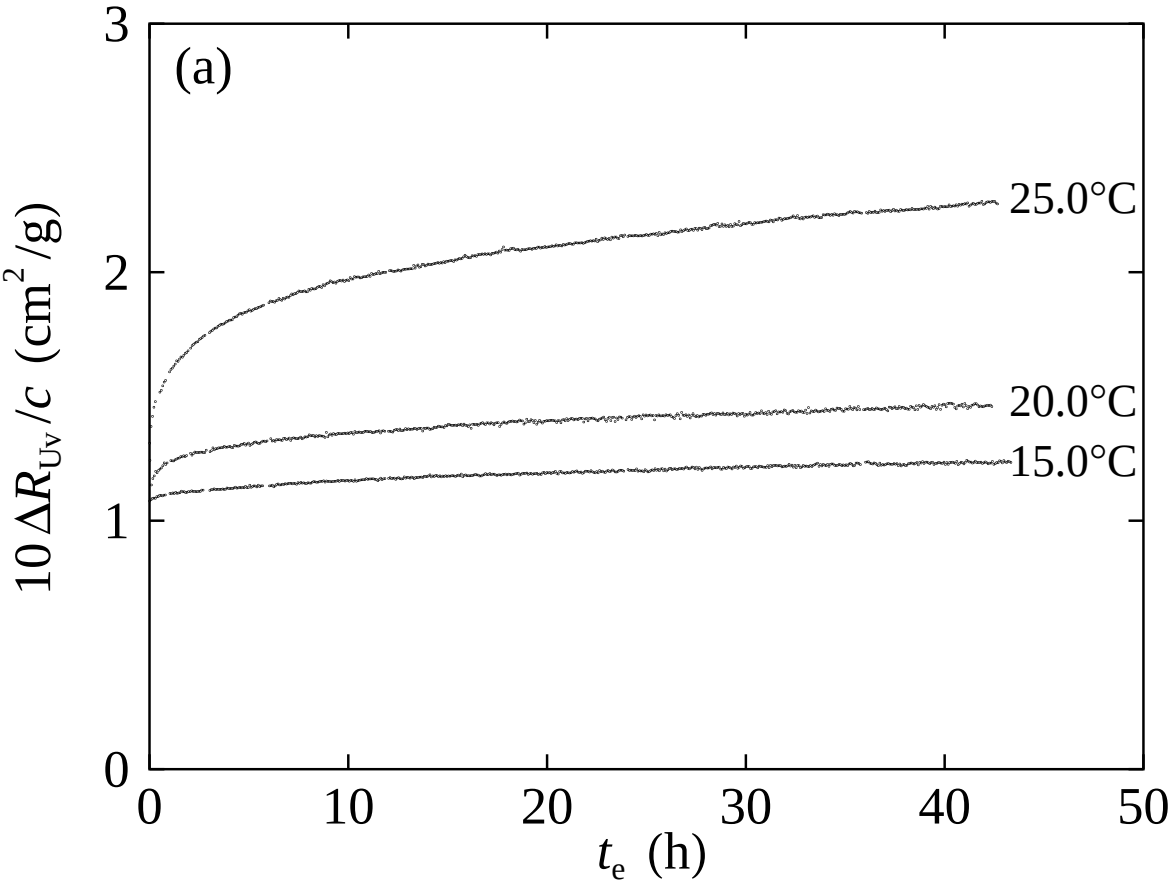

Figure 5.3(a). Plots of $\Delta R_{\mathrm{Uv}}/c$ at $\theta = 90°$ against t_{e} for the aqueous solution of the sample L7 at $w = 0.1026$ % at 15.0, 20.0, and 25.0 °C.

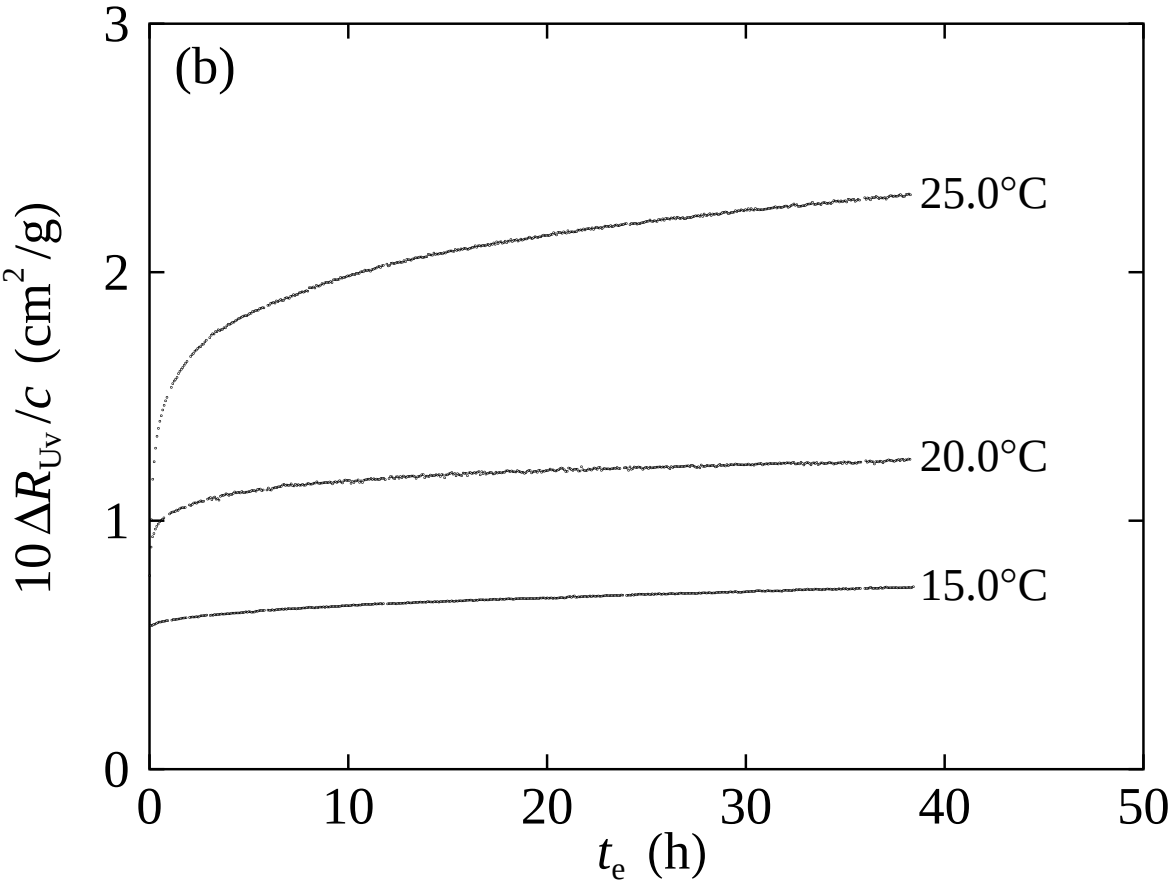

Figure 5.3(b). Plots of $\Delta R_{\mathrm{Uv}}/c$ at $\theta = 90°$ against t_{e} for the aqueous solution of the sample L7 at $w = 1.346$ % at 15.0, 20.0, and 25.0 °C.

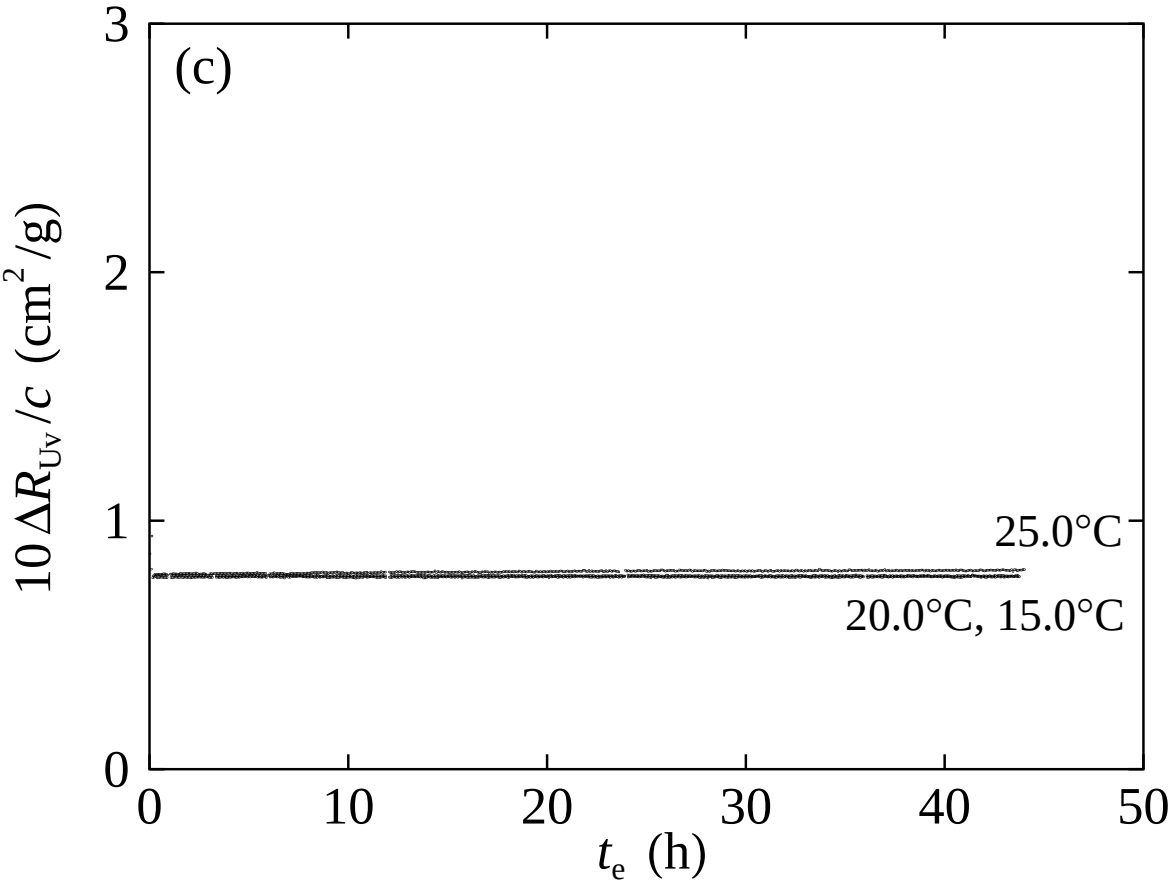

Figure 5.3(c). Plots of $\Delta R_{\mathrm{Uv}}/c$ at $\theta = 90°$ against t_{e} for the aqueous solution of the sample T7 at $w = 0.1022\%$ at 15.0, 20.0, and 25.0 °C.

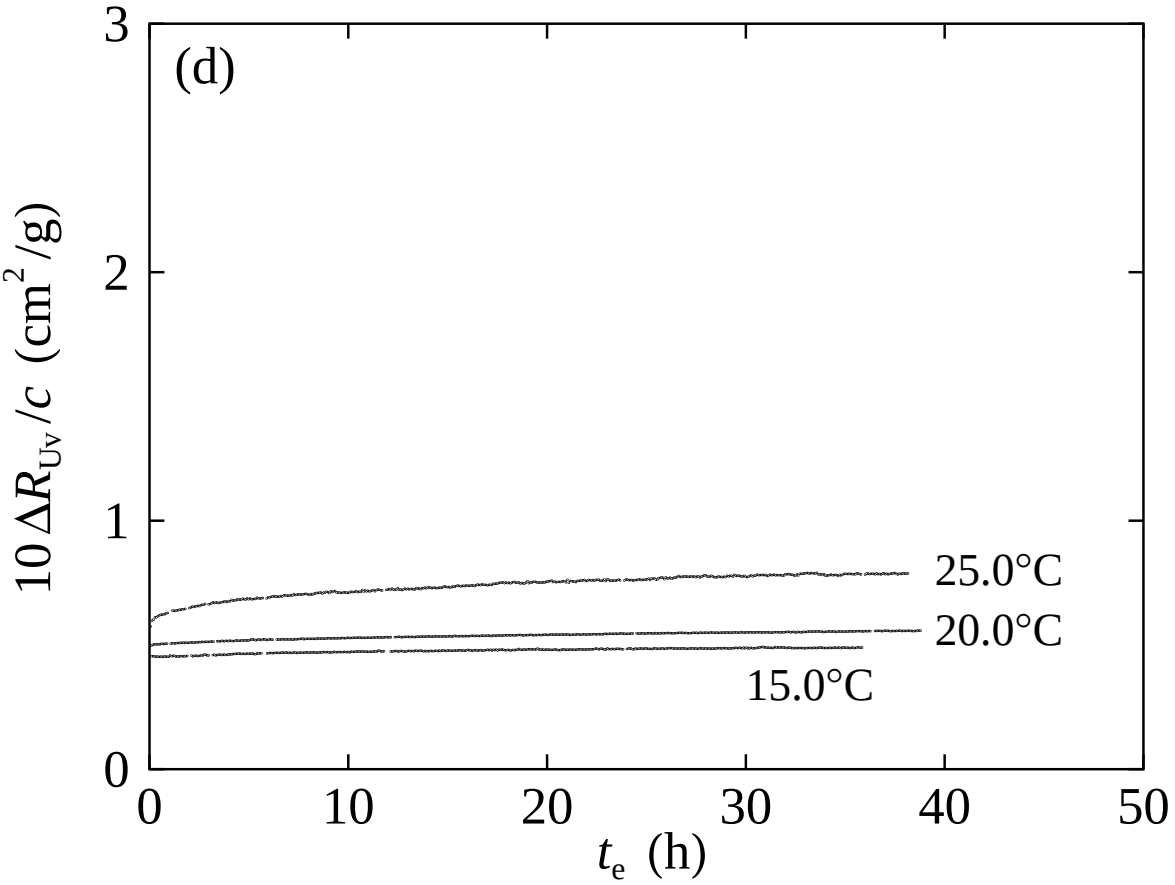

Figure 5.3(d) Plots of $\Delta R_{\mathrm{Uv}}/c$ at $\theta = 90°$ against t_{e} for the aqueous solution of the sample T7 at $w = 1.360\%$ at 15.0, 20.0, and 25.0 °C.

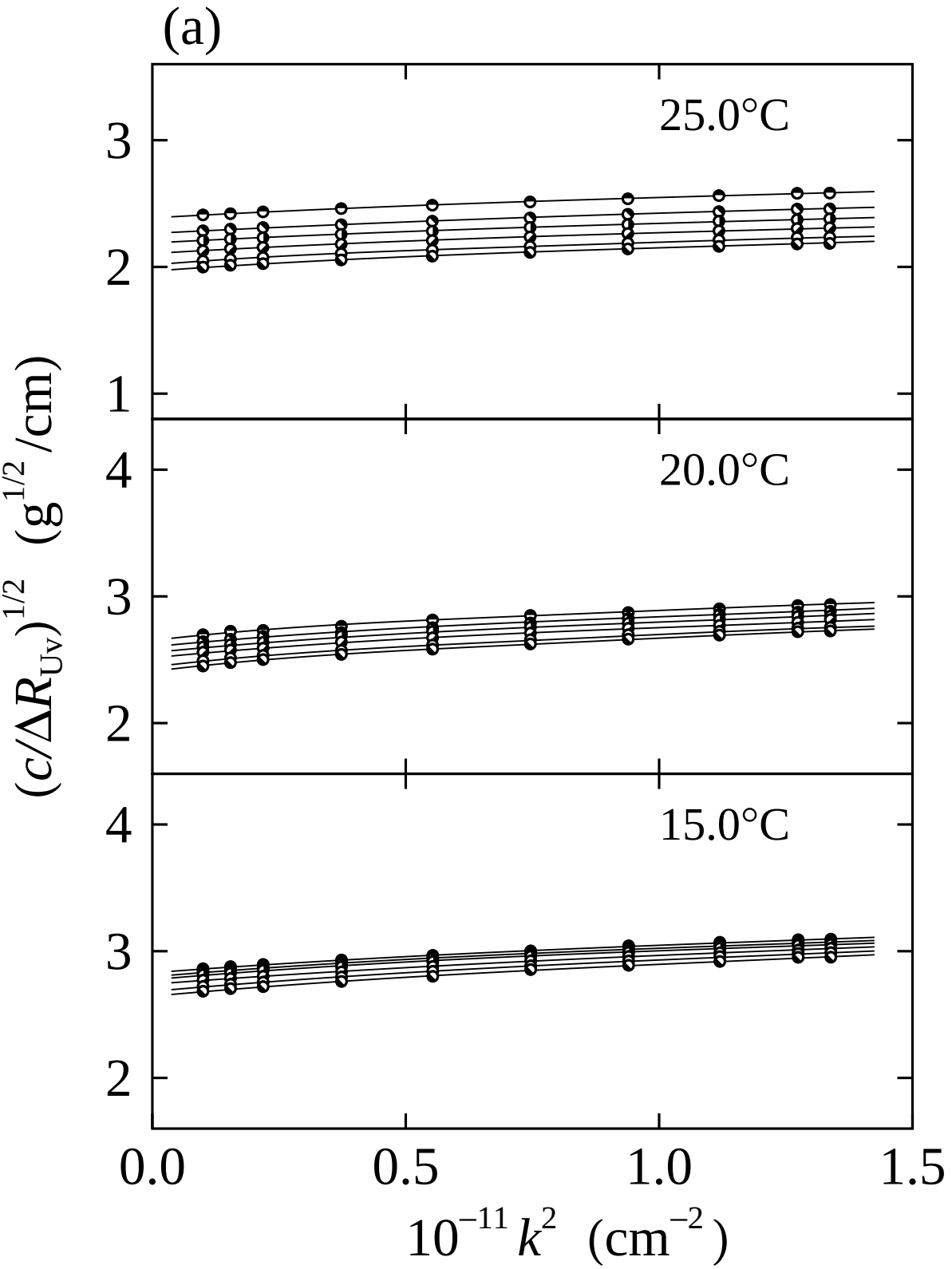

Figure 5.4(a). Plots of $(c/\Delta R_{\mathrm{Uv}})^{1/2}$ against k^2 for the aqueous PNIPA solution of the sample L7 at $w = 0.1026$ % at 15.0, 20.0, and 25.0 °C. The half-filled circles represent the experimental values with their direction distinguishing the values at $t_{\mathrm{e}} \simeq 1$ h (◓), 3 h (◔), 6 h (◑), 12 h (◕), 24 h (◒), and 36 h (◐) from top to bottom, and the solid curves connect smoothly the data points.

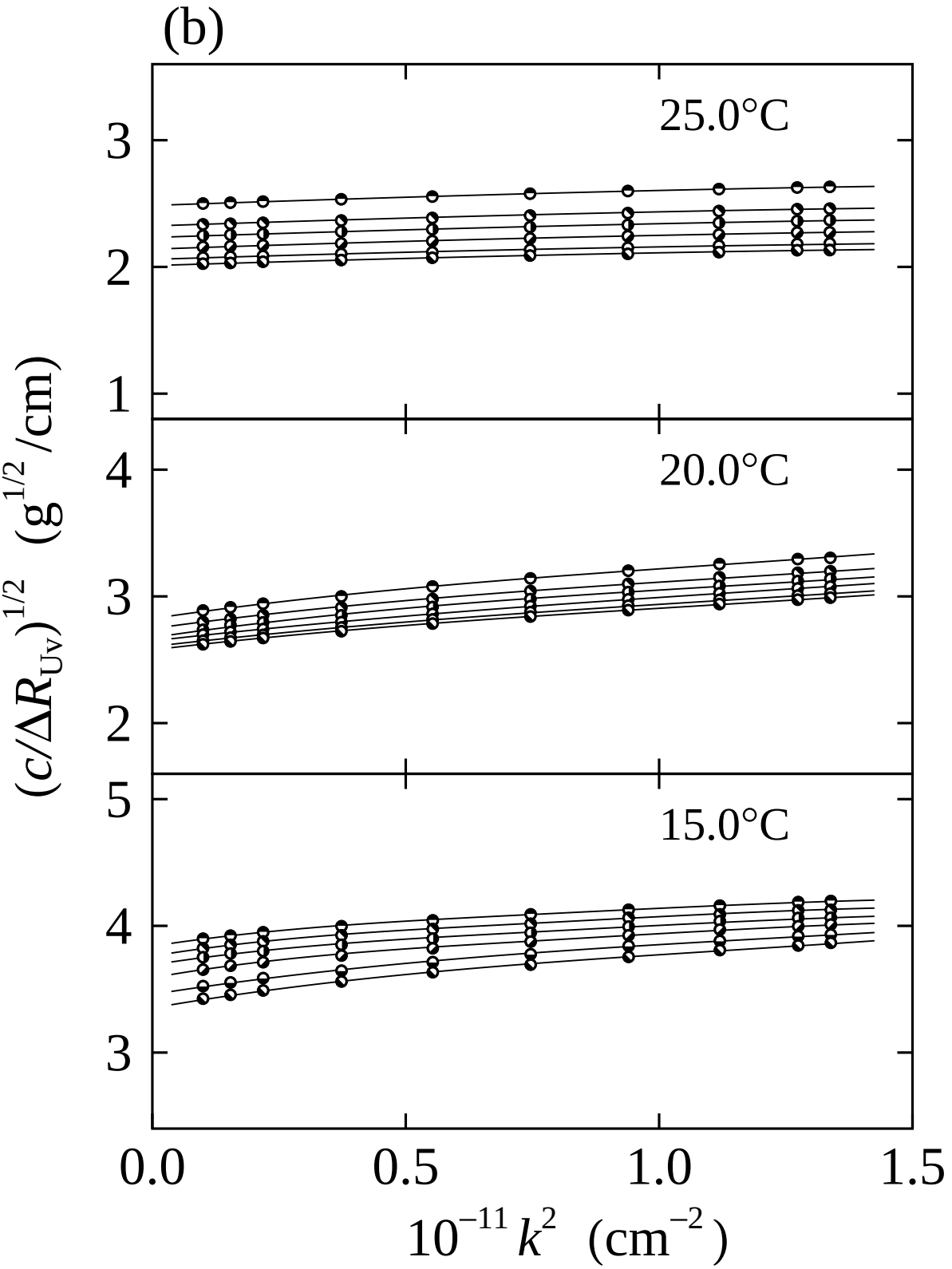

Figure 5.4(b). Plots of $(c/\Delta R_{\mathrm{Uv}})^{1/2}$ against k^2 for the aqueous PNIPA solution of the sample L7 at $w = 1.346\%$ at 15.0, 20.0, and 25.0 °C. The half-filled circles represent the experimental values with their direction distinguishing the values at $t_{\mathrm{e}} \simeq 1$ h (◓), 3 h (◔), 6 h (◑), 12 h (◪), 24 h (◒), and 36 h (◕) from top to bottom, and the solid curves connect smoothly the data points.

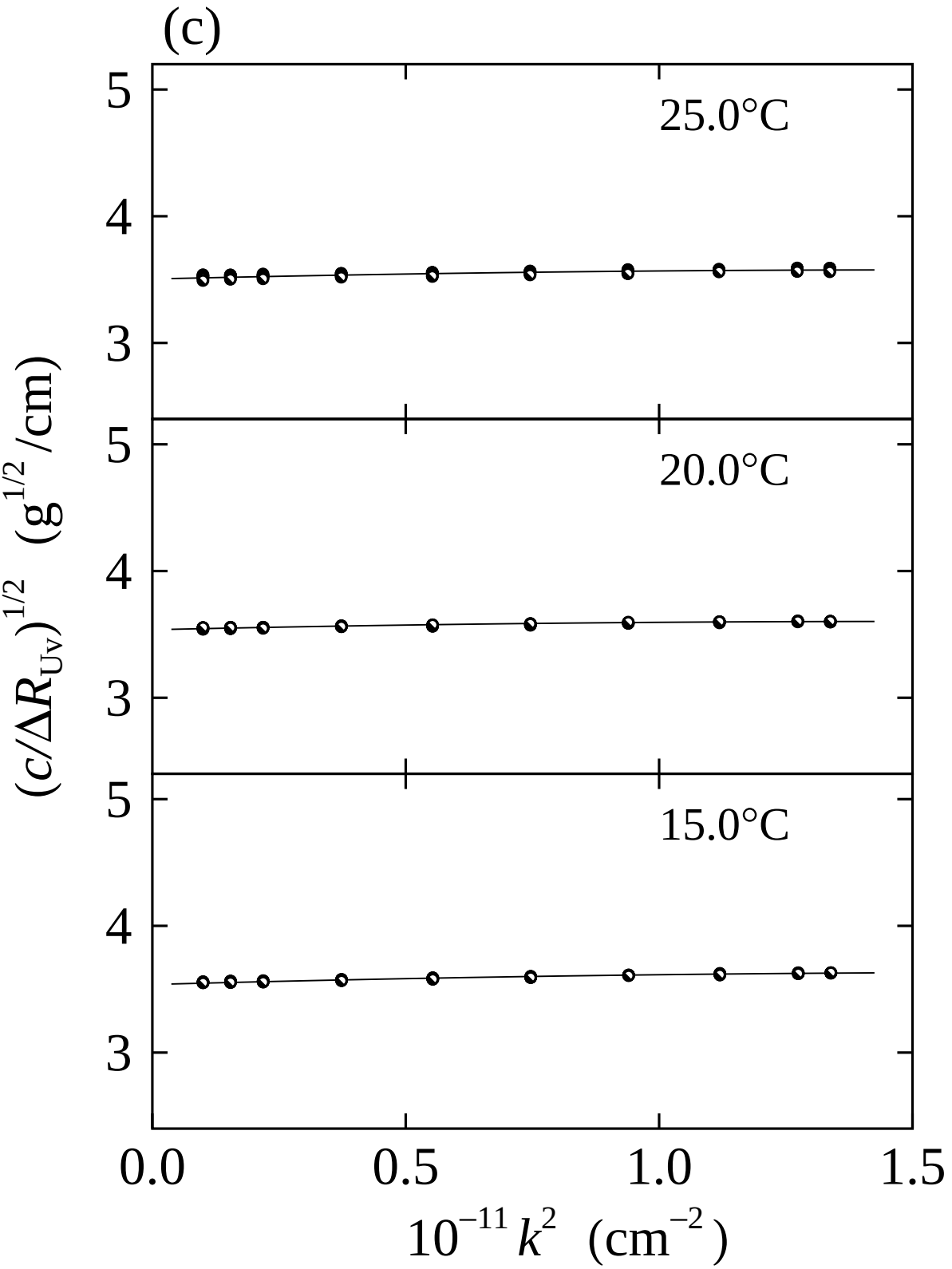

Figure 5.4(c). Plots of $(c/\Delta R_{\mathrm{Uv}})^{1/2}$ against k^2 for the aqueous PNIPA solution of the sample T7 at $w = 0.1022\%$ at 15.0, 20.0, and 25.0 °C. The half-filled circles represent the experimental values with their direction distinguishing the values at $t_{\mathrm{e}} \simeq 1$ h (◓), 3 h (◔), 6 h (◑), 12 h (◕), 24 h (◒), and 36 h (◔) from top to bottom, and the solid curves connect smoothly the data points.

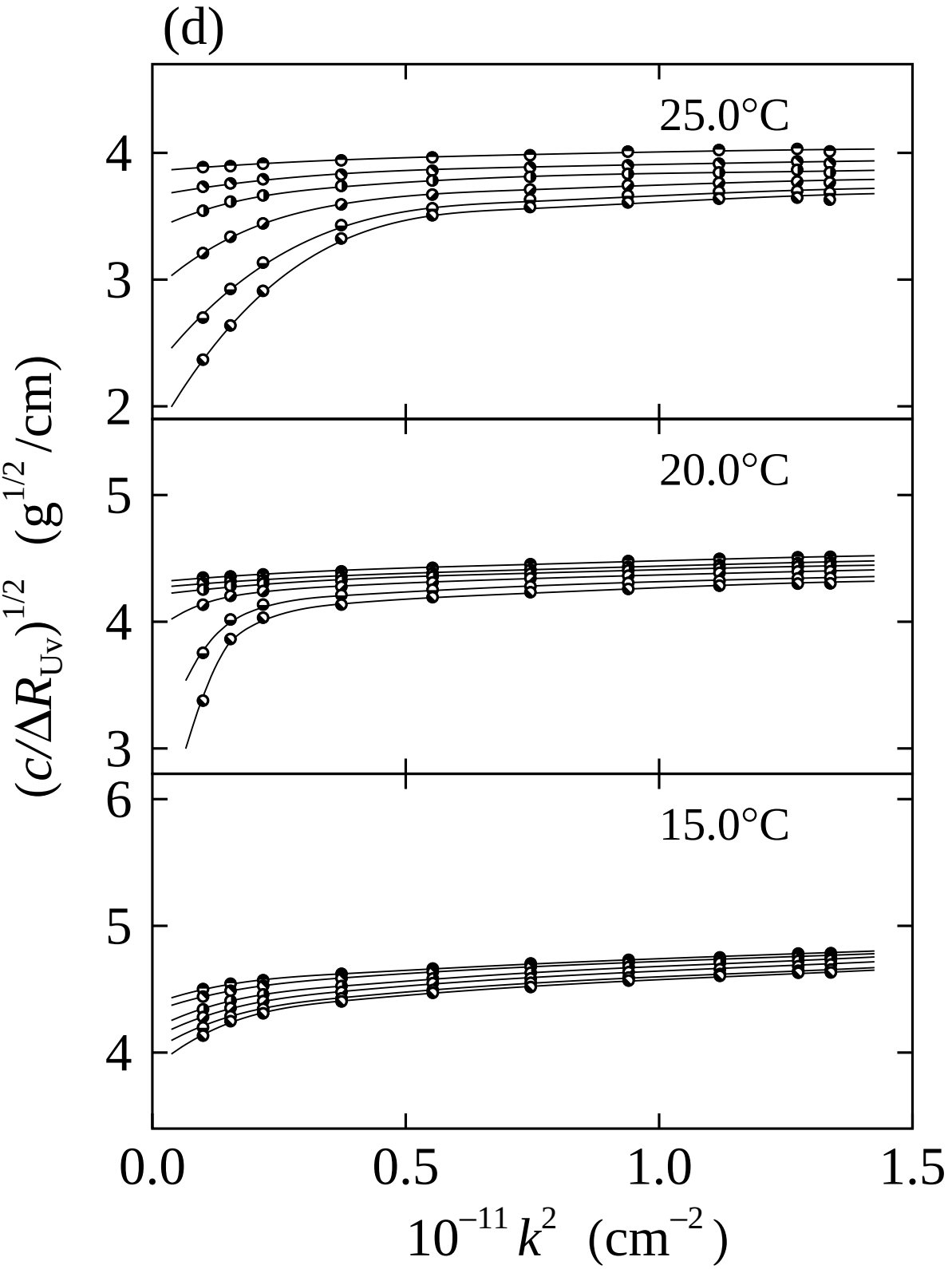

Figure 5.4(d). Plots of $(c/\Delta R_{\mathrm{Uv}})^{1/2}$ against k^2 for the aqueous PNIPA solution of the sample T7 at w =1.360% at 15.0, 20.0, and 25.0 °C. The half-filled circles represent the experimental values with their direction distinguishing the values at $t_{\mathrm{e}} \simeq$ 1 h (◓), 3 h (◔), 6 h (◑), 12 h (◪), 24 h (◒), and 36 h (◕) from top to bottom, and the solid curves connect smoothly the data points.

5.3.3 Dynamic Light Scattering

The dynamic LS data for $g^{(2)}(t)$ as a function of t obtained for the methanol solutions of both the PNIPA samples L7 and T7 were confirmed to follow single-exponential decays over the whole ranges of θ and c, so that the (z-average) translational diffusion coefficient D (at infinite dilution) of isolated PNIPA chains could be determined for the two samples following a standard procedure:[15] the slope Γ (first cumulant) of the plot of $(1/2)\ln[g^{(2)}(t) - 1]$ against t was first determined at each θ and c, then the apparent diffusion coefficient $D^{(\mathrm{LS})}(c)$ at finite c was determined as a limiting value of Γ/k^2 in the limit of $k^2 \to 0$ at each c, and finally D was determined by an extrapolation of $D^{(\mathrm{LS})}(c)$ to $c = 0$. The values of D so determined for the samples L7 and T7 in methanol at 25.0 °C are 5.51×10^{-7} and 5.74×10^{-7} cm^2/s, respectively. In Table 5.2 are given the values of the hydrodynamic radius R_{H} calculated from the defining equation,

$$R_{\mathrm{H}} = k_{\mathrm{B}}T/6\pi\eta_0 D \tag{5.2}$$

with k_{B} the Boltzmann constant and T the absolute temperature and with those D values.

Table 5.2. Values of R_{H} for the samples L7 and T7 in methanol at 25.0 °C

sample	R_{H} (nm)
L7	7.2_9
T7	6.9_9

On the other hand, the data for the aqueous solutions were found not to follow single-exponential decays, since there were scatterers of different sizes other than the isolated PNIPA chains, as expected from the above-mentioned results of static LS. Then, by the use of the FORTRAN program package CONTIN,[16] we decomposed $[g^{(2)}(t) - 1]^{1/2}$ at a given k into a series of exponential-decay functions as

$$[g^{(2)}(t) - 1]^{1/2} = \sum_{i=1}^{n_f} A(\tau_i, k)\, e^{-t/\tau_i} \tag{5.3}$$

where τ_i ($i = 1, 2, \cdots, n_f$) is the ith relaxation time and $A(\tau_i, k)$ is the amplitude of the ith component e^{-t/τ_i}. The quantity $A(\tau, k)$ as a function of the relaxation time τ also has the meaning of the distribution of τ. In practice, we adopted $n_f = 150$ and distributed

τ_i at regular intervals in the logarithmic scale over the range from 1 μs to 1 s. Figure 5.5 shows plots of $g^{(2)}(t) - 1$ at $\theta = 20°$ and at $t_e \simeq 36$ h against the logarithm of t (in s) and those of $A(\tau, k)$ (as a function of τ) against the logarithm of τ (in s) for the four aqueous solutions of the sample L7 at $w = 0.103$ (a) and 1.35% (b) and of the sample T7 at $w = 0.102$ (c) and 1.36% (d), at 15.0, 20.0, and 25.0 °C. The unfilled circles represent the experimental values and the solid curves connect smoothly the data points.

Corresponding to the LS results shown in Figure 5.4, $A(\tau, k)$ as a function of τ is bimodal for all the aqueous solutions except that of the sample T7 at $w = 0.102\%$, implying that there are two classes of scatterers having different sizes. For the solutions of the sample L7 at $w = 1.35\%$ and of the sample T7 at $w = 1.36\%$, $A(\tau, k)$'s obtained at other θ and t_e are always bimodal, although the results are omitted here. The class having larger τ ($\simeq 10^{-2}$ s) may be considered to be large aggregates, and the other one ($\tau \simeq 10^{-3}$ s) seems to correspond to isolated PNIPA chains. As for the solution of the sample T7 at $w = 0.102\%$, $A(\tau, k)$ is unimodal, implying that appreciably large aggregates may not be formed. It may be seen from the figure, the number of the aggregates is larger in the solution of the sample L7 than in that of the sample T7 if their concentrations are the same.

5.4 Discussion

In the previous section, it is clearly shown that the cloud point in the aqueous solutions at least of the linear PNIPA sample having the diphenylmethyl end group synthesized by living anionic polymerization does not directly correspond to the binodal point and that there exist rather large aggregates in the aqueous solutions of both the PNIPA samples synthesized by living anionic and radical polymerization, at a temperature considerably lower than the cloud point, if the concentration is not extremely dilute. It is then desirable to get some information about the size of the aggregates. By an application of the method proposed by Kanao *et al.*[11] for an analysis of dynamic LS data for a polymer solution in which isolated polymer chains and their aggregates coexist, we analyze the dynamic LS data for the solutions of the sample L7 at $w = 1.35\%$ and of the sample T7 at $w = 1.36\%$, for which $A(\tau, k)$ is definitely bimodal, in order to estimate the hydrodynamic radius R_H and mean-square radius of gyration $\langle S^2 \rangle$ at finite c.

5.4.1 Hydrodynamic Radius

Under the assumptions that the solution includes only a small amount of aggregates, interactions between them may be neglected, and the lifetime of each aggregate is much longer than its translational relaxation time, the mutual diffusion coefficient D_{fast} of the

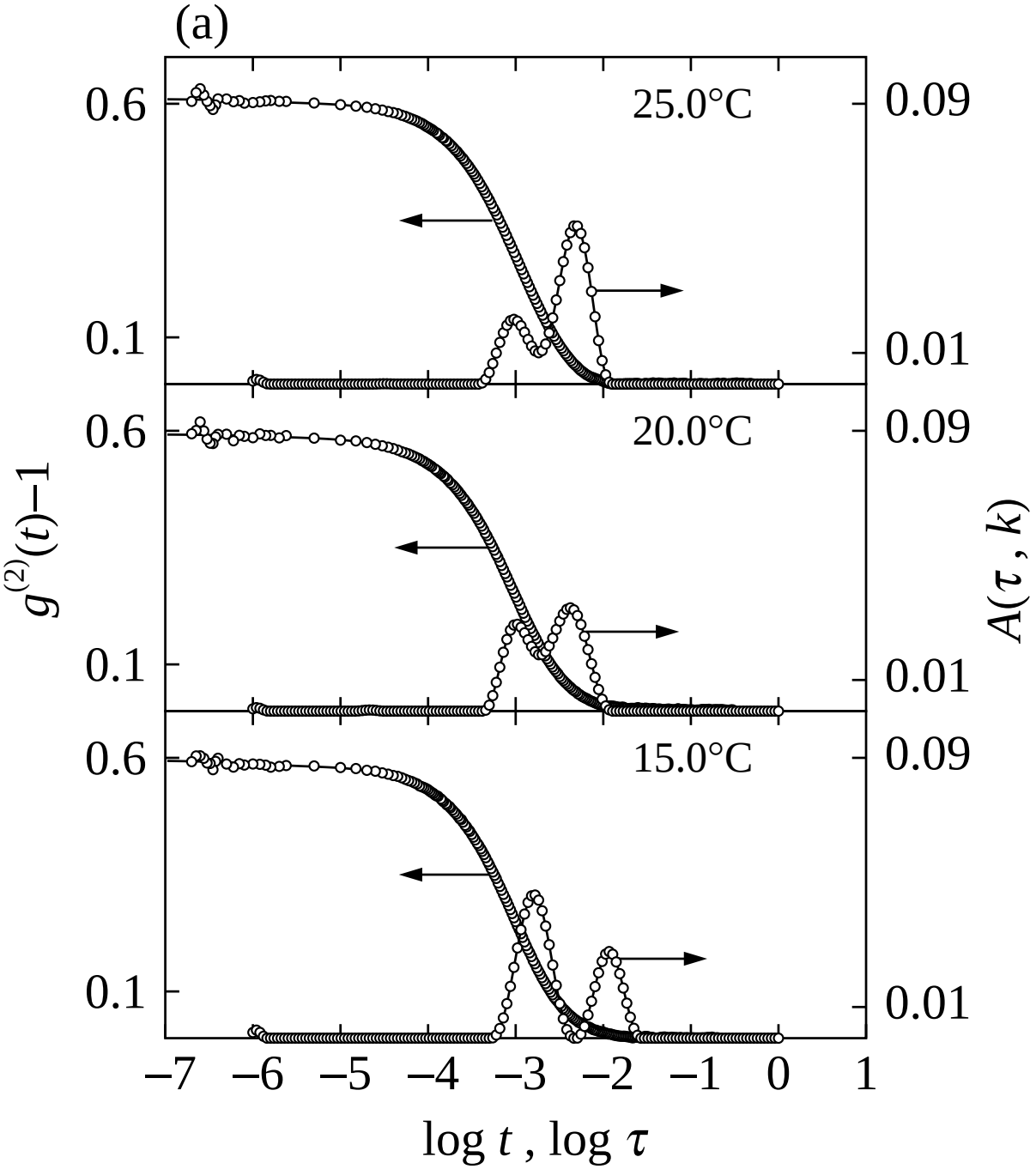

Figure 5.5(a). Plots of $g^{(2)}(t) - 1$ at $\theta = 20°$ and $t_e \simeq 36$ h against the logarithm of t (in s) and those of $A(\tau, k)$ against the logarithm of τ (in s) for the aqueous solution of the sample L7 at $w = 0.103\%$ at 15.0, 20.0, and 25.0 °C. The unfilled circles represent the experimental values and the solid curves connect smoothly the data points.

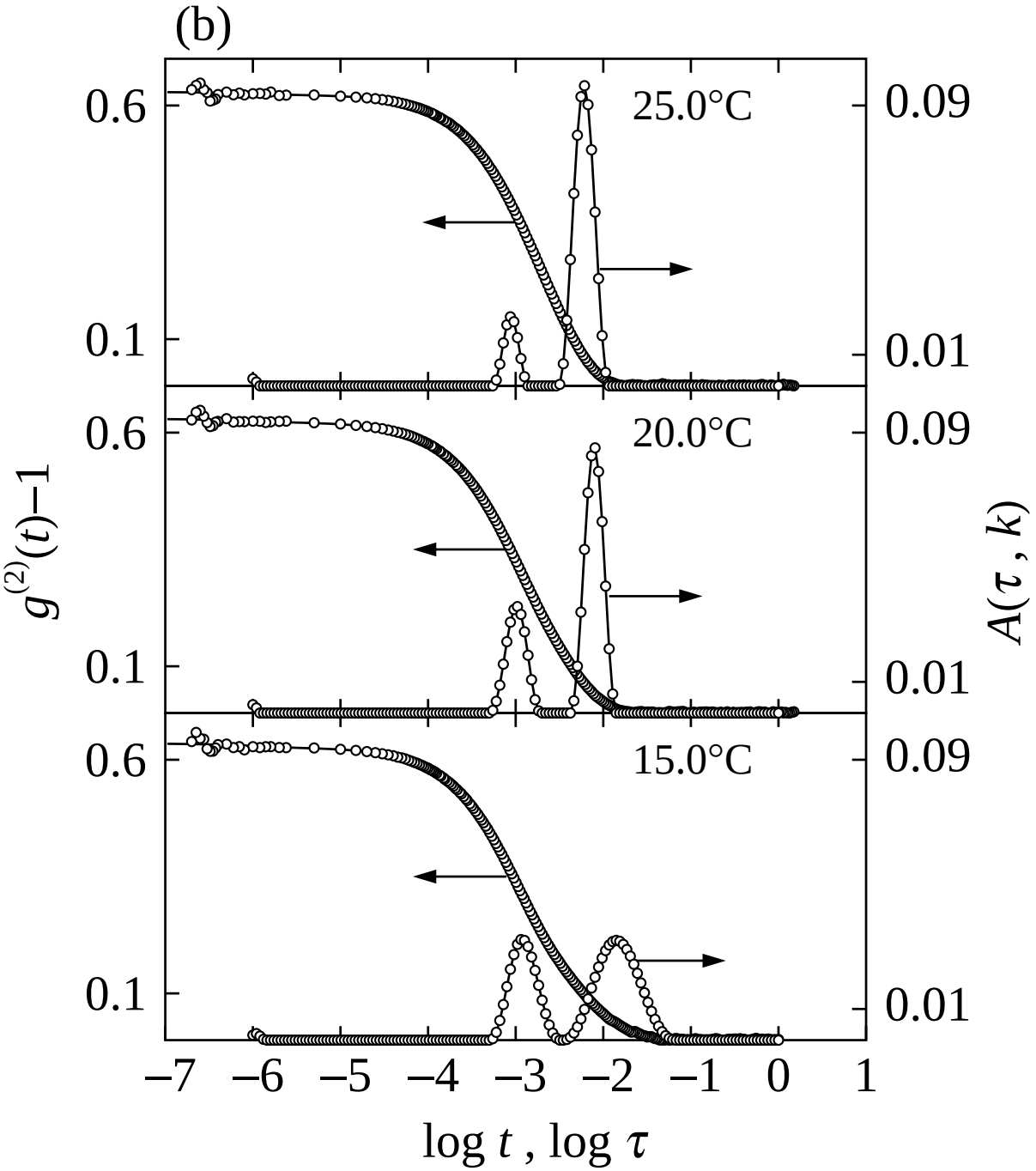

Figure 5.5(b). Plots of $g^{(2)}(t) - 1$ at $\theta = 20°$ and $t_e \simeq 36$ h against the logarithm of t (in s) and those of $A(\tau, k)$ against the logarithm of τ (in s) for the aqueous solution of the sample L7 at w =1.35% at 15.0, 20.0, and 25.0 °C. The unfilled circles represent the experimental values and the solid curves connect smoothly the data points.

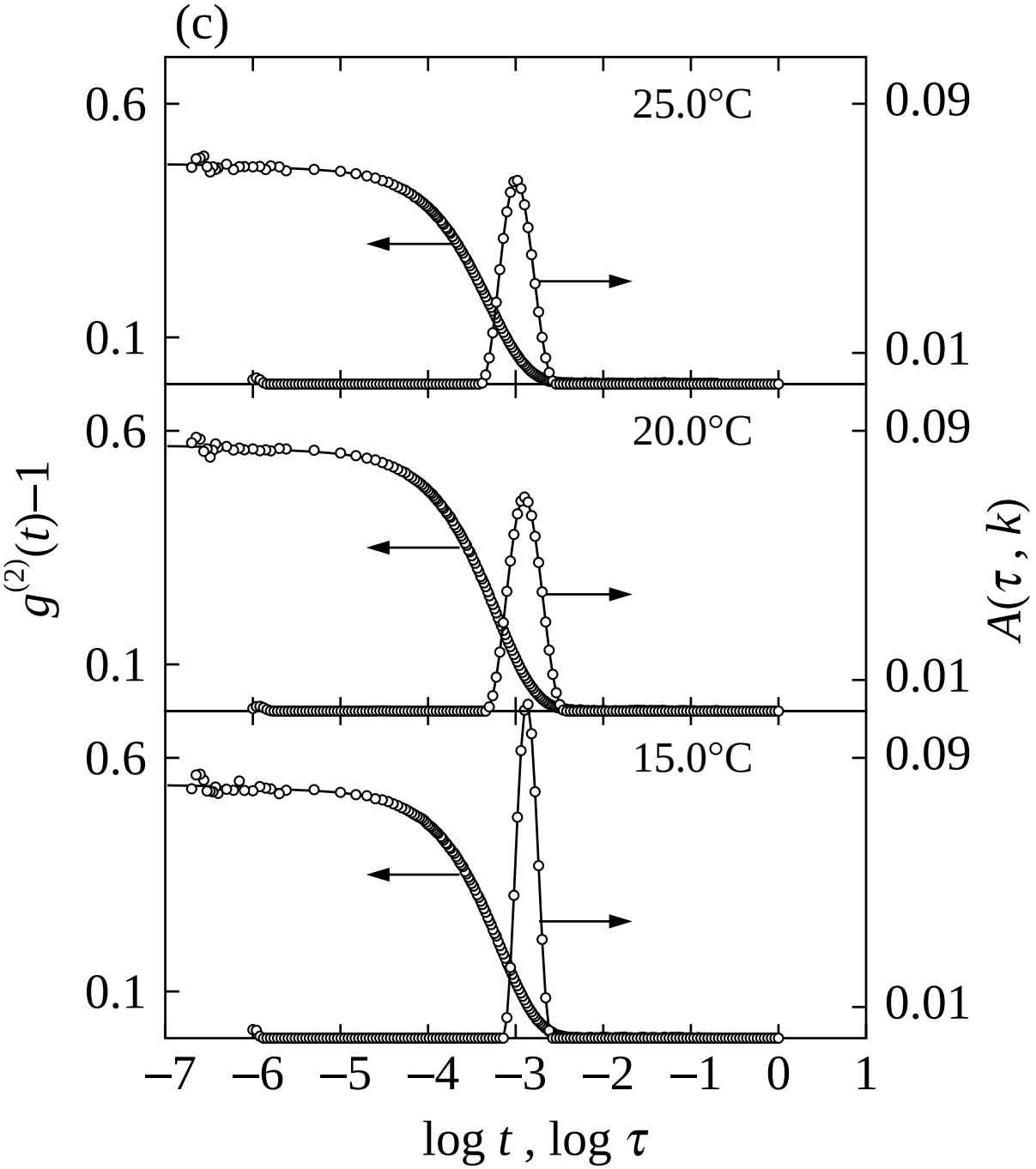

Figure 5.5(c). Plots of $g^{(2)}(t) - 1$ at $\theta = 20°$ and $t_e \simeq 36$ h against the logarithm of t (in s) and those of $A(\tau, k)$ against the logarithm of τ (in s) for the aqueous solution of the sample T7 at $w = 0.102\%$ at 15.0, 20.0, and 25.0 °C. The unfilled circles represent the experimental values and the solid curves connect smoothly the data points.

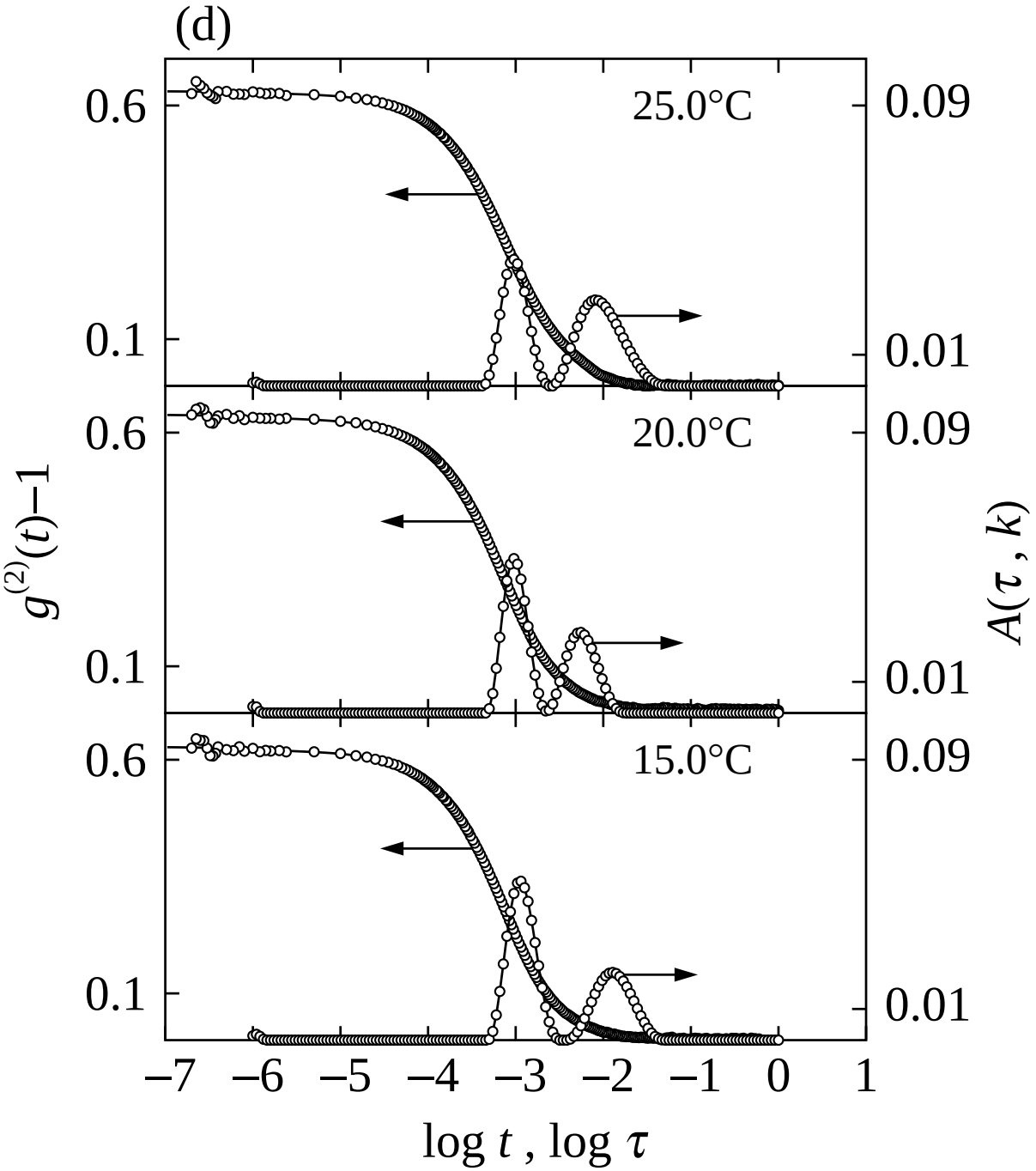

Figure 5.5(d). Plots of $g^{(2)}(t) - 1$ at $\theta = 20°$ and $t_e \simeq 36$ h against the logarithm of t (in s) and those of $A(\tau, k)$ against the logarithm of τ (in s) for the aqueous solution of the sample T7 at w =1.36% at 15.0, 20.0, and 25.0 °C. The unfilled circles represent the experimental values and the solid curves connect smoothly the data points.

isolated polymer chains at finite c and the z-average diffusion coefficient $D_{\rm slow}$ of the aggregates may be given by[11]

$$D_\alpha = \lim_{k\to 0} \Gamma_\alpha/k^2 \qquad (\alpha = \text{fast, slow}) \tag{5.4}$$

with

$$\Gamma_\alpha = \sum_{\tau_i\in\alpha \text{ mode}} {\tau_i}^{-1} A(\tau_i, k) \Big/ \sum_{\tau_i\in\alpha \text{ mode}} A(\tau_i, k) \qquad (\alpha = \text{fast, slow}) \tag{5.5}$$

where τ_i belongs to a set of relaxation times named "fast mode" if τ_i is shorter than an appropriate threshold value which may divide the distribution $A(\tau, k)$ shown in Figures 5.5b and 5.5d into two modes, and to another set named "slow mode" otherwise.

For instance, Figure 5.6 shows plots of Γ_α/k^2 against k^2 for the aqueous solutions of the sample L7 at $w = 1.35\%$ (a) and of the sample T7 at $w = 1.36\%$ (b), at 25.0 °C and at $t_{\rm e} \simeq 36$ h. The unfilled and filled circles represent the values for α = fast and slow, respectively. The data point at the left end in each plot corresponds to the plot of $A(\tau, k)$ at 25.0 °C shown in Figures 5.5b and 5.5d. The values of $\Gamma_{\rm fast}/k^2$ ($\bigcirc$) for both the solutions are independent of k^2 within experimental error in the whole range of k^2 examined, so that $D_{\rm fast}$ may be evaluated as a mean of the experimental values for each solution, which is represented by the horizontal line. The values of $D_{\rm fast}$ so estimated for the sample L7 at 15.0, 20.0, and 25.0 °C are $2.9_2 \times 10^{-7}$, $3.5_1 \times 10^{-7}$, and $4.1_4 \times 10^{-7}$ cm^2/s, respectively, and those for the sample T7 are $2.9_3 \times 10^{-7}$, $3.2_6 \times 10^{-7}$, and $3.4_2 \times 10^{-7}$ cm^2/s, respectively. On the other hand, the values of $\Gamma_{\rm slow}/k^2$ ($\bullet$) for both the solutions appreciably depend on k^2 in the range of large k^2 ($\gtrsim 2 \times 10^{10}$ cm^{-2}), so that we estimate $D_{\rm slow}$ by an extrapolation of $\Gamma_{\rm slow}/k^2$ to $k^2 = 0$ following the curve connecting smoothly the data points for each solution as shown in Figure 5.6. The values of $D_{\rm slow}$ so estimated for the sample L7 at 15.0, 20.0, and 25.0 °C are $2.8_5 \times 10^{-8}$, $4.7_5 \times 10^{-8}$, and $5.8_6 \times 10^{-8}$ cm^2/s, respectively, and those for the sample T7 are $2.7_1 \times 10^{-8}$, $3.9_8 \times 10^{-8}$, and $3.7_0 \times 10^{-8}$ cm^2/s, respectively.

From the values of D_α so determined, we define the hydrodynamic radius $R_{{\rm H},\alpha}$ by

$$R_{{\rm H},\alpha} = \frac{k_{\rm B}T}{6\pi\eta_\alpha D_\alpha} \qquad (\alpha = \text{fast, slow}) \tag{5.6}$$

where $\eta_{\rm fast}$ and $\eta_{\rm slow}$ are the viscosity coefficients of fluids around the isolated polymer chains and aggregates and are set equal to those of the solvent (η_0) and solution (η), respectively.[11] We note that $R_{\rm H,fast}$ is not the hydrodynamic radius in the strict sense of the term, since $D_{\rm fast}$ is the mutual diffusion coefficient at finite c. We also note that the solution viscosity η is used in the definition of $R_{\rm H,slow}$ since the translational motion of the aggregates is very slow compared to that of the isolated chains and therefore the aqueous

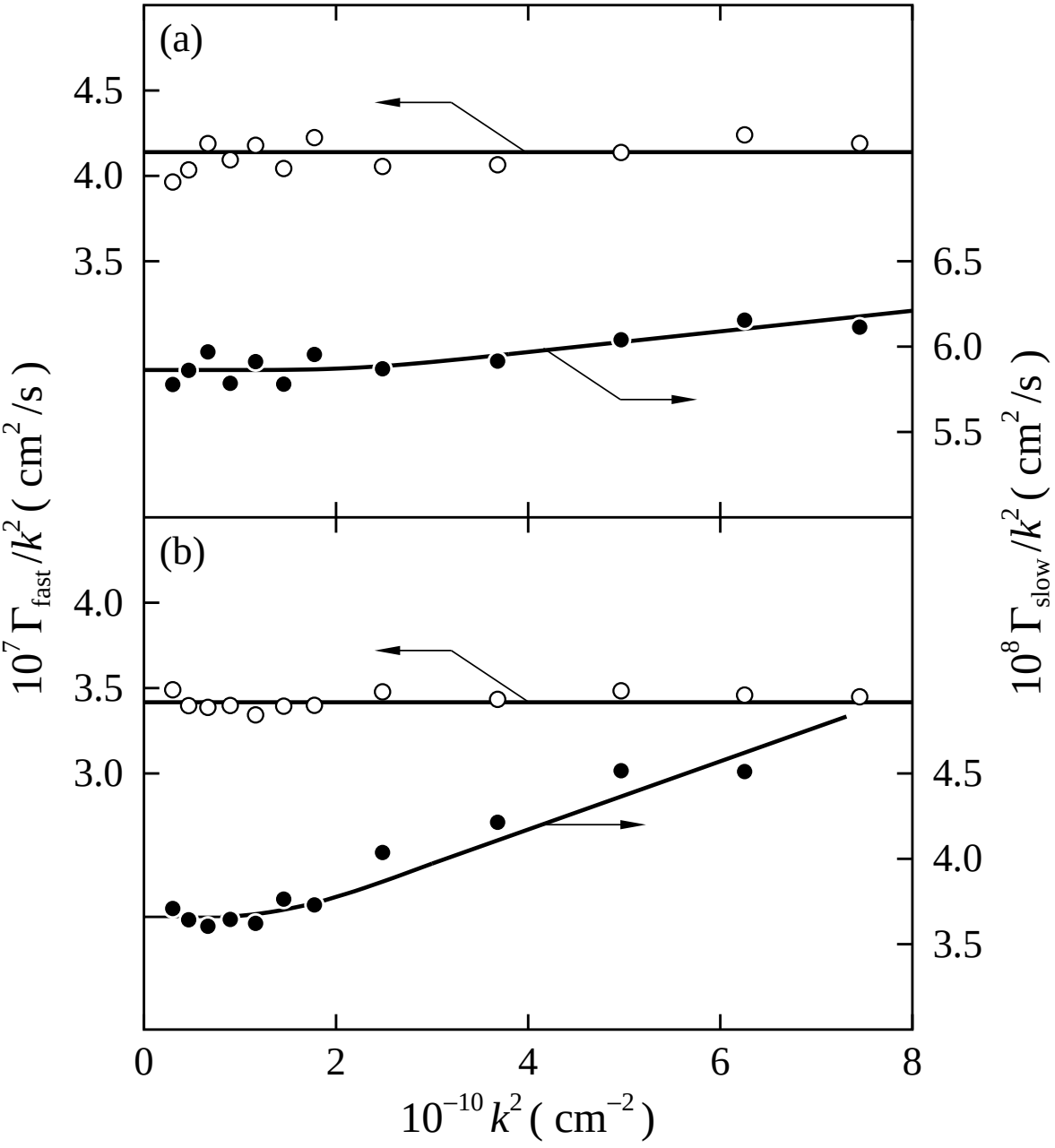

Figure 5.6. Plots of $\Gamma_{\mathrm{fast}}/k^2$ (○) and $\Gamma_{\mathrm{slow}}/k^2$ (●) against k^2 for the aqueous solutions of the sample L7 at $w = 1.35\%$ (a) and of the sample T7 at $w = 1.36\%$ (b), at 25.0 °C and at $t_{\mathrm{e}} \simeq 36$ h. The horizontal line associated with each plot of $\Gamma_{\mathrm{fast}}/k^2$ indicates the mean of the experimental values and the curve associated with each plot of $\Gamma_{\mathrm{slow}}/k^2$ connects smoothly the data points.

solution of the isolated chains may be considered to act as a continuous fluid around the aggregates. Here, it has been assumed that the aggregate can hardly contribute the observed η since its concentration is extremely low as assumed above.[11]

Table 5.3. Values of $R_{\mathrm{H,fast}}$ and $R_{\mathrm{H,slow}}$ for the samples L7 and T7 in water at 15.0, 20.0, and 25.0 °C and at $t_{\mathrm{e}} \simeq 36$ h

		$R_{\mathrm{H,fast}}$ (nm)			$R_{\mathrm{H,slow}}$ (nm)		
sample	w, %	15.0 °C	20.0 °C	25.0 °C	15.0 °C	20.0 °C	25.0 °C
L7	1.35	6.3_6	6.1_0	5.9_3	$37._1$	$26._6$	$25._8$
T7	1.36	6.3_5	6.5_8	7.1_9	$38._3$	$31._3$	$40._3$

In Table 5.3 are given the values of $R_{\mathrm{H,fast}}$ and $R_{\mathrm{H,slow}}$ calculated from eq 5.6 with the above-mentioned values of D_{fast} and D_{slow}, respectively. The values of $R_{\mathrm{H,fast}}$ so obtained for the samples L7 and T7 in aqueous solutions are comparable to the respective values of R_{H} for them in methanol at 25.0 °C given in Table 5.2, confirming that the fast mode may be ascribed to the translational motion of the isolated PNIPA chains. The values of $R_{\mathrm{H,slow}}$ are 4—6 times as large as the corresponding values of $R_{\mathrm{H,fast}}$.

5.4.2 Mean-Square Radius of Gyration

Since $A(\tau, k)$ as a function of τ is definitely bimodal for the aqueous solutions of the sample L7 at $w = 1.35\%$ and the sample T7 at $w = 1.36\%$ as mentioned above, $\Delta R_{\mathrm{Uv}}(k)$ determined from the time-averaged scattering intensity $\bar{I}$ may be divided into the two contributions $\Delta R_{\mathrm{Uv,fast}}(k)$ and $\Delta R_{\mathrm{Uv,slow}}(k)$ from the fast- and slow-mode components, respectively, as follows,

$$\Delta R_{\mathrm{Uv},\alpha}(k) = \Delta R_{\mathrm{Uv}}(k) \sum_{\tau_i \in \alpha \text{ mode}} A(\tau_i, k) \Big/ \sum_{i=1}^{n_f} A(\tau_i, k) \qquad (\alpha = \text{fast, slow}) \tag{5.7}$$

Under the assumptions that the solution includes only a small amount of aggregates and interactions between them may be neglected, the z-average mean-square radius of gyration $\langle S^2 \rangle_{\mathrm{slow}}$ of the aggregates may be estimated from[11]

$$\left[\frac{\Delta R_{\mathrm{Uv,slow}}(0)}{\Delta R_{\mathrm{Uv,slow}}(k)} \right]^{1/2} = 1 + \frac{1}{6} \langle S^2 \rangle_{\mathrm{slow}} k^2 + \cdots \tag{5.8}$$

with the values of $\Delta R_{\mathrm{Uv,slow}}(k)$ defined by eq 5.7. Although a similar analysis of dynamic LS data can be found elsewhere,[17–19] its theoretical background was not adequately justified, as pointed out by Kanao *et al.*[11]

Figure 5.7 shows plots of $[\Delta R_{\mathrm{Uv,slow}}(0)/\Delta R_{\mathrm{Uv,slow}}(k)]^{1/2}$ against k^2 for the aqueous solutions of the sample L7 at $w = 1.35\%$ (a) and of the sample T7 at $w = 1.36\%$ (b), at 15.0, 20.0, and 25.0 °C and at $t_e \simeq 36$ h. The unfilled circles represent the experimental values and the solid curves connect smoothly the data points. The dot-dashed line segment associated with each curve indicates its initial tangent. The values of $\langle S^2\rangle_{\mathrm{slow}}^{1/2}$ evaluated from the slopes of those initial tangents are given in the third, fourth, and fifth columns of Table 5.4. It is seen that $\langle S^2\rangle_{\mathrm{slow}}^{1/2}$ is appreciably larger for the sample T7 than for the sample L7 at each temperature.

Table 5.4. Values of $\langle S^2\rangle_{\mathrm{slow}}^{1/2}$ and ρ_{slow} for the samples L7 and T7 in water at 15.0, 20.0, and 25.0 °C and at $t_e \simeq 36$ h

		$\langle S^2\rangle_{\mathrm{slow}}^{1/2}$ (nm)			ρ_{slow}		
sample	w, %	15.0 °C	20.0 °C	25.0 °C	15.0 °C	20.0 °C	25.0 °C
L7	1.35	$40._7$	$24._6$	$17._8$	1.1_0	0.9_2	0.6_9
T7	1.36	$61._1$	$32._2$	$49._2$	1.6_0	1.0_3	1.2_2

5.4.3 Reduced Hydrodynamic Radius

Finally, we consider the density profile of the aggregate on the basis of values of the ratio ρ of $\langle S^2\rangle^{1/2}$ to R_{H},

$$\rho = \langle S^2\rangle^{1/2}/R_{\mathrm{H}} \tag{5.9}$$

its reciprocal ρ^{-1} being called the reduced hydrodynamic radius.[20] It is well known that the ρ value of an isolated solute in dilute solution is sensitive to its density profile, *i.e.*, $\rho = 1.2$—1.5 for a random coil (Gaussian density profile) and $\rho = 0.775$ for a rigid sphere with a uniform density.[20] The ρ value becomes even smaller than 0.775 if the density profile in the rigid sphere concentrates at its center rather than its periphery.[11,21]

In the sixth, seventh, and eighth columns of Table 4 are given the values of ρ_{slow} for the slow mode in the aqueous PNIPA solutions at 15.0, 20.0, and 25.0 °C, respectively,

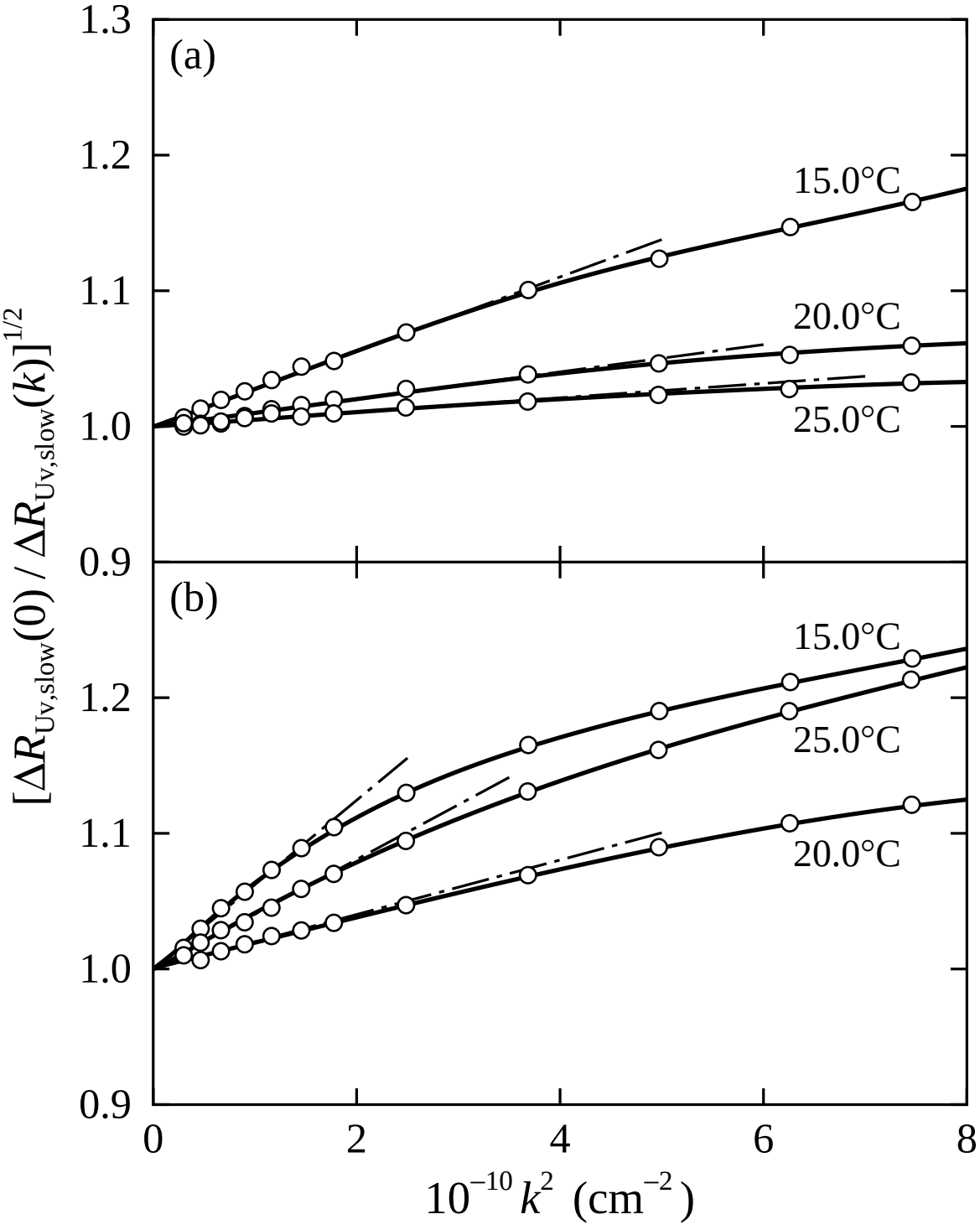

Figure 5.7. Plots of $[\Delta R_{\mathrm{Uv,slow}}(0)/\Delta R_{\mathrm{Uv,slow}}(k)]^{1/2}$ against k^2 for the aqueous solutions of the sample L7 at $w = 1.35\%$ (a) and of the sample T7 at $w = 1.36\%$ (b), at 15.0, 20.0, and 25.0 °C and at $t_{\mathrm{e}} \simeq 36$ h. The unfilled circles represent the experimental values and the solid curves connect smoothly the data points. The dot-dashed line segment associated with each curve indicates its initial tangent.

and at $t_e \simeq 36$ h calculated from eq 5.9 with the values of $R_{H,slow}$ and $\langle S^2 \rangle_{slow}^{1/2}$ given in Tables 3 and 4, respectively. The value of ρ_{slow} at each temperature is smaller for the sample L7 than for the sample T7. For the sample L7, ρ_{slow} decreases from 1.1 to 0.7 with increasing temperature. As for the sample T7, it takes a minimum 1.0 at 20.0 °C. The results for ρ_{slow} along with $R_{H,slow}$ and $\langle S^2 \rangle_{slow}^{1/2}$ indicate that the aggregates in the aqueous solutions of the sample L7 seem to be densely packed spheres of small size, while those of the sample T7 look like loosely packed random coils of large size.

The above-mentioned differences in the size and density profile of the aggregates and also in the number of them (Figure 5.5) between the aqueous solutions of the samples L7 and T7 may be regarded as arising from the differences in the primary structure and in the chain end group, *i.e.*, the sample L7 has the linear structure and the diphenylmethyl group at one end, while the sample T7 has the random-branched structure with a small number of branch points and the isobutyronitrile group at almost every end. The diphenylmethyl group may be considered to be more hydrophobic than the isobutyronitrile group, so that an attractive interaction between the chain end groups in an aqueous solution seems stronger for the sample L7 than for the sample T7. Linear PNIPA chains having hydrophobic groups at one end can form only star-like aggregates, while random-branched PNIPA chains having hydrophobic groups at almost every end can even form networks.

Concerning the shape and number of aggregates in aqueous PNIPA solutions, it is pertinent to refer here to literature LS data for aqueous solutions of telechelic hydrophobically modified PNIPA (HM-PNIPA)[22,23] — a linear PNIPA chain with strong hydrophobic groups at both the chain ends. It was shown that the HM-PNIPA samples with $M_w = 1.2 \times 10^4$—4.9×10^4 formed aggregates in aqueous solutions at 20—30 °C and at 1×10^{-4}—1×10^{-2} wt% and that there remained no isolated HM-PNIPA chain. Further, from a rather detailed analysis of the LS data, it was supposed that the aggregates were flower micelles consisting of 10—40 HM-PNIPA chains.

5.5 Conclusion

A rather detailed examination has been made of the transmittance of light passing through the 4.91 wt% aqueous solution of the linear PNIPA sample of $M_w = 7.23 \times 10^4$, which was synthesized by living anionic polymerization and has the diphenylmethyl group at the initiating end, in the vicinity of its cloud point. In contrast to the case of a typical phase separation as observed in cyclohexane solutions of a-PS in which the transmittance decreases very steeply to zero, even though the solution temperature is fixed at a constant value very close to its cloud point, the transmittance was found to be held at a constant

value between 0 and 100% near the cloud point in the aqueous PNIPA solution. The indication is that the cloud point in the aqueous PNIPA solution does not correspond to the binodal point.

Static and dynamic LS measurements have then been carried out for aqueous solutions of the above-mentioned linear PNIPA sample and also of another PNIPA sample, which was synthesized by radical polymerization and has random-branched structure with the isobutyronitrile group at almost every chain end, at temperatures considerably lower than the cloud point where the solutions are apparently transparent. It was found that both the PNIPA samples in aqueous solution form aggregates, whose number, size, and density profile depend on the kind of end group and also on the primary structure. The linear PNIPA chains with the diphenylmethyl group at one end seem to form densely-packed spherical aggregates of small size, while the random-branched PNIPA chains with the isobutyronitrile group at almost every end prefer to form large aggregates like loosely-packed random coils.

References

1. T. Kawaguchi, Y. Kojima, M. Osa, and T. Yoshizaki, *Polym. J.*, **40**, 455 (2008).
2. T. Kawaguchi, Y. Kojima, M. Osa, T. Yoshizaki, *Polym. J.*, **40**, 528 (2008).
3. K. Kobayashi, S. Yamada, K. Nagaoka, T. Kawaguchi, M. Osa, and T. Yoshizaki, *Polym. J.*, submitted.
4. T. Ishizone and M. Ito, *J. Polym. Sci., Polym. Chem. Ed.*, **40**, 4328 (2002).
5. M. Ito and T. Ishizone, *Designed Monomers and Polymers*, **7**, 11 (2004).
6. M. Ito and T. Ishizone, *J. Polym. Sci., Polym. Chem. Ed.*, **44**, 4832 (2006).
7. Gj. Deželić and J. Vavra, *Croat. Chem. Acta*, **38**, 35 (1966).
8. D. N. Rubingh and H. Yu, *Macromolecules*, **9**, 681 (1976).
9. F. Spieweck and H. Bettin, *Technishes Messen*, **59**, 285 (1992).
10. B. L. Johnson and J. Smith, In *Light Scattering from Polymer Solutions*; M. B. Huglin, Ed.; Academic Press: London, 1972; Chapter 2.
11. M. Kanao, Y. Matsuda, and T. Sato, *Macromolecules*, **36**, 2093 (2003).
12. G. Jones and H. J. Fornwalt, *J. Am. Chem. Soc.* **60**, 1683 (1938).
13. National Astronomical Observatory of Japan, Ed. *Rika Nenpyo. Tables for Scientific Data*; Maruzen: Tokyo, 2003.
14. G. C. Berry, *J. Chem. Phys.*, **44**, 4550 (1966).
15. T. Konishi, T. Yoshizaki, and H. Yamakawa, *Macromolecules*, **24**, 5614 (1991).
16. S. W. Provencher, *Comput. Phys. Commun.*, **27**, 213; 229 (1982). See also the URL: `http://s-provencher.com/pages/contin.shtml`

17. M. Sedlák, *J. Chem. Phys.*, **105**, 10123 (1996).
18. A. Sehgal and T. A. P. Seery, *Macromolecules*, **31**, 7340 (1998).
19. S. Kanai and M. Muthukumar, *J. Chem. Phys.*, **127**, 244908 (2007).
20. H. Yamakawa, "Helical Wormlike Chains in Polymer Solutions," Springer, Berlin, 1997.
21. X. Wang, X. Qiu, and C. Wu, *Macromolecules*, **31**, 2972 (1998).
22. P. Kujawa, F. Tanaka, and F. M. Winnik, *Macromolecules*, **39**, 3048 (2006).
23. R. Nojima, T. Sato, X. Qiu, and F. M. Winnik, *Macromolecules*, **41**, 292 (2008).

List of Publications

CHAPTER 2

1. Cloud Points in Aqueous Poly(*N*-isopropylacrylamide) Solutions; T. Kawaguchi, Y. Kojima, M. Osa, and T. Yoshizaki, *Polym. J.*, **40**, 455—459 (2008).

CHAPTER 3

2. Primary Structure of Poly(*N*-isopropylacrylamide) Synthesized by Radical Polymerization. Effects of Polymerization Solvents; T. Kawaguchi, Y. Kojima, M. Osa, and T. Yoshizaki, *Polym. J.*, **40**, 528—533 (2008).

CHAPTER 4

3. Characterization of Linear Poly(*N*-isopropylacrylamide) and Cloud Points in its Aqueous Solutions; K. Kobayashi, S. Yamada, K. Nagaoka, T. Kawaguchi, M. Osa, and T. Yoshizaki, *Polym. J.*, in press.

CHAPTER 5

4. Is a "Cloud-Point Curve" in Aqueous Poly(*N*-isopropylacrylamide) Solution the Binodal?; T. Kawaguchi, K. Kobayashi, Masashi. Osa, and T. Yoshizaki, *J. Phys. Chem. B*, submitted.

Other Publications

1. Second Virial Coefficient and Gyration-Radius Expansion Factor of Oligo- and Poly(α-methylstyrene)s near the Θ Temperature; T. Kawaguchi, M. Osa, T. Yoshizaki, and H. Yamakawa, *Macromolecules*, **37**, 2240—2248 (2004).
2. Unique Effects of 2,3,5,6,7,8-Hexasilabicyclo[2.2.2]octan-1-yl Moiety on Photophysical Properties of π-Conjugated System; M. Shimizu, T. Kawaguchi, K. Oda, and T. Hiyama, *Chem. Lett.*, **36**, 412—413 (2007).

Acknowledgement

The present study has been carried out at the Department of Polymer Chemistry, Graduate School of Engineering, Kyoto University under the guidance of Professor Takenao Yoshizaki. The author would like to thank Professor Takenao Yoshizaki for his guidance, suggestions of the problems, numerous valuable comments, and constant encouragement, and his critical reading of the manuscript. The author has been learning from him many things about polymer science. This must also be acknowledged.

The author is indebted to Professor Emeritus Yoshiyuki Einaga of Nara Women's University and Professor Takahiro Sato of Osaka University for their valuable comments and constant encouragement throughout this work.

The author wishes to thank Associate Professor Yo Nakamura for their encouragement and helpful discussions and Lecturer Masashi Osa, Mr. Yosuke Kojima, Mr. Satoshi Yamada, Mr. Kunihiko Kobayashi, and Mr. Kouta Nagaoka for their active collaborations.

The author's thanks are also tendered to all the members in the laboratory of Polymer Molecular Science for their help.

Finally, the author wishes to thank his parents, Sadaji Kawaguchi and Machiyo Kawaguchi, for their support and encouragement.